ESL INCORPORATED • A SUBSIDIARY OF TRW INC.
495 JAVA DRIVE • P.O. BOX 510 • SUNNYVALE, CA 94086

TIME INTEGRATING OPTICAL SIGNAL PROCESSING

FINAL TECHNICAL REPORT

JULY 1981

Todd R. Bader
Peter Kellman
Harry N. Shaver

Research sponsored by the Air Force Office of Scientific Research
under Contract F49260-78-C-0102

UNCLASSIFIED

SECURITY CLASSIFICATION OF THIS PAGE (When Data Entered)

REPORT DOCUMENTATION PAGE	READ INSTRUCTIONS BEFORE COMPLETING FORM
1. REPORT NUMBER: AFOSR-TR-81-0700	2. GOVT ACCESSION NO.: AD-A106 778	3. RECIPIENT'S CATALOG NUMBER
4. TITLE (and Subtitle): Time Integrating Optical Signal Processing.	5. TYPE OF REPORT & PERIOD COVERED: Final rpt. 1 Aug 1980 — 31 Jul 1981
	6. PERFORMING ORG. REPORT NUMBER
7. AUTHOR(s): Todd R. Bader; Peter N. Kellman; Harry N. Shaver	8. CONTRACT OR GRANT NUMBER(s): F49620-78-C-0102
9. PERFORMING ORGANIZATION NAME AND ADDRESS: ESL Incorporated, 495 Java Dr., Sunnyvale, CA 94086	10. PROGRAM ELEMENT, PROJECT, TASK AREA & WORK UNIT NUMBERS: 61102F; 2305/B1
11. CONTROLLING OFFICE NAME AND ADDRESS: AFOSR/NE, Bldg. 410, Bolling AFB, DC 20332	12. REPORT DATE: July 81
	13. NUMBER OF PAGES: 80
14. MONITORING AGENCY NAME & ADDRESS (if different from Controlling Office)	15. SECURITY CLASS. (of this report): Unclassified
	15a. DECLASSIFICATION DOWNGRADING SCHEDULE

16. DISTRIBUTION STATEMENT (of this Report)

Approved for public release; distribution unlimited.

17. DISTRIBUTION STATEMENT (of the abstract entered in Block 20, if different from Report)

18. SUPPLEMENTARY NOTES

19. KEY WORDS (Continue on reverse side if necessary and identify by block number)

Optical Signal Processing
Optical Correlators
Acousto-Optic Signal Processing
Time Integrating

20. ABSTRACT (Continue on reverse side if necessary and identify by block number)

Optical signal processing architectures using time integration on the detector array provide a highly flexible, multipurpose, wideband, realtime processor. A key feature of the time integrating concept is the ability to perform very large time-bandwidth product processing operations on signals without having to store the entire time history of the signal as a spatial record. Further, these signal processing operations may be realized with either coherent or non-coherent optical systems.

DD FORM 1 JAN 73 1473

UNCLASSIFIED

SECURITY CLASSIFICATION OF THIS PAGE (When Data Entered)

20. ABSTRACT (Continued)

In the first phase of the program, a comprehensive treatment of time integrating acousto-optic signal processing was undertaken. This treatment includes a synthesis and evaluation of alternative architectures and a detailed statistical analysis of processor performance. New developments include the extension of one-dimensional time integrating optical correlation to two-dimensional processing, the concepts of interferometric detection with electronic reference, and the generalization of these signal processing techniques to complex computation. One- and two-dimensional complex signal processing algorithms have been developed for non-coherent optical realizations. Detailed analysis has been made for complex spectral analysis and ambiguity function processing. Complex computation using real correlation processing has been analyzed.

In the second phase of the program, new architectures were developed for signal processing using time integration and a comparative analysis of alternate techniques for one-dimensional spectrum analysis was performed. Coherent and non-coherent time integrating schemes were considered and a new hybrid space/time integrating approach was detailed. The hybrid approach was shown to exhibit important characteristics related to sensitivity and dynamic range, including the suppression of effects due to optical scattering, special sidelobes and multisignal handling ability. A new approach to ambiguity function processing that utilizes space and time integration in two-dimensions exhibits superior performance in dynamic range and permits high resolution Doppler search.

The final phase of the program continued the extension of optical architectures development that resulted in several new space/time integrating system configurations for correlation and triple product processing and a space-integrating triple product and four product ambiguity processor. Experimental results were presented to demonstrate the application of chirps as spatially distributed local oscillators for interferometric spectrum analysis and to provide a quantitative evaluation of a time-integrating ambiguity function processor.

TIME INTEGRATING
OPTICAL SIGNAL PROCESSING

FINAL TECHNICAL REPORT

JULY 1981

Todd R. Bader
Peter Kellman
Harry N. Shaver

Research sponsored by the Air Force Office of Scientific Research
under Contract F49260-78-C-0102

TABLE OF CONTENTS

TABLE OF CONTENTS

1. INTRODUCTION.

This program was a three year effort to analyze and develop new acousto-optic techniques for signal processing that utilize time integration in one and two dimensions. The following paragraphs in this section summarize the results of the first two years (phases 1 and 2). Sections 2 and 3 present a review of the results of the final phase, which includes the extension of system architectures to achieve high performance processing and an investigation of realizability considerations, including laboratory measurements of some time-integrating processing systems.

1.1 Summary of Phase I.

1.1.1 Architectures.

Time integrating optical signal processing has been generalized for one- and two-dimensional complex signal processing. Signal processing architectures utilizing actively generated reference waveforms such as chirps realize a wide range of algorithms, and variable time integration allows further flexibility. The class of signal processing operations achieved with time integrating acousto-optic techniques has been described, and hybrid architectures using both time and space integration have been discussed. Particularly attractive is the multi-purpose capability of the time integrating optical processor, e.g., the same optical system is used for both spectral analysis and ambiguity function processing.

1.1.2 Optical Processor Realizations.

Several optical realizations were analyzed including interferometric and non-interferometric implementations. Interfereometric techniques are based on linear electric field modulation and non-interferometric techniques are based on linear intensity modulation.

1.1.2 -- Continued

The concept of interferometric detection with electronic reference was introduced. In this implementation, a local oscillator is added to the acoustic modulation rather than a coherent optical reference added to the image. This method, therefore, permits non-coherent optical implementation, with the advantage of directly modulated diode light sources and increased immunity to artifacts of coherent optical imaging systems. The correlation is performed at a carrier, thereby enabling complex operation. Furthermore, the interferometric method circumvents the difficult requirements for acoustic modulation at a high diffraction efficiency bias point, which is necessary for linear operation in the non-interferometric technique.

1.1.3 Statistical Analysis.

Fundamental limitations were established with regards to signal-to-noise and signal-to-bias ratios. The reduction in signal-to-noise ratio due to detection noise and bias variation was analyzed. It was shown that the average bias reduces the dynamic range and that the bias variation cause a loss in sensitivity. Expressions were derived for the optical processor output that include the signal dependent bias contribution. This contribution may be filtered or subtracted. Several schemes were analyzed.

The optical implementation, utilizing acousto-optic input and integrating image sensor output devices, creates a processor that is highly compatible with signal processing systems. Such implementation affords very large time-bandwidth product signal processing without the input signal storage requirement associated with spatial integrating methods. The requirement for high resolution large dynamic range output image sensors becomes the key device limitation. Acousto-optic devices are available with time-bandwidth product much greater than the number of resolvable image samples.

1.1.3 -- Continued

The key attributes of time integrating techniques are summarized in the following: extremely large time-bandwidth correlations may be performed, independent of the device time-bandwidth product; a flexible, multi-purpose processor is realized by use of actively generated reference waveforms and variable time integration; an important class of two-dimensional algorithms, including complex spectral analysis and ambiguity function processing, may be performed without having to store the entire time history as a spatial history; the system may be implemented with non-coherent diode sources, acousto-optic devices, and integrating image sensors.

1.2 Summary of Phase II.

Efforts during this phase concentrated on system architectures for spectrum analysis, including a comparative analysis of various approaches to one-dimensional processing, dynamic range studies and implementation requirements, and coherent hybrid approaches to ambiguity function processing.

1.2.1 One-Dimensional Spectrum Analysis.

Many acousto-optic techniques are available for spectrum analysis. The interferometric schemes can be divided into three groups: time-integrating, space-integrating and hybrid space/time integrating. These have been analyzed to establish their capabilities with respect to each other and in comparison with an acousto-optic (non-interferometric) power spectrum analyzer (which we will call a Bragg receiver).

A Bragg receiver measures the signal power spectrum, so that long detector integration can be used to gain signal-to-noise ratio for narrowband signals and to ease the detector read rate requirements. A major difficulty with the Bragg receiver is the limitation on the

1.2.1 -- Continued

dynamic range imposed by the detector noise. A common characteristic of all the interferometric approaches is the considerable improvement of the dynamic range attained by measuring the complex amplitude spectrum.

1.2.1.1 Time Integrating Techniques.

A number of configurations for time integration spectrum analysis, both coherent and incoherent, have been analyzed. Their major characteristics may be summarized as follows:

- The bandwidth is limited to about 25% of the Bragg cell bandwidth by chirp transition effects.
- Chirps that are not highly uniform in amplitude and linear in phase can produce spurious signals. A noisy chirp will produce a noisy spectrum when a signal is present.
- Multiple signal handling capacity is low. Unit modulation can occur only for a narrowband signal. The dynamic range therefore degrades as the spectrum becomes more dense.
- Counterpropagating schemes sometimes require an external delay of τ (equal to the Bragg cell delay) for the chirp signal applied to one of the cells. Also, whenever a baseband signal is mixed with a CW or chirp, the product must be generated single sideband to avoid a 3 dB loss in dynamic range.
- Optical scatter noise is suppressed. Light scattered from optical elements is not Doppler-shifted, and

1.2.1.1 -- Continued

therefore the only components in the exposure that do not integrate to zero are products containing only scatter elements. The dynamic range referred to scatter noise is twice as large (in dB) for time-integrating techniques as it is for a Bragg receiver.

1.2.1.2 Space Integrating Interferometric Techniques.

The configuration considered here is one using a pulsed coherent source, such as a laser diode, to generate a snapshot of the amplitude spectrum. The chief attraction of this technique is the removal of the requirement for a chirp. An additional favorable aspect of the pulsed laser scheme is that, unlike the time-integration techniques and wider-band hybrid techniques, the reference wave does not need to be diffracted by a Bragg cell. Since the reference wave needs to illuminate all the diodes in the detector array, a low efficiency diffraction of the reference wave could have a serious impact on the system light budget, especially at wide bandwidths.

Optical scatter, however, is not suppressed unless a supplementary Bragg cell is used in the reference arm of the interferometer, complicating the design.

Laser diodes are presently the only realistic pulsed light source for this application. Diode sources with adequate coherence and sufficient peak and average output powers are available, but the transverse mode structures of these devices are grossly inadequate.

1.2.1.3 Coherent Hybrid Techniques.

The coherent hybrid approach to interferometric spectrum analysis described here uses both space integration and time integration. In summary

1.2.1.3 -- Continued

- Spectral sidelobes are down by a factor of two in dB compared with the above techniques and with the Bragg receiver. Sidelobes of the very bright zero order (undiffracted by the acoustic wave) that extend into the signal band are similarly suppressed. This inherent sidelobe suppression is the result of the combined effect of the localization of the signal illumination at the detector by spatial integration (i.e., the optical Fourier transform) and localization of the interference fringe pattern by time integration.

- As in the purely time-integration techniques, scatter noise from optical elements is suppressed. Dynamic range relative to scatter noise is doubled in dB compared with that of the Bragg receiver.

- Hybrid techniques, unlike time-integrating techniques are not sensitive to chirp noise and chirp-related intermodulation distortion.

- The multiple signal handling capability of a hybrid spectrum analyzer is not degraded from that of a Bragg receiver. Whereas time-integration techniques degrade in dynamic range by 10 log N due to the buildup of bias terms when N equal amplitude signals are present, hybrid and space-integrating techniques spatially separate the light associated with signals of different frequency.

1.2.2 Dynamic Range and Implementation Factors.

Dynamic range for interferometric detection was shown to be limited by the detector noise (of variance σ^2) to

1.2.2 -- Continued

$$DR = (V_{sat}/\sigma)^2/8 \quad ,$$

where V_{sat} is the detector saturation voltage. Since for a Bragg receiver $DR = V_{sat}/\sigma$, the gain in dynamic range is considerable.

Shot noise due to the bias can be significant in large dynamic range systems. Large saturation values for the detector and high light powers are required to avoid this limitation.

Other serious dynamic range limits, as mentioned above, can be overcome with the correct system architecture. Time-integration suppresses scatter noise, and, in addition, hybrid techniques overcome chirp distortion and noise and also suppress sidelobes.

Chirp linearity requirements and the effects of nonlinearities were investigated. It was found that resolution considerations permit larger percent linearity error for time integrating techniques, but the requirement to suppress intermodulation terms imposes a much more severe linearity requirement for time integrating than for hybrid techniques.

1.2.3 Ambiguity Function Processing.

A hybrid ambiguity function concept was developed that utilizes a space-integrating ambiguity function generator in one arm of an interferometer and a chirp-generated spatially distributed local oscillator in the other arm. Time integration detection yields an estimate of the ambiguity function with finer Doppler resoltuion (than a space integrating technique) but with a signal-dependent bias localized in the delay direction. It was shown that a multiplicity of correlation peaks does not result in a decreased dynamic range due to bias buildup, as it does in purely time integrating techniques, provided that the peaks are separated by at least one delay resolution element.

2. ARCHITECTURES.

It has become apparent that there is an innumerable variety of architectures, implementation variations and algorithms possible with acousto-optic techniques, and that optimum architectures for one algorithm are not generally optimum for another algorithm. Furthermore, implementational variations may differ widely in performance, relative to signal-to-noise ratio, bandwidth and other important parameters. It is further recognized that the driving motivation for A-O processing is the ability to process data at very high rates. With these considerations in mind it is highly relevant to compare and contrast A-O techniques, time integrating, space integrating and hybrid architectures for correlation, generalized triple product processing and ambiguity function generation. In the paragraphs below we discuss some extensions of previously described configurations and introduce several new architectures.

2.1. Correlation.

In this section one dimensional A-O techniques for signal correlation are discussed. The performance of time-integrating, space-integrating and hybrid configurations are compared with one another and with respect to the performance of an ideal correlator.

2.1.1 Ideal Correlator.

Let

$$S_1(t) = S(t-t_0) + n_1(t) \qquad (2\text{-}1)$$

$$S_2(t) = S(t) + n_2(t)$$

be complex signals plus noise; the cross-correlation function between these signals is defined as

2.1.1 -- Continued

$$R_{12}(\tau) = E\{S_1(t)S_2^*(t-\tau)\} \quad , \tag{2-2}$$

where E {} represents an ensemble average. The time integrated estimate of the correlation is

$$\hat{R}_{12}(\tau) = \frac{1}{T}\int_0^T S_1(t)S_2^*(t-\tau)\,dt \quad . \tag{2-3}$$

The output signal-to-noise ratio for the correlation estimate is defined as

$$SNR(\tau) = \frac{|E\{\hat{R}_{12}(\tau)\}|^2}{E|\hat{R}_{12}(\tau)|^2} \quad . \tag{2-4}$$

If B is the signal bandwidth (assumed equal to both noise bandwidths) then Equations 2-1 through 2-4 lead to the SNR at the peak of the correlation

$$SNR(t_0) = \frac{BT\ SNR_1\ SNR_2}{1 + SNR_1 + SNR_2} \tag{2-5}$$

for signals of constant modulus, and when SNR_1 and SNR_2 are small. SNR_1 and SNR_2 are the input signal-to-noise ratios for S_1 and S_2, respectively;

$$SNR_1 = \frac{R_S(0)}{R_1(0)} \tag{2-6}$$

$$SNR_2 = \frac{R_S(0)}{R_2(0)}$$

where $R_1(0)$, $R_2(0)$ and $R_S(0)$ are the input noise and signal powers, respectively.

2.1.2 Acousto-Optic Time-Integrating Correlator.

There are many variations of A-O time-integrating correlators. For the present discussion we will choose the noncoherent configuration in which a light source is modulated in intensity according to

$$I_1(t) = 1 + m_1|S_1(t)|\cos[2\pi ft + \phi_1(t)] \quad , \tag{2-7}$$

and the Bragg cell is driven so that the diffraction efficiency at a point τ from the transducer is $I_2(t-\tau)$, where

$$I_2(t) = 1 + m_2|S_2(t)|\cos[2\pi ft + \phi_1(t)] \quad . \tag{2-8}$$

It is assumed that $f \geq 3B/2$. The input gains m_1 and m_2 are adjusted so that

$$m_1^2\, E[|S_1(t)|^2] = m_1^2[R_S(0) + R_1(0)] \leq 1 \tag{2-9}$$

$$m_2^2\, E[|S_2(t)|^2] = m_2^2[R_S(0) + R_2(0)] \leq 1 \quad .$$

The light diffracted from the Bragg cell, imaged onto the detector array, is integrated for timeT, after which the voltage output from the diode at τ is

$$V(\tau) = \frac{V_B}{T} \int_0^T I_1(t) I_2(t-\tau)\, dt + V_d(\tau) \quad , \tag{2-10}$$

where V_B is the accumulated bias and V_d is the electrical noise added by the detector. From Equations 2-7 and 2-8,

$$V(\tau) = V_B + V_S(\tau) + V_d(\tau) \tag{2-11}$$

2.1.2 -- Continued

where

$$V_S(\tau) = \frac{m_1 m_2 V_B}{2} |\hat{R}_{1,2}(\tau)| \cos[2\pi f\tau + \psi(\tau)] \quad , \qquad (2\text{-}12)$$

and where

$$R_{1,2}(\tau) = |\hat{R}_{1,2}(\tau)| \exp[j\psi(\tau)] \quad .$$

With appropriate demodulation the signal can be detected with an output signal-to-noise ratio given by

$$SNR'(t_0) = \frac{E\left\{\frac{1}{2}\left(\frac{m_1 m_2 V_B}{2}\right)^2 |\hat{R}_{12}(t_0)|^2\right\}}{E\left\{\frac{1}{2}\left(\frac{m_1 m_2 V_B}{2}\right)^2 [\hat{R}_{12}^2(t_0) - R_{12}^2(t_0)]\right\} + \sigma_d^2} \qquad (2\text{-}13)$$

where σ_d^2 is the mean of $|V_d(\tau)|^2$ times the number of detector elements per delay bin. With the signals of Equations 2-1 and 2-2, this reduces to

$$SNR'(t_0) \approx \frac{SNR(t_0)}{1 + \frac{\alpha BT}{M^2}} \quad . \qquad (2\text{-}14)$$

In this example $\alpha = 8$. $SNR(t_0)$ is the SNR for an ideal correlator (Equation 2-5), and $M = V_B/\sigma_d$ represents the dynamic range of the detector. A value of V_B equal to the saturation voltage determines the limiting performance. Equation 2-14 quantifies the limit of processing gain for a noncoherent time-integrating correlator. For example, if the saturation-to-rms noise of an element of a detector array is 1000, and if there are 8 sampling elements per correlation width, the limiting value of M^2 is 8×10^6, and 60 dB of processing gain is achievable. This may not be adequate for some applications

2.1.2 -- Continued

when used as an auto-correlator with a low input SNR. The dynamic range limitation is aggravated by the presence of other signals in the signal band, which contribute to the bias.

The bandwidth of the Bragg cell in this noncoherent time-integrating configuration must be at least twice the signal bandwidth, since a reference tone must be placed at a frequency at least 3B/2 away from the center of the band.

Noncoherent schemes using two Bragg cells permit the use of a bright light source, such as an arc lamp, that cannot be directly modulated. Two Bragg cells, one imaged onto the other in a counter-propagating mode, also permit correlations to be measured over twice the relative delay as a single cell correlator. The same bandwidth and dynamic range considerations as outlined above apply, however.

A coherent time-integrating correlator can be implemented so that the Bragg cells have the same bandwidth as the signal. We assume a configuration in which two Bragg cells are in separate arms of an interferometer, such that the signal amplitudes, represented by the optical amplitudes diffracted from the cells, are imaged onto a linear detector array. The power density on the array is

$$I(t,\tau) = \left| m_1 S_1(t-\tau) + m_2 S_2(t+\tau) e^{j2\pi f\tau} \right|^2 , \qquad (2\text{-}15)$$

where the exponential describes the effect of the offset angle between the beams. The time integrated array output is

$$V(\tau) = V_B \left\{ 1 + \frac{2m_1 m_2}{V_B} \left| \hat{R}_{12}(\tau) \right| \cos[2\pi f\tau + \phi(\tau)] \right\} + V_d \qquad (2\text{-}16)$$

2.1.2 -- Continued

where the bias is

$$V_B = \frac{m_1^2}{T} \int_0^T |S_1(t-\tau)|^2 dt + \frac{m_2^2}{T} \int_0^T |S_2(t+\tau)|^2 dt \qquad (2\text{-}17)$$

It can be shown that the output SNR for this coherent technique used as an auto-correlator is given by Equation 2-14 with $\alpha = 2$, indicating that the processing gain limitation is 6 dB less serious than for a noncoherent technique. Interference can degrade the performance of a coherent correlator also.

2.1.3 Noncoherent Space-Integrating Correlator.

The noncoherent correlator with two Bragg cells can be used, with slight modification, as a space-integrating processor. If the input to one cell is a time-reversed version of the input to the other, and if the linear detector array is replaced by a single large-area wideband detector, the cross-correlation of the signals is contained in the time-varying output of the detector:

$$V(t) = V_B + \frac{m_1 m_2 V_B}{2} \hat{R}_{12}(2t)\cos[4\pi ft + \psi(2t)] + V_d \qquad (2\text{-}18)$$

The correlation function is on a temporal carrier and, therefore, requires a detector with a wide bandwidth. A detector with a large active area has a large capacitance, making it difficult to provide wideband response with high dynamic range. A space-integrating correlator provides processing gain equal to the time-bandwidth product of the Bragg cells, and therefore limits its usefulness when large processing gain is required, particularly in an auto-correlator. When used as a cross-correlator, the frequency of both signals must be equal to an accuracy of the reciprocal of the integration time (as for all

2.1.3 -- Continued

linear correlators). A sequential search through frequency may be required; to minimize total search time it is desirable to provide the minimum processing gain required to detect the signal. In those cases where space integration provides adequate gain, a space-integrating correlator may be a useful device for rapid search. Coherent implementations, however, can provide significant advantages. These advantages include the capability for parallel search over frequency; such configurations perform simultaneous cross-correlation and spectrum analysis and are referred to as ambiguity function processors.

2.1.4 Coherent Space/Time-Integrating Correlator.

The technique described here is a coherent optical approach that exploits the advantages of space integration processing and yet permits the extended gain provided by time-integration. It is also hybrid in the sense that the technique includes a digital processing step; this occurs, however, after time integration where the data rates are compatible with digital techniques.

The approach is illustrated in Figure 2-1, and is basically an integrating acousto-optic power spectrum analyzer followed by a digital Fourier transform. The input to the Bragg cell is the sum of the two signals being correlated. The optical power integrated over time T_2 on the detector results in an exposure

$$E(f) = \int_0^{T_2} |A_1(f,t) + A_2(f,t)|^2 dt \quad , \qquad (2\text{-}19)$$

where for A_1 and A_2 are the optical Fourier transform estimates of signals S_1 and S_2:

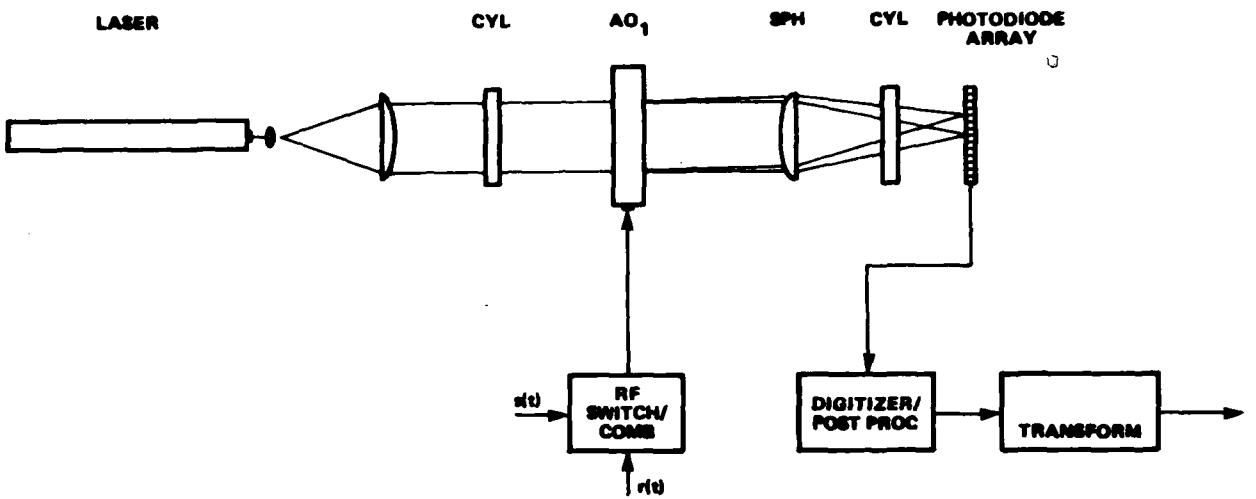

Figure 2-1. Space/Time Integrating Correlator.

2.1.4 -- Continued

$$A(f,t) = \int_0^{T_1} S(t-\tau)e^{j2\pi f}\,dt \quad . \tag{2-20}$$

where T_1 is the Bragg cell delay. The detector output is proportional to E(f), plus detector noise $V_d(\tau)$. The Fourier transform of the result, performed digitally, is

$$W(\tau) = \frac{V_B}{P}\,|\hat{R}_{12}(\tau)|\cos\phi(\tau) + n(\tau) \quad . \tag{2-21}$$

The FT of the bias term occurs at $\tau = 0$ and has been ignored. V_B is the bias level of the detector, $n(\tau)$ is the FT of the detector noise, where

$$E[n^2(\tau)] = (B/T_1)E[V_d^2(f)] \quad ,$$

and

$$P = \int_0^{T_2} [|A_1|^2 + |A_2|^2]dt$$

$$= [R_{S1}^1(0) + R_{S2}^2(0)]/B \quad . \tag{2-22}$$

Equation 2-21 indicates that the real output of the correlation estimate is obtained. A second measurement with S_2 shifted in phase by 90° yields the quadrature component.

A calculation of the output signal-to-noise ratio for signals and noise are defined in Equation 2-1 leads to

2.1.4 -- Continued

$$SNR'(t_0) = \frac{SNR(t_0)}{1 + \frac{2BT_2}{BT_1}\left(\frac{1}{M}\right)^2} \quad , \qquad (2\text{-}23)$$

i.e., $\alpha = 2/BT_1$. The processing gain achievable for a hybrid space/time integrating correlator is, therefore, larger than that for a purely time-integrating correlator by at least a factor BT_1. This improvement in performance over purely time-integrating techniques is directly analogous to the signal handling ability and dynamic range improvement in the hybrid space/time spectrum analyzer and the hybrid ambiguity function processor reported earlier (see the Interim Technical Report, 1980). This technique of measuring the joint spectral density with the detector array also permits the excision (or at least limitation) of narrowband interference signals occurring in the band before digital Fourier transformation. It is also tolerant of point blemishes.

2.2 Triple Product Correlator.

A triple product processor performs the estimate

$$\hat{R}(\tau_1,\tau_2) = \frac{1}{T}\int_0^T S_1(t)S_2(t-\tau_1)S_3(t-\tau_3)dt \quad , \qquad (2\text{-}24)$$

which can be implemented optically in a variety of ways. Below we contrast two techniques, one purely time integrating, the other a scheme that employs both space-integration and time-integration.

2.2.1 Noncoherent Time Integrating Processor.

The noncoherent correlator of subsection 2.1.2 can be expanded to two dimensions by passing the light diffracted from the

2.2.1 -- Continued

Bragg cell through a second cell orthogonal to the first driven by the third signal. The second Bragg cell produces a diffracted intensity.

$$I_3(t-\tau_2) = 1 + m_3 s_3(t-\tau_3) \qquad (2\text{-}25)$$

S_3 is assumed to be real. Both Bragg cells are imaged onto a two dimensional photodetector array. The important term of the triple product exposure integral over time T is

$$V_S(\tau_1,\tau_2) = \frac{m_1 m_2 m_3 V_B}{2} |\hat{R}(\tau_1,\tau_2)| \cos[2\pi f\tau_1 + \psi(\tau_1,\tau_2)] \qquad (2\text{-}26)$$

where the correlation estimate is on a carrier in the τ_1 direction, in this example. The output SNR can be shown again to be given by Equation 2-14 with $\alpha = 8$. This means that the noncoherent two-dimensional triple product correlator permits the same processing gain as the one-dimensional device. For cross-correlation of noisy signals, where large processing gain is desired, this technique will frequently be inadequate, especially if interfering signals are present. The Bragg cell bandwidth again must be at least twice the signal bandwidth. (The full Bragg cell bandwidth may be used if the measurement is made without a carrier twice.) Coherent time-integrating techniques can provide some improvement, as in the one-dimensional case, but not nearly as much as hybrid space/time integrating techniques.

2.2.2 Coherent Space/Time Processor.

The optical configuration shown in Figure 2-2 generates a two dimensional cross-spectral density that is transformed into the triple product integral by a digital Fourier transform. Light from a coherent source is split into two arms each containing a Bragg cell. The light diffracted from each of the orthogonally oriented cells,

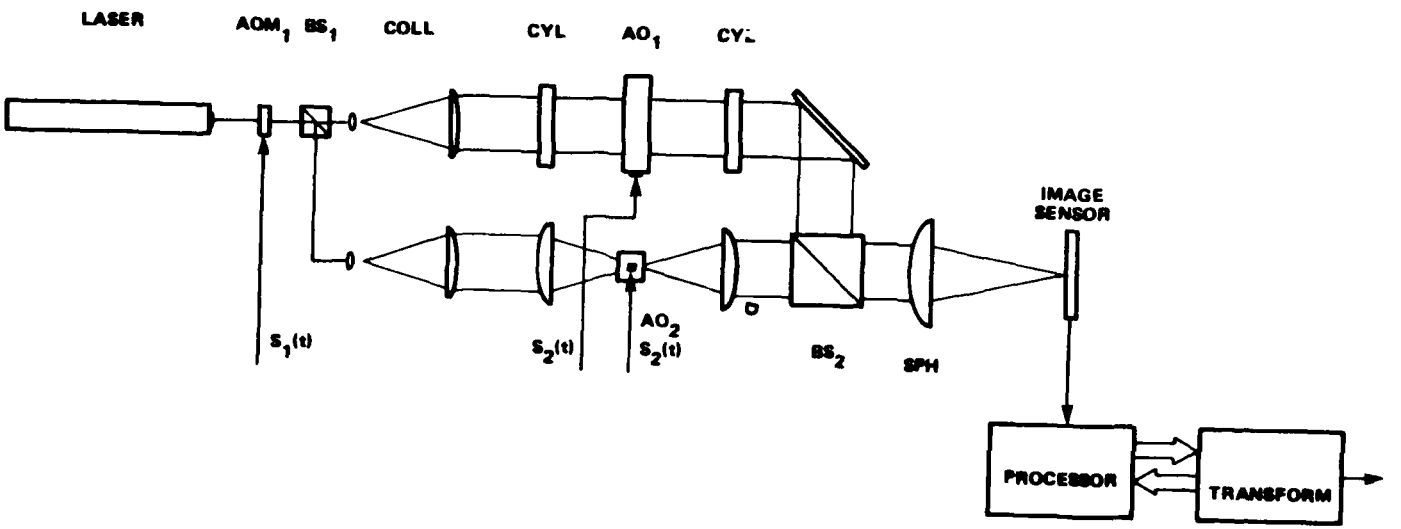

Figure 2-2. Space/Time Integrating Triple Product Processor.

2.2.2 -- Continued

driven by S_2 and S_3, is optically Fourier transformed onto a two-dimensional detector array, where the optical power density is

$$I(f_1,f_2,t) = |A_1(f_1,t) + A_2(f_2,t)|^2 \quad , \tag{2-27}$$

where A_1 and A_2 are the spectral amplitude estimates of S_1 and S_2 as defined in Equation 2-20. The light source is modulated in intensity by a third Bragg cell. The time integrated power density produces a detector output signal

$$V(f_1,f_2) = V_B \int_0^{T_2} [1 + S_3(t)]|A_1(f_1,t) + A_2(f_2,t)|^2 dt \quad . \tag{2-28}$$

The two dimensional digital Fourier Transform produces auto-correlation lines at $\tau_1 = 0$, $\tau_2 = 0$, a diagonal cross-correlation line between S_1 and S_2, and the term of interest

$$V_S(t) = V_B|\hat{R}(\tau_1,\tau_2)|\cos\psi(\tau_1,\tau_2) \tag{2-29}$$

The second quadrature component is obtained by a second measurement with the identical input signals but with one of the signals having a 90° phase shift imposed. The processing gain permitted with this technique is limited by Equation 2-14 with $\alpha = 2/BT_1$, as in the one-dimensional space/time integrating correlator. In addition to the large gain that is achievable, this technique permits relatively simple suppression of narrowband interference signals after time-integration but before the digital transform. Point blemishes on large two-dimensional photodetector arrays are almost impossible to avoid with the present state of technology, and these are particularly troublesome

2.2.2 -- Continued

when they occur in the correlation domain. However, in the spectral domain, as in the present case, blemishes are not particularly damaging, as their effect is more or less uniformly distributed over the correlation field after Fourier transformation.

2.2.3 Space-Integrating Triple Product Processor.

A space-integrating processor that computes the triple product integral is shown in Figure 2-3. The first Bragg cell has a diffracted optical amplitude that, when imaged onto the second Bragg cell, is proportional to the signal traveling opposite to that in the second Bragg cell. The light diffracted from the second cell is $S_1(x+t)S_2(x-t)$. This is imaged in the x direction through the third Bragg cell onto plane P; the plane of the third cell, driven by $S_3(t)$, is imaged in the y direction onto plane P. The result is Fourier transformed in the direction $v = (x+y)/\sqrt{2}$ and imaged in direction $2 = (x-y)/\sqrt{2}$ onto the detector plane. The resulting amplitude is

$$E(t,w) = \int S_1[(v+w)/\sqrt{2}+t]S_2[(v+w)/\sqrt{2}-t]S_3[(v-w)/\sqrt{2}+t]e^{j2\pi vx}dv$$

$$= e^{j2\pi(w-\sqrt{2}t)z}\int S_1(\xi)S_2(\xi-2t)S_3(\xi-w\sqrt{2})e^{j2\pi\sqrt{2}\xi z}d \quad . \quad (2\text{-}30)$$

At $z = 0$ the detected intensity is

$$|E|^2 = |R[2t,\sqrt{2}w]|^2 \quad , \quad (2\text{-}31)$$

recognized as the square of the triple product integral, with $\tau_1 = 2t$ $\tau_2 = \sqrt{2}w$. A linear photodiode array with parallel outputs placed along $z = 0$ permits very high speed processing in those cases in which a processing gain equal to the time bandwidth product of the Bragg cell

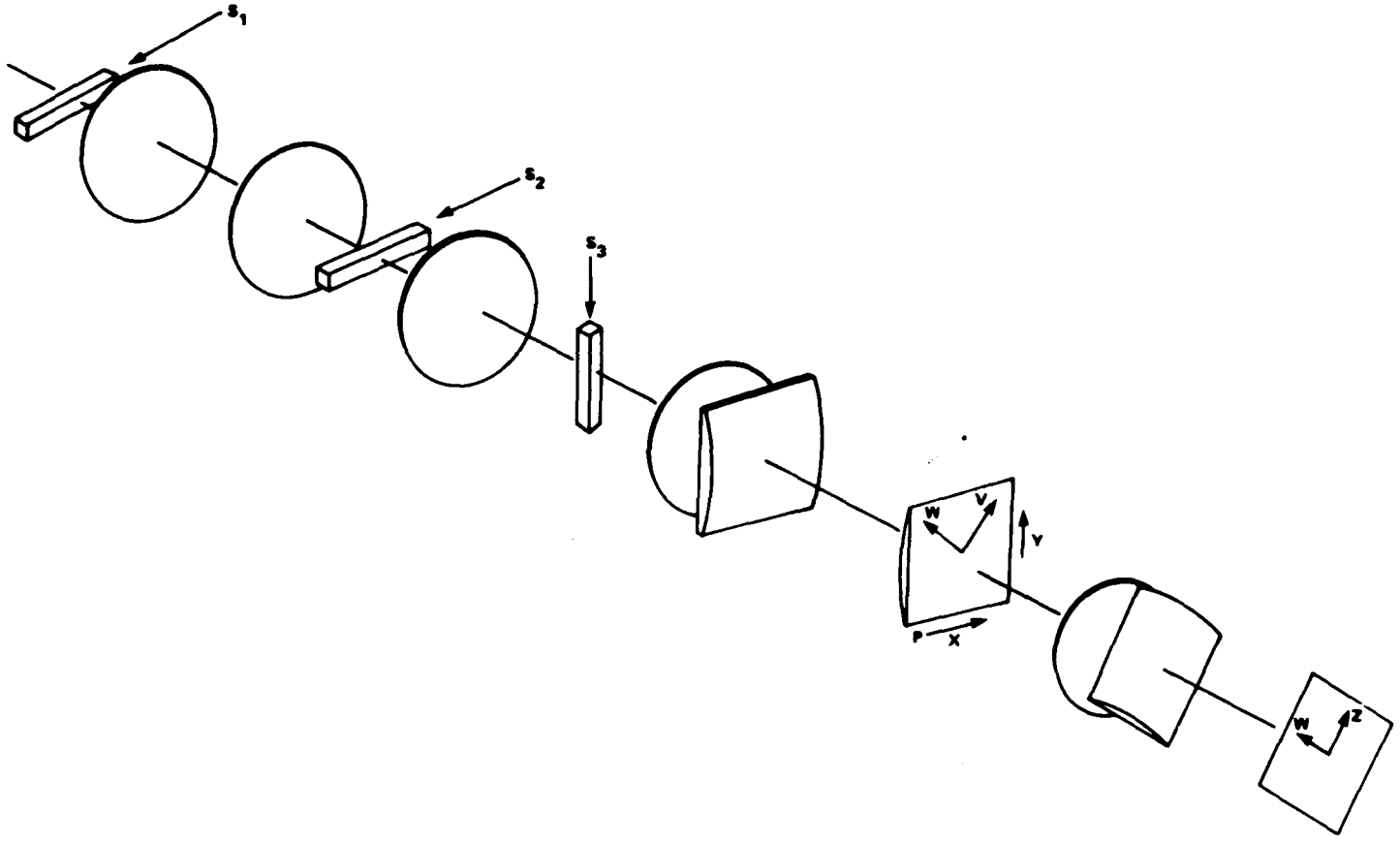

Figure 2-3. Coherent Space-Integrating Triple Product Processor.

2.2.3 -- Continued

is sufficient. Detector processing considerations are similar to those of the one-dimensional space-integrating ambiguity processor.

A triple product processor can be used in a linear carrier-dependent mode, where frequency must be known. The processor of Figure 2-3 can, in principal, be expanded to a three-product ambiguity processor by implementing a two-dimensional detector array in which all elements have parallel outputs. Very high processing speeds would be achievable with this processor. The detector array problem, however, is extremely difficult. Some compromises might be made to provide some, but not all, of the frequency coverage, such as placing a number (say N) of linear arrays equally spaced in the plane, with a consequent reduction in Doppler search time by a factor N.

2.3 Ambiguity Function Processing.

When a correlation is performed, for example, between an unknown signal and a hypothesized signal, the frequency of the unknown signal must be known to an accuracy of at least the reciprocal of the correlation integration time. If it is not, a search through frequency is required. Cross-correlation between a received signal and a multipath component also requires a search through frequency if the relative Doppler shift is not known to the required accuracy. Ambiguity function processors permit simultaneous correlations to be performed between a signal of unknown frequency and a signal with many hypothesized frequencies.

Below we discuss several types of ambiguity functions that promise to be of value in substantially reducing processing time in applications requiring search through delay and Doppler.

2.3.1 Triple Product Ambiguity Processor.

Any processor that generates the triple product integral can be used for ambiguity processing by making one input a chirp and premultiplying one of the signal inputs with the same chirp. For reasons discussed above and in earlier reports, time-integrating processors have some disadvantages compared with space/time integrating hybrid techniques. A difficulty with a wideband ambiguity processor using time integration is that a wideband highly linear chirp is required, if a triple product processor is used directly, or else the processor must be reconfigured to use a narrower bandwidth Bragg cell with which one could use a digitally generated chirp.

Wideband analog chirps can be generated with a VCO, for example, but the linearity of such a device, even with the most sophisticated linearization techniques presently available, is not nearly adequate. Highly linear surface acoustic wave (SAW) devices with wide bandwidths are becoming available (see Section 3). These suffer the severe disadvantages, however, of having a fixed delay and bandwidth and cannot be fabricated with the very large chirp time-bandwidth product required for high Doppler resolution.

2.3.2 One-Dimensional Space Integrating Processor.

An extension of the one-dimensional space-integrating correlator can be configured to permit parallel frequency search. Figure 2-4 illustrates a correlator that performs parallel frequency testing. Coherent light diffracted from a Bragg cell driven by $S_1(t)$ is imaged onto a second cell driven by $S_2(-t)$ so that the signals are counterpropagating. The light diffracted from the second cell is optically Fourier transformed onto an array of photodiodes with parallel outputs. The optical power density in the array plane is

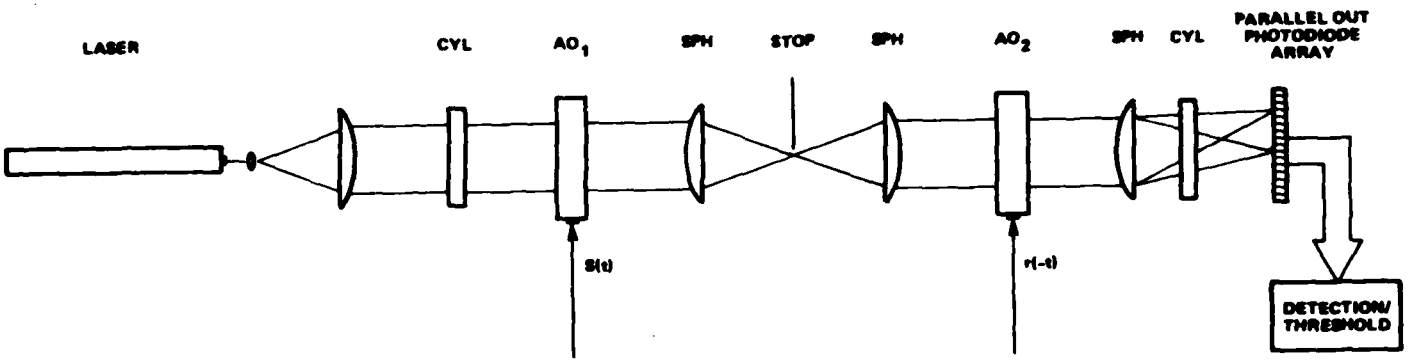

Figure 2-4. Space-Integrating Ambiguity Function Processor.

2.3.2 -- Continued

$$I(t) = \left| \int_0^T S_1(t-\tau) S_2^*(-t-\tau) e^{j2\pi f_d t} \right|^2 \qquad (2\text{-}32)$$

$$= |\hat{x}_{12}(f,t)|^2 \quad .$$

The detector array senses the absolute sqare of the ambiguity function, where time is the correlation axis and position in the diode array is the frequency axis. Since there is no time-integration processing, this technique is only useful when the processing gain equal to the time bandwidth product of the Bragg cells is sufficient. In such cases this device could be a valuable tool for very rapid search, since ambiguity surfaces can be generated at very high rates due to the channelization in frequency. Note that for a signal bandwidth B = 200 MHz, for example, with a signal length T = 20 μs, a Bragg cell bandwidth of 400 MHz and time-bandwidth product of 500, a search of 10^5 ambiguity surfaces per second results, each surface containing 8×10^5 delay-frequency elements. The surfaces would be detected by a linear array of 250 photodiodes, each with a 200 MHz video bandwidth.

For applications requiring only threshold detection, post-detection processing architectures can be several levels of complexity. The technique providing the highest degree of sensitivity is to implement a synchronous video integrator on each channel, thus noncoherently adding successive ambiguity planes. This post-detection integration generates further processing gain over and above that provided by the coherent space integration. The size, speed, versatility and quantity of these channel processors make this approach presently impractical. A realistic approach is to threshold each channel and process threshold crossings to detect signals while minimizing errors. The probability of false alarm (P_{fa}) is a function of the threshold level, which affects sensitivity. In the above example a threshold-to-noise ratio of 12 dB

2.3.2 -- Continued

(corresponding to $P_{fa} = 2.5 \times 10^{-7}$ for each delay bin) provides a P_{fa} of 10^{-3} over a 4000 bin delay range. If each frequency channel is revisited for confirmation the net P_{fa} is 10^{-6} for each frequency channel over 20 μs, or one confirmed error every 20 seconds. The same false alarm rate can be achieved with a 5 dB threshold-to-noise ratio if each delay bin of each frequency channel can be tested for confirmation. The detailed behavior and requirements for various post-process schemes (including channel integration of threshold crossings) need to be determined.

In an alternate arrangement, the second Bragg cell, driven by a digitally stored and time-reversed signal, is narrower bandwidth but with larger delay than the first cell, driven by a wideband signal. The imaging optics provides a magnification equal to the ratio B_2V_1/B_1V_2 where B_1 and V_1 are the signal bandwidths and acoustic velocity of the first cell, etc. This alternate scheme reduces the processing rate by a factor of about 2, but has the advantage of greatly reducing the bandwidth requirement for the memory feeding the second cell. For a system composed of a $PbMoO_4$ and a $(TeO_2)_s$ Bragg cell, the memory speed requirement is reduced from 200 Msamples/s to 20 Msamples/s, as compared with a system containing two PbMoOy cells.

3. IMPLEMENTATIONS.

A consideration of some practical limitations and constraints for A-O processors and some experimental measures of performance were made to evaluate to some degree the realizability of high performance systems based on the concepts developed during the first two phases of this effort. The experimental efforts included a laboratory bench version of a coherent hybrid space/time integrating spectrum analyzer and a packaged brassboard noncoherent two-dimensional ambiguity function processor.

3.1 Space/Time Integrating Spectrum Analyzer.

An experimental configuration of the one-dimensional coherent hybrid spectrum analyzer of Figure 3-1 was implemented. The intent was to present an uncomplicated and straightforward illustration of the concept discussed in detail in the Annual Technical Report of 1980. The parameters of the experiment were chosen to provide such an illustration with devices and components immediately available to us, and no attempt was made to maximize those parameters, such as bandwidth and time-bandwidth product, that would otherwise be important in the design of a high performance system.

The optoelectronic devices used in the experiment were a 5 mW fundamental transverse mode HeNe laser, two slow shear mode TeO_2 Bragg cells and a Reticon CCPD1024 charge coupled photodiode array. The portions of the bandwidth and time delay of the Bragg cells that were utilized in the experiment were, respectively, 5.3 MHz and 6 μs.

3.1.1 Chirp Spatially Distributed Local Oscillators.

One of the Bragg cells in this interferometric system is driven by a reference signal that contains all the frequencies in the analysis band, in order to generate a coherent optical reference wave

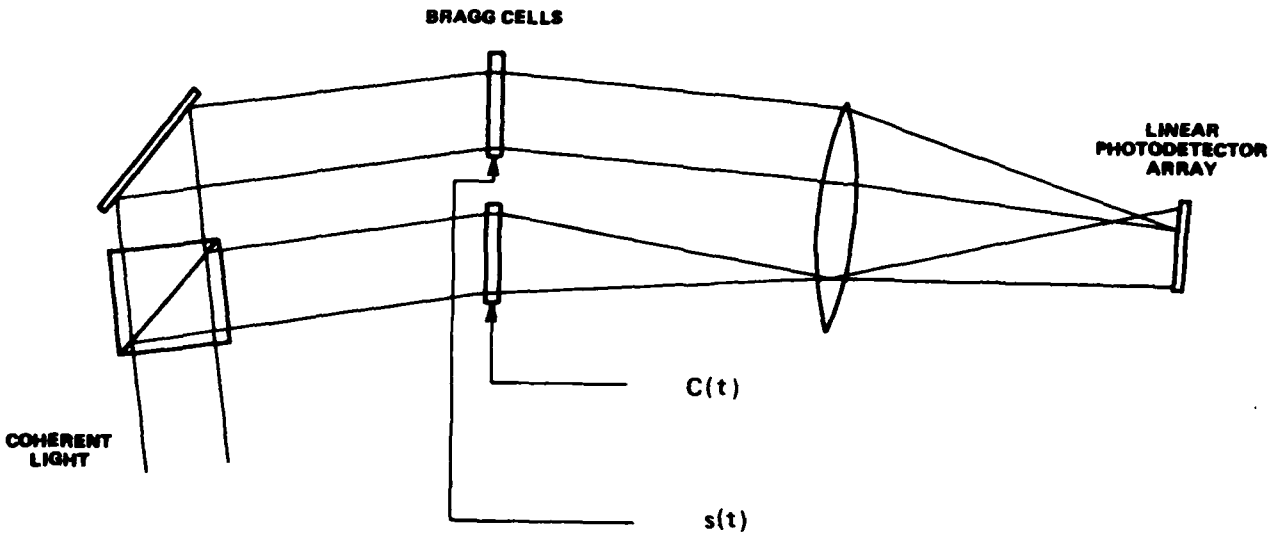

Figure 3-1. One Dimensional Coherent Hybrid Spectrum Analyzer.

3.1.1 -- Continued

to interfere with the signal optical wave at the detector. It is desired that this reference have a uniform power density across the band. The reference waveform used in these experiments was a periodic chirp, generated digitally, with a variable bandwidth (up to about 20 MHz) and a variable chirp time. The chirp time was set a 6 μs. The baseband chirp was mixed single sideband with a 50 MHz local oscillator as the reference waveform driving the Bragg cell. The optical power spectra of chirps with bandwidths 5.3 MHz, 10.6 MHz and 21.2 MHz are shown in Figure 3-2 as detected by the CCD photodiode array. These exhibit the familiar Fresnel ringing pattern that is most pronounced for small time bandwidth products (BT). For comparison, Figure 3-3 shows the calculated moduli of the Fourier transforms of chirps with BT values of 20, 21, 100 and 300. Note that the details of the ringing structure are very sensitive to BT, as evidenced by the patterns for BT = 20 and BT = 21. The power spectrum of a chirp in practice may be degraded by amplitude and phase errors in the chirp temporal waveform. These types of errors are usually negligible for digitally generated chirps. Achievable bandwidths, however, are limited by the rise-time limitations of digital systems. A voltage controlled oscillator (VCO) can produce very wide band chirps, but linearity problems are severe and chirp-to-chirp coherence (a necessity for these applications) is extremely difficult to achieve. Surface acoustic wave (SAW) linear dispersive filters are approaching adequate amplitude and phase behavior and are highly periodic (chirp-to-chirp coherent), controlled by the timing of the RF pulses feeding the filter. Figure 3-4a shows the spectrum (using an HP spectrum analyzer) of a RAC SAW filter of 500 MHz bandwidth and 0.5 μs dispersive delay. Figure 3-4b shows a portion of the spectrum at an expanded scale; the comb structure illustrates the periodic nature of the chirp (chirps were made contiguous with an 0.5 μs period).

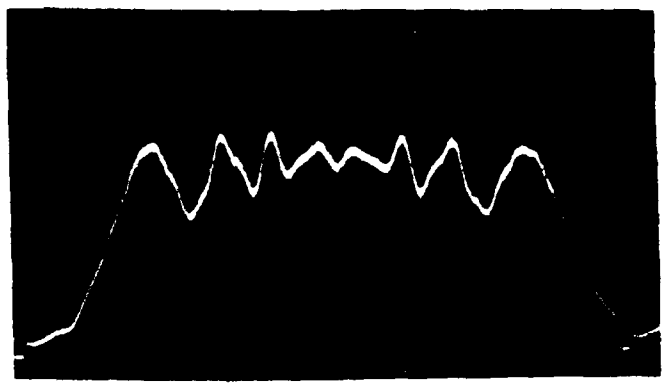

BT = 32

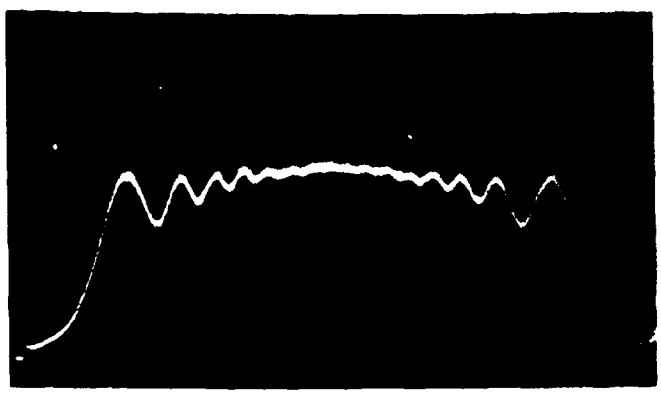

BT = 64

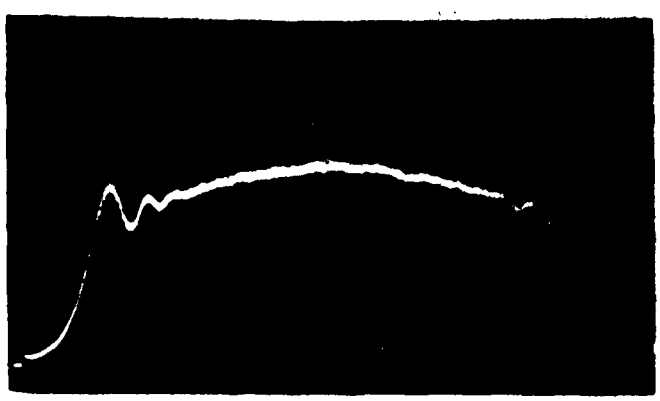

BT = 128

Figure 3-2. Acousto-Optic Measuremnt of Power Spectrum of Digitally Generated Chirps.

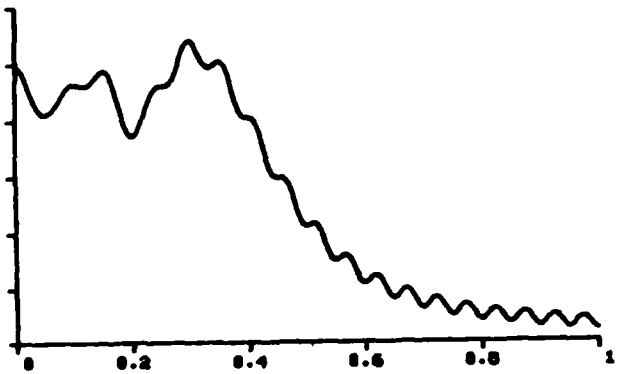

BT = 20

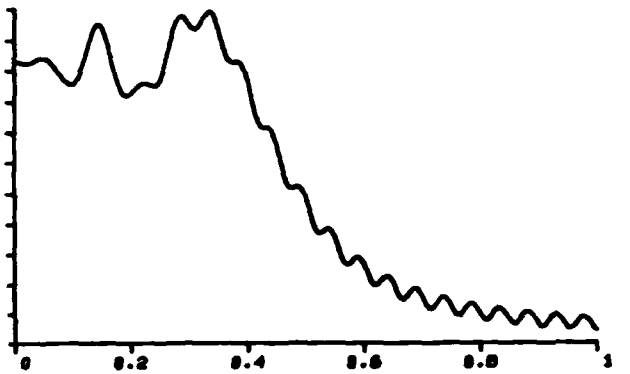

BT = 21

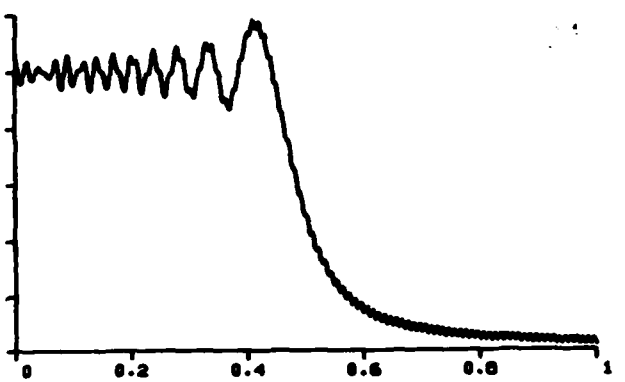

BT = 100

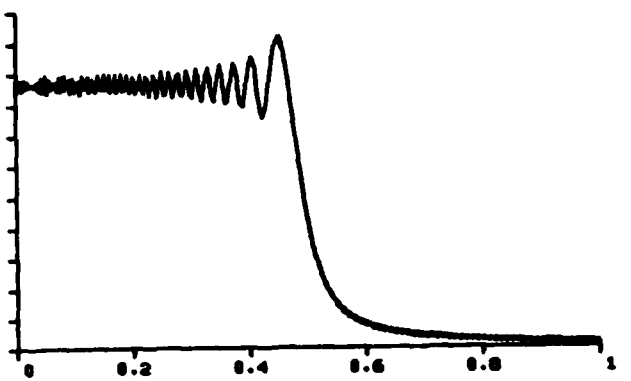

BT = 300

Figure 3-3. Calculated Modulus of the Fourier Transform of a Chirp.

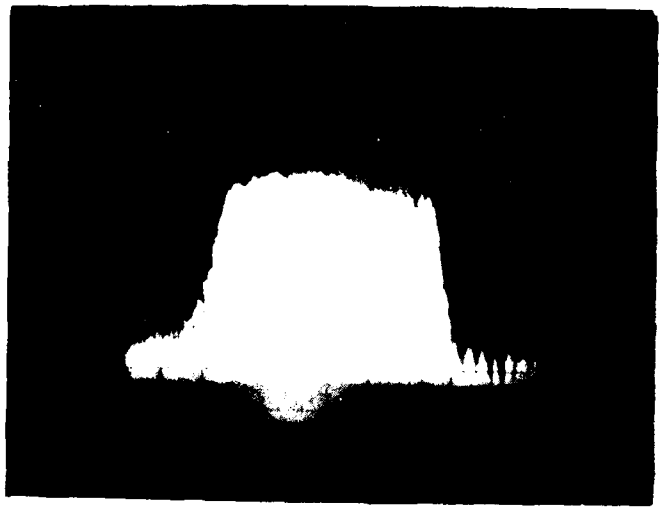

a) Horizontal Scale: 100 MHz/div.
Vertical Scale : 10 dB/div.

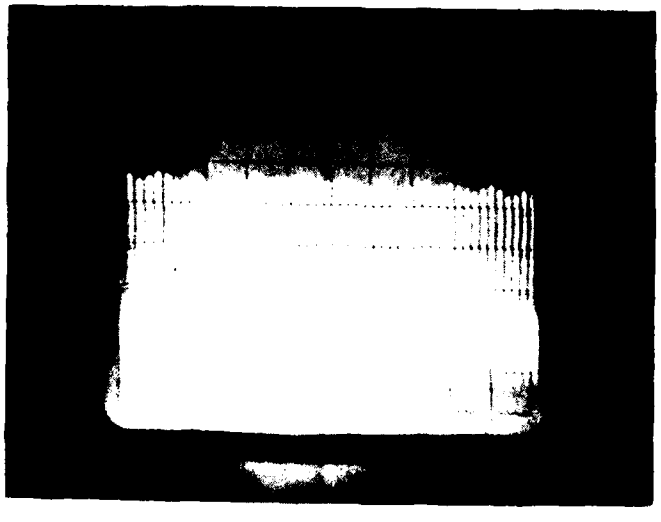

b) Horizontal Scale: 10 MHz/div.
Vertical Scale : 10 dB/div.

Figure 3-4. Spectrum of a SAW Dispersive Filter.

3.1.2 Experimental Results.

For the spectrum analyzer experiment a 0-5.3 MHz chirp was generated digitally in 6 μs and mixed single sideband with a 50 MHz local oscillator as the reference waveform driving one Bragg cell. The other Bragg cell was driven by a single tone within the analysis band (~50-55.3 MHz). Figure 3-5 shows the integrated intensity in the detector plane, as reflected in the serially addressed output of the photodiode array. Figure 3-5a shows the bias over the band due to the Fourier transformed chirp reference and the localized interference fringe pattern on an additional localized bias generated by the pure tone signal. In this experiment BT = 32, so that the chirp spectrum nonuniformity is quite pronounced. Nevertheless, the spatial frequency content is near spatial baseband. Highpass filtering of the output shown in Figure 3-5a results in the signal shown in Figure 3-5b, where the reference bias structure and that due to the signal have been removed.

The Reticon CCPD1024 integrates the incident optical power density for 250 μs, about the shortest time in which the CCD register can transfer the 1024 charge elements. Since the Bragg cell delay and chirp period are 6 μs, we are integrating by a factor of 42 longer than prescribed. The effects of such a long exposure is to introduce a frequency comb filter. The teeth of the comb response are separated by $1/T$ = 167 kHz and the width of a tooth is $1/T^1$ = 4 kHz, which was observed. When the frequency is tuned to a peak, the intensity integrated for T^1 is (T^1/T) times the intensity integrated for time T.

The 1980 Annual Technical Report presented an analysis of the dynamic range characteristics of direct detection and interferometric detection, demonstrating the advantages of the latter. Figure 3-6 shows a comparison of the measured detector outputs for direct detection and for interferometric detection. For Figure 3-6a the reference path is blocked so that only the light diffracted from the

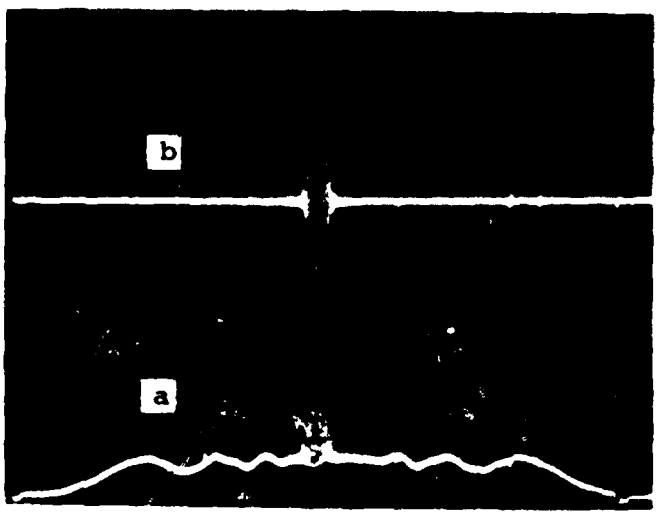

Figure 3-5. Signal Plus Reference Spectrum and High Pass Filtered Version.

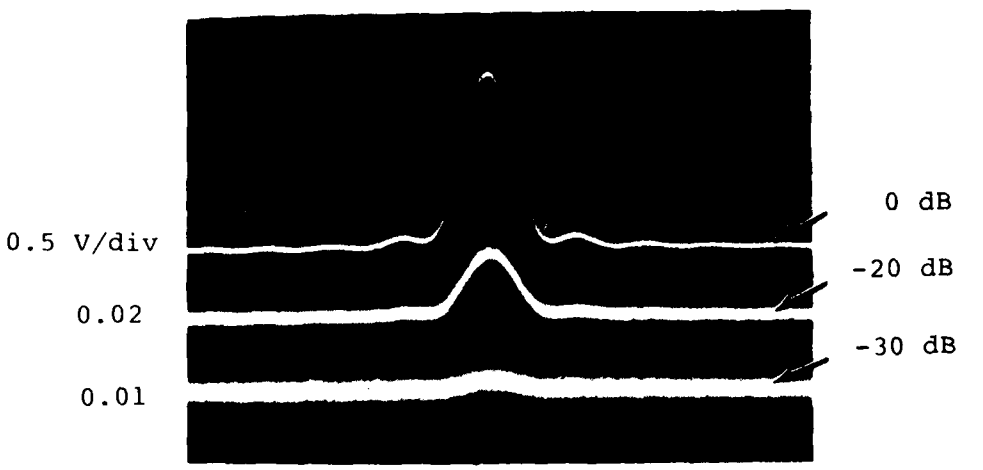

(A) DIRECT DETECTION

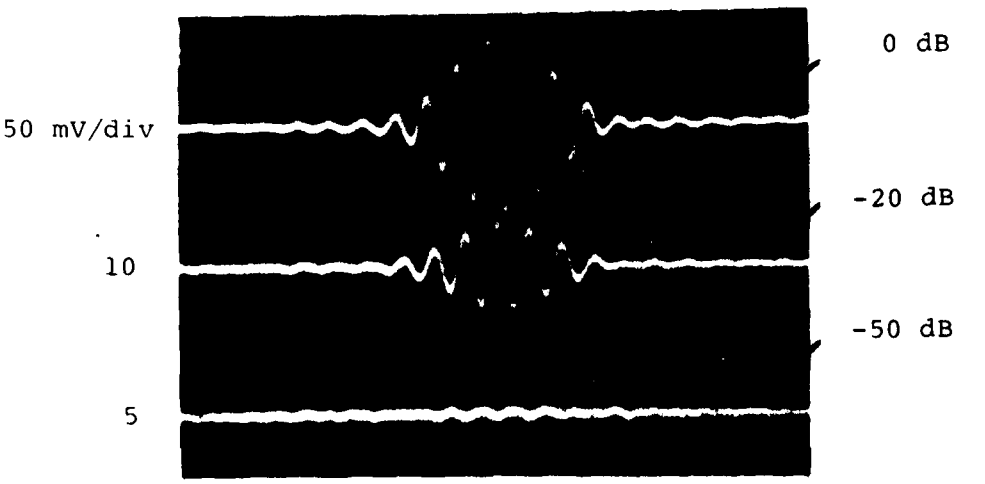

(B) INTERFEROMETRIC DETECTION

Figure 3-6. Dynamic Range Comparison.

3.1.2 -- Continued

signal Bragg cell illuminates the detector. The top trace corresponds to a signal level that just saturates the detector and the lower traces correspond to 20 dB and 30 dB attenuation of the signal. These traces were obtained with two forms of noise reduction; a single frame of the detector output in the absence of a signal was subtracted from the detector output in the presence of the signal, and the result was passed through a lowpass filter. The background subtraction served to reduce the effects of diode-to-diode nonuniformities in dark current, and the lowpass filter constrained the detector noise bandwidth to the signal bandwidth. Figure 3-6b shows the results when the reference wave was added. Background subtraction and bandpass filtering were performed. A signal is seen to be still detectable when it is 50 dB below the maximum signal (upper trace) for interferometric detection, compared with a barely detectable signal 30 dB down for direct detection.

The spectral line shape for interferometric detection is shown in Figure 3-7. Figure 3-7a was obtained by interfering the signal spectral line with a reference wave that was generated by driving the reference Bragg cell with the same signal tone and spreading the diffracted light uniformly over detector. The reference wave has, therefore, a Doppler frequency shift that is independent of position. The interference pattern has approximately a sine envelope, following the shape of the spectral amplitude of the signal, a result of the spatially integrated Fourier transform. This would also result from a snapshot exposure when the reference wave is not the same frequency as the signal. A purely time integrating spectrum analyzer exhibits the same spectral line shape, a result of integration over the exposure time window. Figure 3-7a illustrates the resulting line shape with the hybrid space/time integrating technique. The rapidly decaying sidelobes are evident. This data demonstrates the characteristics derived theoretically that the sidelobes for a coherent hybrid spectrum analyzer are lower by a factor of two in dB compared with a purely space-integrating system, whether the latter is interferometric or square-law.

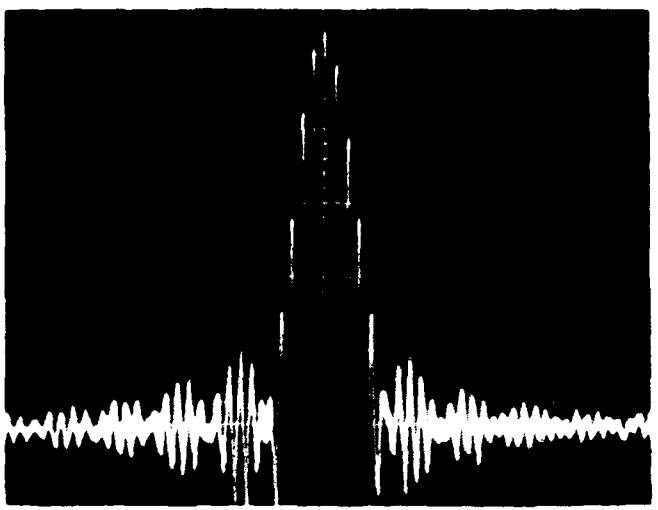

(A) TIME INTEGRATING OR INTERFEROMETRIC SPACE INTEGRATING

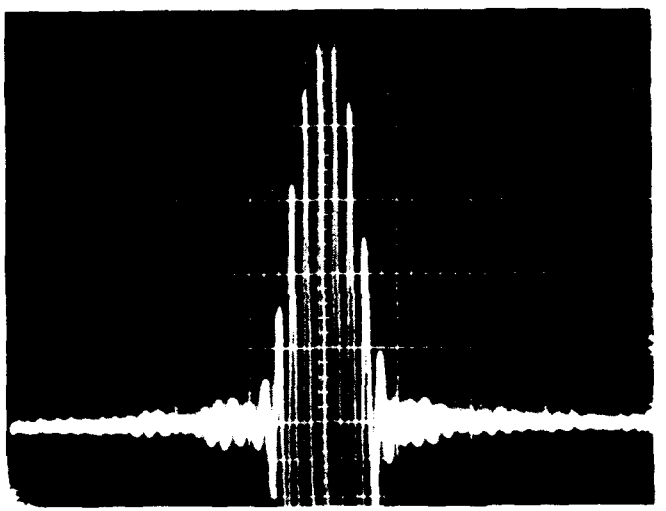

(B) HYBRID SPACE/TIME INTEGRATING

Figure 3-7. Spectral Side Sidelobe Comparison.

3.2 Performance Evaluation of a Time Integrating A-O Processor.

A two dimensional implementation of a time integrating acousto-optic signal processor, configured to compute the cross ambiguity function, has been quantitatively evaluated in a limited series of tests. Although the tests are limited in scope, the results provide significant insights into the performance limitations and capabilities of a real implementation. The performance results are compared with those of an ideal cross-correlation processor.

3.2.1 Ambiguity Function Processor Description.

The ambiguity function processor is based on a time integrating acousto-optic signal processing architecture developed at ESL. Time integrating acousto-optic processors realize flexible, multi-purpose complex signal processing architectures based on correlation algorithms. Interest in time integrating techniques is due to the attractive device technology as well as flexibility in time integrating algorithms. An important consequence of time integrating techniques is the ability to operate on signals with very large time-bandwidth without having to store the entire time history as a spatial record. Therefore, an important class of two-dimentional and multi-channel algorithms may be performed without requiring two-dimensional spatial light modulators. Acousto-optic devices and charge coupled image sensors are particularly well suited for time integrating processor implementation. Further, these signal processing techniques may be realized with either coherent or non-coherent optical systems.

The theory of operation is summarized in the following section. For more detailed explanation of time integrating techniques, refer to the earlier reports (Time Integrating Optical Signal Processing, Annual Technical Report, 1 August 1978-31 July 1979, Contract F49620-78-C-0102 and Interim Report on Time Integrating Signal Processing, September 1980, Contract F49620-78-C-0102).

3.2.1.1 Theory of Operation.

Two-dimensional integral transforms, for which the kernel is decomposable in the proper way, may be implemented by time integrating optical processing. An important example is ambiguity function processing. Consider the optical realization shown conceptually in Figure 3-8. The optical train has a modulated illumination source, two acoustic delay line light modulators, and a matrix array of detectors. This configuration may be employed for several functions, determined by input signal and reference waveforms.

The light diffracted by the first acousto-optic modulator A01, is diffracted by the second, A02, in an orthogonal direction. Both acoustic signals are imaged on the detector plane. The desired image plane intensity distribution has a term proportional to the product of acoustic signals, $s_1(t-\tau_1)s_2(t-\tau_2)$, where $\tau_1 = y/v$ and $\tau_2 = x/v$ are time variables. The resultant detected output voltage is proportional to the integrated charge. This structure implements integrals of the form:

$$R(\tau_1,\tau_2) = \int_T s_0(t)s_1(t-\tau_1)s_2(t-\tau_2)dt$$

In this configuration, all signals are real. In order to perform complex computation, the real and imaginary components are used to modulate a carrier in quadrature.

The cross ambiguity function may be implemented using the two-dimensional optical system shown in Figure 3-8. The cross ambiguity function between complex signals x(t) and y(t) may be defined as

$$A_{xy}(\tau,f) = \int_0^T x(t)y^*(t-\tau)e^{-j2\pi ft}dt$$

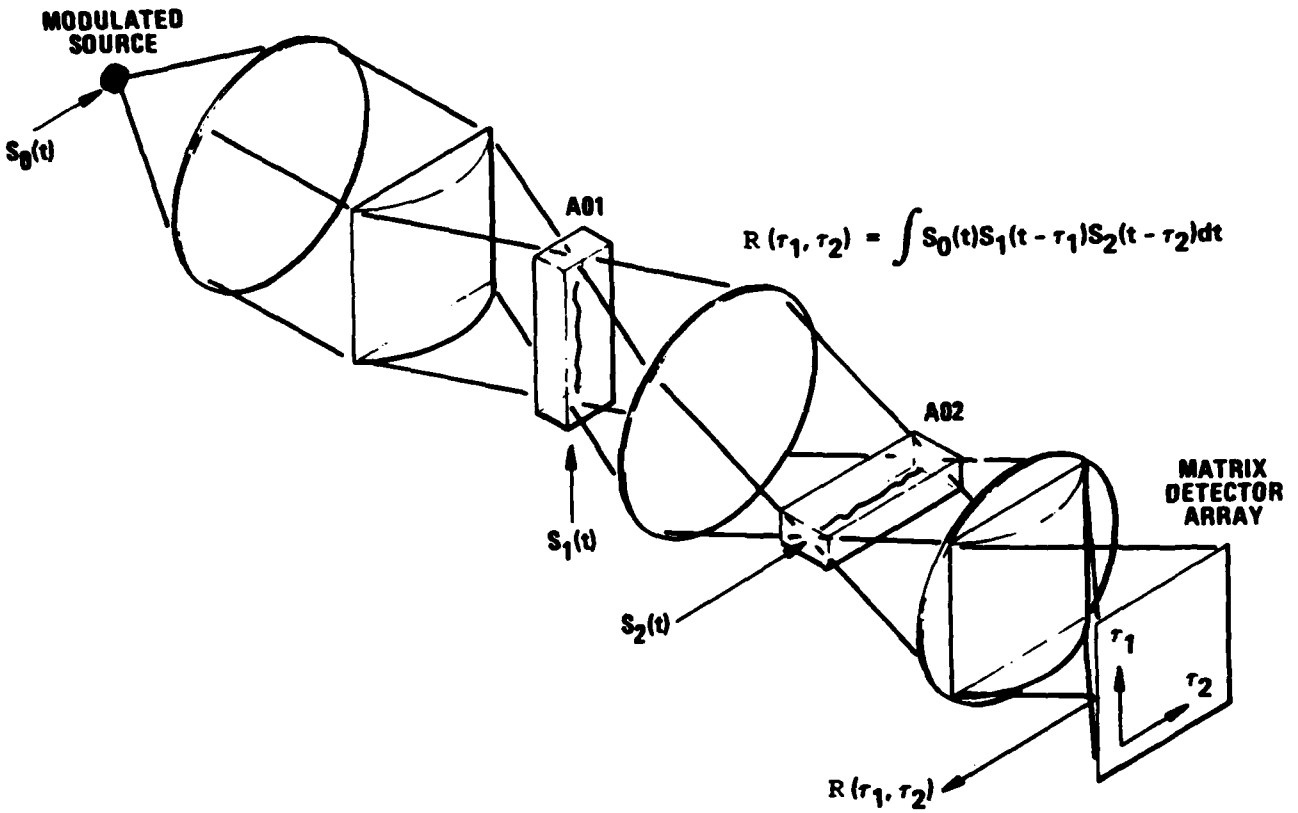

Figure 3-8. Two-Dimensional Time Integrating Processor with Modulated Diode Source.

3.2.1.1 -- Continued

where the variables τ and f may be interpreted as delay and Doppler, respectively. The spectral analysis operation is performed using the chirp algorithm. Define the complex input signals $s_0(t)$, $s_1(t)$, and $s_2(t)$ by

$$s_0(t) = x(t)e^{-i\alpha\pi t^2}$$

$$s_1(t) = y^*(t)$$

$$s_2(t) = e^{i\alpha\pi t^2} \quad .$$

The output is given by

$$R(\tau_1,\tau_2) = \int x(t)e^{-i\alpha\pi t^2} y^*(t-\tau_1)e^{i\alpha\pi(t-\tau_2)^2} dt$$

$$= e^{i\alpha\pi\tau_2^2}\int x(t)y^*(t-\tau_1)e^{-i2\pi\alpha t\tau_2}dt$$

$$= A_{xy}(\tau_1,\alpha\tau_2)e^{i\alpha\pi\tau_2^2} \quad .$$

The quadratic phase term may be ignored if magnitude square calculation is desired. The variables τ_1 and τ_2 correspond to delay and Doppler, respectively. The Doppler resolution is commensurate with the integration time; the analysis bandwidth is determined by the chirp bandwidth and acoustic delay. A coarse resolution may be maintained during a signal acquisition period, and a higher resolution zoom can be achieved by longer integration. Multiple correlation peaks or targets can be processed simultaneously since a linear system implementation is used.

3.2.1.2 Acousto-Optic Subsystem.

The time integrating signal processor has been implemented with a non-coherent optical system using a diode source as shown in Figure 3-8. Devices include a Hitachi HLP-40 light emitting diode, Fairchild CCD221 charge coupled image sensor, and Isomet acousto-optic devices. The diode has a 30 MHz 3-dB bandwidth and is biased at an average optical power of approximately 20 mW. The image sensor has 488 x 380 elements and is operated with an integration period of 33.33 msec (30 frames per second). The acousto-optic device have a 30 MHz 1-db bandwidth and both use a delay range of approximately 20 μsec.

In order to realize complex computation with real input modulation, the complex signals modulate a local oscillator in quadrature. An interferometric technique with electronic reference is used. The diode is internally modulated with a current driver (at a carrier), and the acoustic devices are modulated at a carrier with a summed reference oscillator. The analog signal processor requires three inputs: input signal 1 multiplied by a chirp waveform, input signal 2, and the reference chirp waveform. The required frequency translations and chirp multiplication are performed in an analog frequency translation unit. The three inputs have the form

$$\text{Re}\left\{ x(t) e^{i(2\pi f_o t - \alpha\pi t^2)} \right\}$$

$$\text{Re}\left\{ y(t) e^{i2\pi f_1 t} \right\}$$

$$\text{Re}\left\{ e^{-i(2\pi f_2 t - \alpha\pi t^2)} \right\}$$

where x(t) and y(t) are the complex input time series, f_o, f_1, and f_2 denote carrier frequencies, and α is the chirp rate.

3.2.1.3 Bias Elimination.

An optical bias results due to the use of intensity modulation. Filtering or subtraction may be used to eliminate the bias. The use of intensity modulation offers a number of advantages in comparison with coherent systems including compact non-coherent optical system realization and increased immunity to artifact noise. Through interferometric detection and complex demodulation, the complex ambiguity function may be computed. In the current unit a bias subtraction scheme is employed, though other techniques may be implemented. The bias subtraction method utilizes two consecutive ambiguity functions where the second calculation has effectively the opposite polarity. That is to say, the first frame consists of the bias plus signal and the second consists of bias minus signal. The two frames are subtracted yielding twice the signal. The throughput rate is decreased by a factor of 2. However, if filtering were used, the bias could be eliminated with a single frame. The bias elimination is performed digitally in a high-speed memory (the DeAnza System IP5000).

The technique that has been implemented to provide two sequential frames -- one representing bias plus the real part of the complex ambiguity function and one representing bias minus the real part of the complex ambiguity function -- is suboptimum. The technique provides an average signal phase difference of 180° between sequential frames (thus allowing bias removal by subtraction) by allowing a differential carrier phase drift rate that is matched to the processor framing rate. Although this implementation provides the desired bias elimination, it uses phase averaging over 180° for each frame to achieve the phase differences of 180° over sequential frames. Analysis has shown that there is a minimum loss of 3.25 dB processing gain as a consequence of this technique. This loss may be easily recovered by using a relatively simple phase switching approach. As a consequence, effective processing gain as measured in the quantitative performance tests were at least 3.25 dB lower than they need to be.

3.2.2 Quantitative Processor Evaluation.

Quantitative evaluation of the A-O processor operating as a gated cross-correlator has been performed by considering processing results from two distinctly different points of view. Both of the approaches consider the dual hypothesis detection process associated with the detection of a peak in the ambiguity plane. The first approach is based on the assumption that the underlying statistics of the detection random variables are unknown and it is necessary to develop the comparison with an ideal processor through measured probability of detection, P_d, and probability of false alarm, P_{fa}, characteristics. In the second approach, the underlying statistics of the detection process are hypothesized (and tested to a limited extent) and measured processor output SNR values are compared with those of an ideal correlator.

3.2.2.1 Test Conditions.

The quantitative tests on the A-O processor all used simulated signals with additive Gaussian noise. The signals of interest have been simulated as a repetitive pulse train with a multipath delay of nominally 25 μs and with PRI variation between 19 μs and 312 μs. The pulse width has been fixed at 1 μs. The input signal-to-noise ratios (both direct signal and multipath) are specified as the ratio of peak signal power (power measured during the 1 μs pulse) to the equivalent noise power measured in a 1-MHz bandwidth. The pre-D bandwidth for the composite signal plus noise was varied from 300 kHz to 1 MHz.

Gated correlation processing was used on all of the tests. The gate was derived from the noisy signal in much the same way in which the process might be automated in a real multipath processing configuration. Specifically the noisy pre-D signal is AM detected and passed to a recursive synchronous video integrator (SVI) that has a length corresponding to the PRI of the desired signal (assumed known *a'priori*).

3.2.2.1 -- Continued

The output of the SVI is reconstructed through a signal synchronizer to provide a repetitive gate signal that is centered on the direct signal and has a width on the order of 2 μs. The width of the gate may be varied to approximately match the signal that has passed through a pre-D filter. The gate signal as well as the pre-D input signal that is used to modulate the LED in the ambiguity function processor are digitally delayed by a pre-computational delay unit that, by adjustment, provides the means to select the delay range to be processed in the ambiguity function processor. That is, the delay window of approximately 20 μs can be centered on any particular delay value by adjustment of the pre-computational delay.

A block diagram of the experimental configuration is shown in Figure 3-9. The ambiguity function processor in this case includes a digital chirp generator, a frequency translation unit, the A-O triple product processor, a camera control unit, and a special purpose digital image processor. The Doppler window is centered on the desired range (positive or negative) by simply tuning the frequency synthesizer. The range of Doppler that is processed is selected by choosing the chirp rate. For the tests that are reported here, the Doppler range is approximately 1.1 kHz.

3.2.2.2 Data Collection.

For each set of conditions a block of data is collected so that subsequent analysis can provide as complete a picture as possible of the processor performance. The processor is set up with controlled and known conditions. These include signal properties such as RFI, pulse width, direct path and multipath SNR's. Processor parameters such as pre-D filtering bandwidth, gate width, Doppler and delay offset, and Doppler range are also established. For each of these fixed conditions, a large sequence of processing runs (generally on the order of 1000, however some at 10,000) are performed to measure the statistical

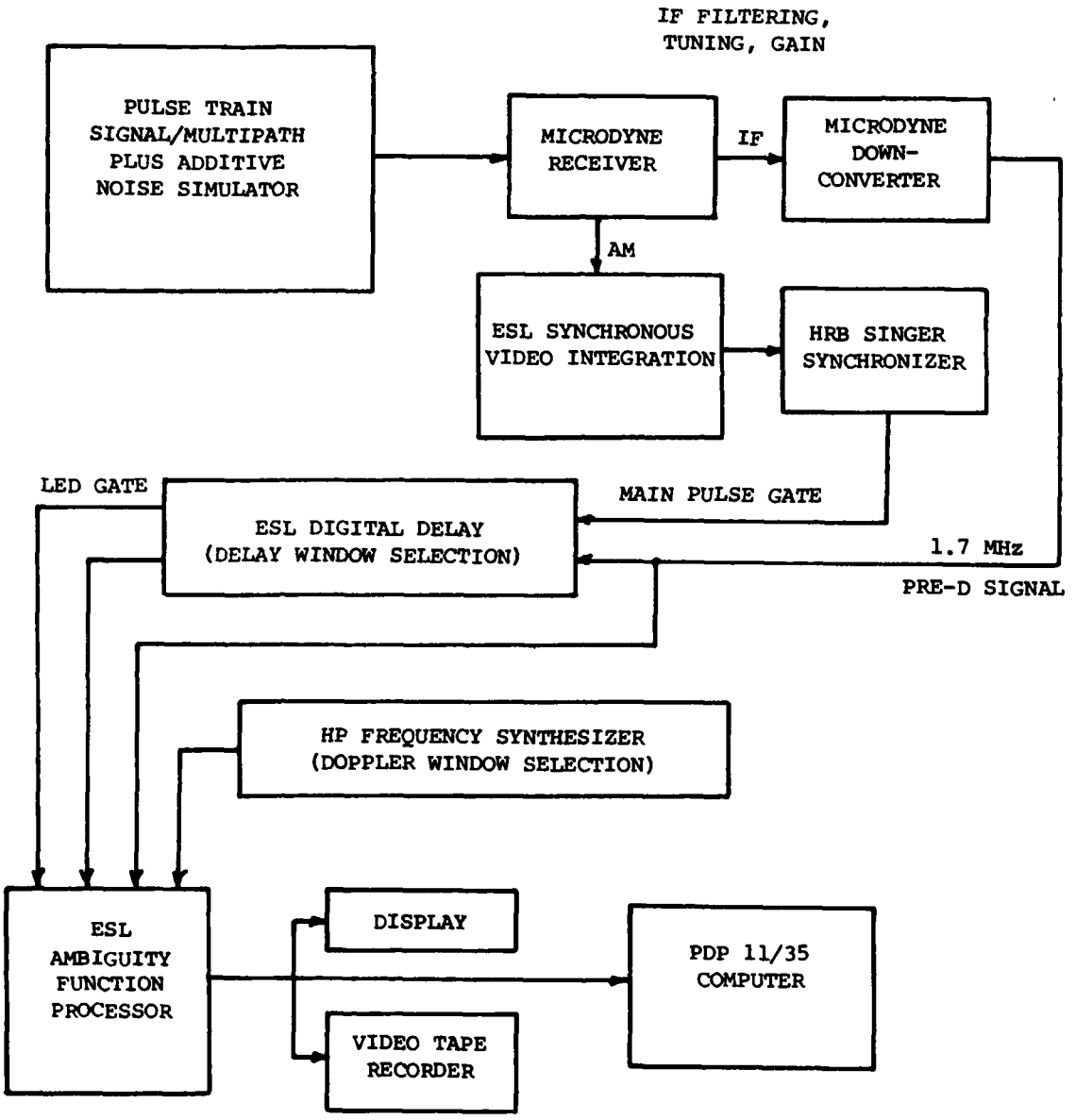

Figure 3-9. Experimental Configuration for Repetitive Pulse Signal Multipath Processing.

3.2.2.2 -- Continued

properties of the ambiguity function envelope in the noise region and in the signal peak region. The properties include the mean, the standard deviation and the cumulative distribution function. The number of points used for the noise only, and signal plus noise CDFs were 10,000 and 1,000 respectively. At a selected threshold value, the P_{fa} is given by one minus the noise only CDF value and P_d is given by one minus the signal plus noise value. As an example from the table, a threshold number of 108 corresponds to a P_{fa} of 10^{-2} and a P_d of 0.39. The additional statistics, mean and standard deviation, are useful in the performance analysis in a way that will be described.

3.2.2.3 Processor Analysis Based on P_{fa} and P_d.

As has been described in the preceeding section, the CDFs of the linearly detected envelope at the peak of the cross ambiguity function and in a "noise only" region of the ambiguity function plane have been measured for various input signal conditions. By varying the threshold on the pair of CDFs a curve of P_d versus P_{fa} may be constructed. This type of curve is normally called a ROC curve or Receiver Operating Characteristic.

Theoretical ROC curves for a detection process based on a decision at the output of a linear envelope detector where the input is either Gaussian noise only or a sinusoid in Gaussian noise are available in the literature. Curves of this type will enable us to relate the measured P_d/P_{fa} characteristics to an equivalent input SNR for the detection of a single sinewave pulse in Gaussian noise.

Receiver operating characteristics for which values of constant SNR are straight lines have been developed by Robertson (G.H. Robertson, "Operating Characteristics for a Linear Detector of CW Signals in Narrow-Band Gaussian Noise", BSTJ, April 1967, pp 755-774).

3.2.2.3 -- Continued

An example of the set of curves is given in Figure 3-10 (from A.D. Whalen, Detection of Signals in Noise, Academic Press, New York, 1971, p. 248). Comparable data are also available in D.K. Barton, Radars, Volume 2, The Radar Equation, Artech House, Inc., 1974, p. 115.

The theoretical results represented by these curves are based on the detection of the envelope of a single pulse of sinusoid in Gaussian noise. Thus, as we superimpose the measured ROC data points, departure of the set of points from a line parallel to those for constant input SNR could be indicative of departure from the Gaussian assumption. Assuming there is nominally a straight line, the "equivalent single pulse input SNR", γ_0 may be estimated by curve matching and interpolation. Measured data values for a variety of input conditions are shown superimposed on the theoretical ROC curves in Figure 3-11.

These data may be compared with an "equivalent single phase input SNR", Γ_0, that has been derived from an analysis of an ideal gated correlator. For idealized gated correlation processing,

$$\Gamma_0 = n \frac{(SNR_1)(SNR_2)}{(SNR_1 + 1)} \quad ,$$

where SNR_1 is the direct path input SNR, SNR_2 is the multipath input SNR, gating is performed on the direct path pulses and n of these pulses are used in the processing.

The results of the data analysis are summarized in Figure 3-12. Based on this comparison, the apparent loss in processing gain relative to an ideal gated cross-correlator ranges from 10.6 dB to 16.8 dB. For these data, the largest apparent loss occurs for conditions under which the expected processing gain is largest. The possible increase in

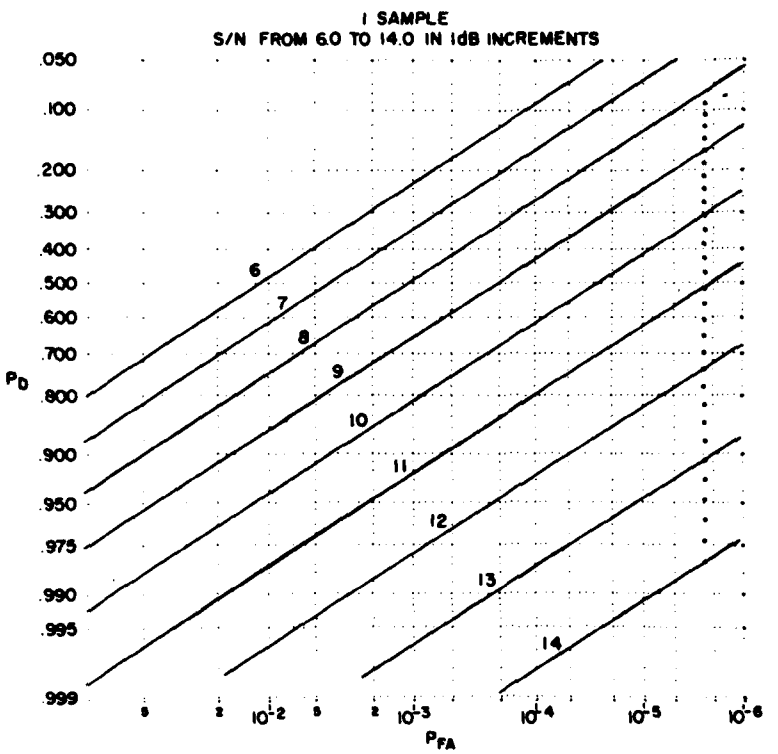

Figure 3-10. Receiver Operating Characteristic for Detecting a Single Sinewave Pulse in White Gaussian Noise.

	Input Filters	Input SNRs	
■	500 kHz	(0 dB SNR)	k = 1
●	300 kHz	(0 dB SNR)	
X	1.0 MHz	(-3 dB, 0 dB, +3 dB)	
□	500 kHz	(+6 dB/-4 dB)	k = 0.32
Δ	500 kHz	(+10 dB/0 dB)	
▽	500 kHz	(+3 dB/-7 dB)	

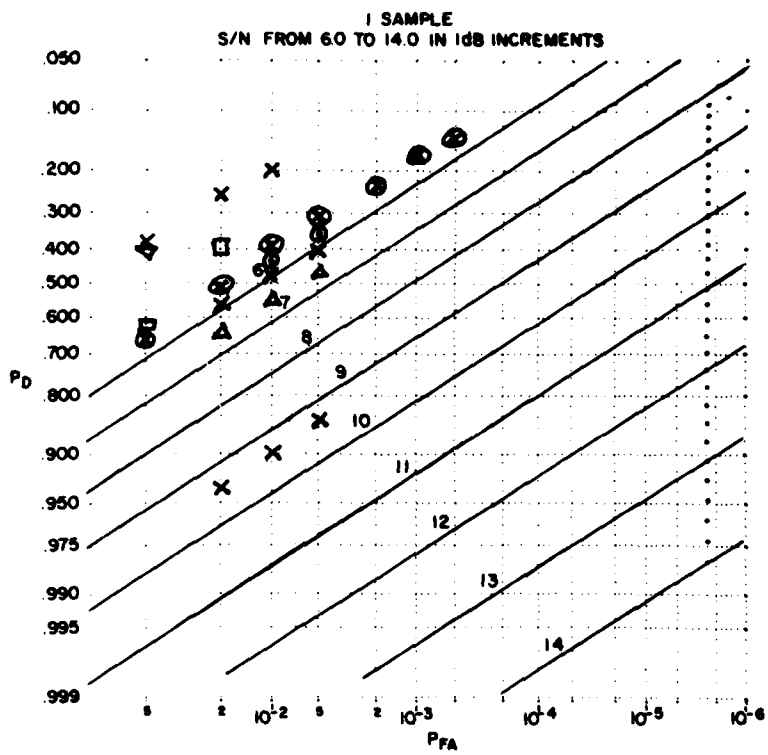

Figure 3-11. A-O Processor Test Results Plotted in Terms of Receiver Operating Characteristics (2 μsec gated processing of 300 μsec PRI input data).

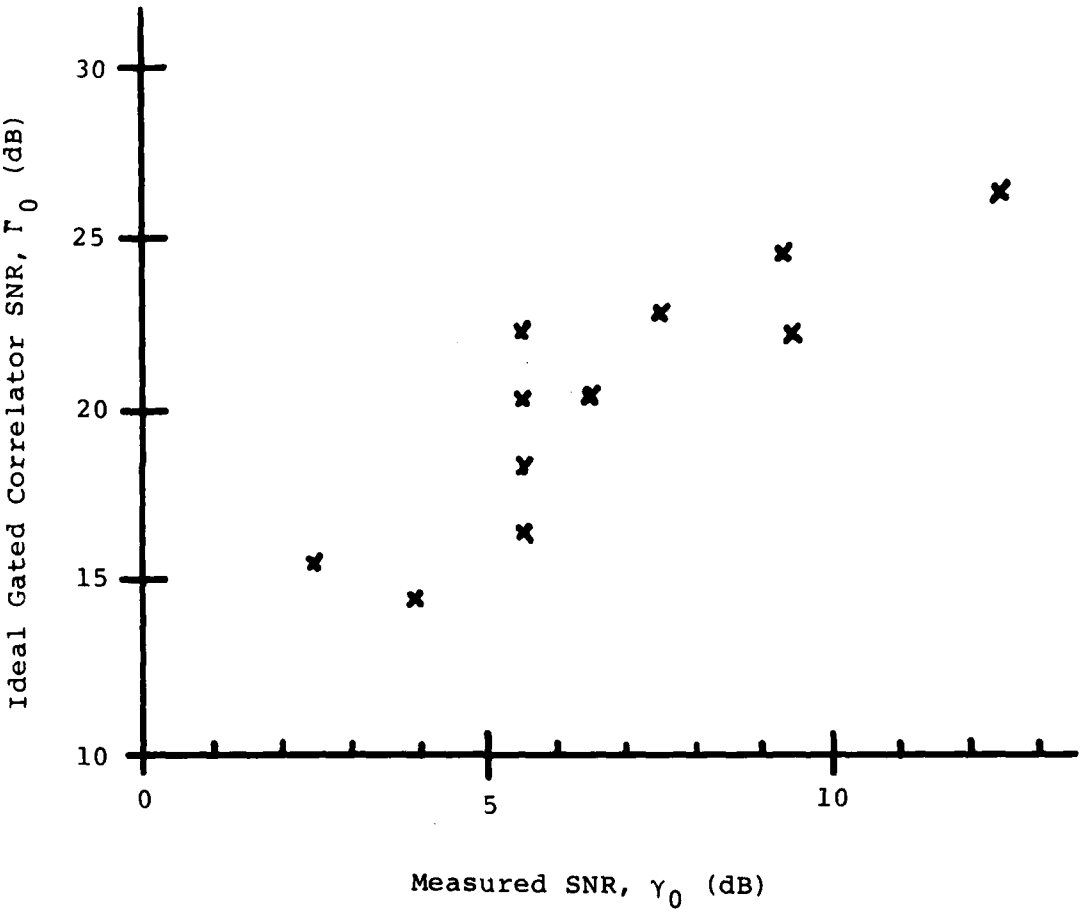

Figure 3-12. A Comparison of Processor Equivalent SNR for an Ideal Gated Cross-Correlator (Parker's Model) and Corresponding Values Derived from Measured P_d/P_{fa} Characteristics of the A-O Processor.

3.2.2.3 -- Continued

apparent loss for high processing gain (a larger number of pulses in the processing interval) will be examined further in a subsequent section.

Another possible insight into processor performance may be available by considering the apparent loss as a function of the multipath SNR. These data are shown in Figure 3-13. A straight line with a slope of 1/2 is superimposed on the data to illustrate a trend.

3.2.2.4 Detector Input Output Relationships.

The P_d/P_{fa} measurements have been used to provide an estimate of the effective SNR, γ_0, at the input to a linear envelope detector. As part of our data collection, the mean and variance of the output of the linear envelope detector have also been measured both in a noise region and at the peak of the ambiguity function. Based on the central limit theorem we might expect the random part of our ambiguity function estimate (before taking the envelope and in any region of the plane) is Gaussian. The fact that the measured ROC data points generally follow straight lines (Figure 3-11) supports a Gaussian assumption. Additional support is provided by the measured statistics. Specifically, the envelope of a zero-mean Gaussian random variable, as is expected in the "noise-only" region of the ambiguity plane, is Rayleigh and the ratio of the mean to the standard deviation is

$$\frac{\mu_n}{\sigma_n} = \frac{(\frac{\pi}{2})^{\frac{1}{2}}}{(2 - \frac{\pi}{2})^{\frac{1}{2}}} \doteq 1.913 \quad .$$

For a set of 21 measurements (each of which represents the computation of a thousand or more ambiguity surfaces), the mean of this ratio is 1.904 and the standard deviation is 0.047.

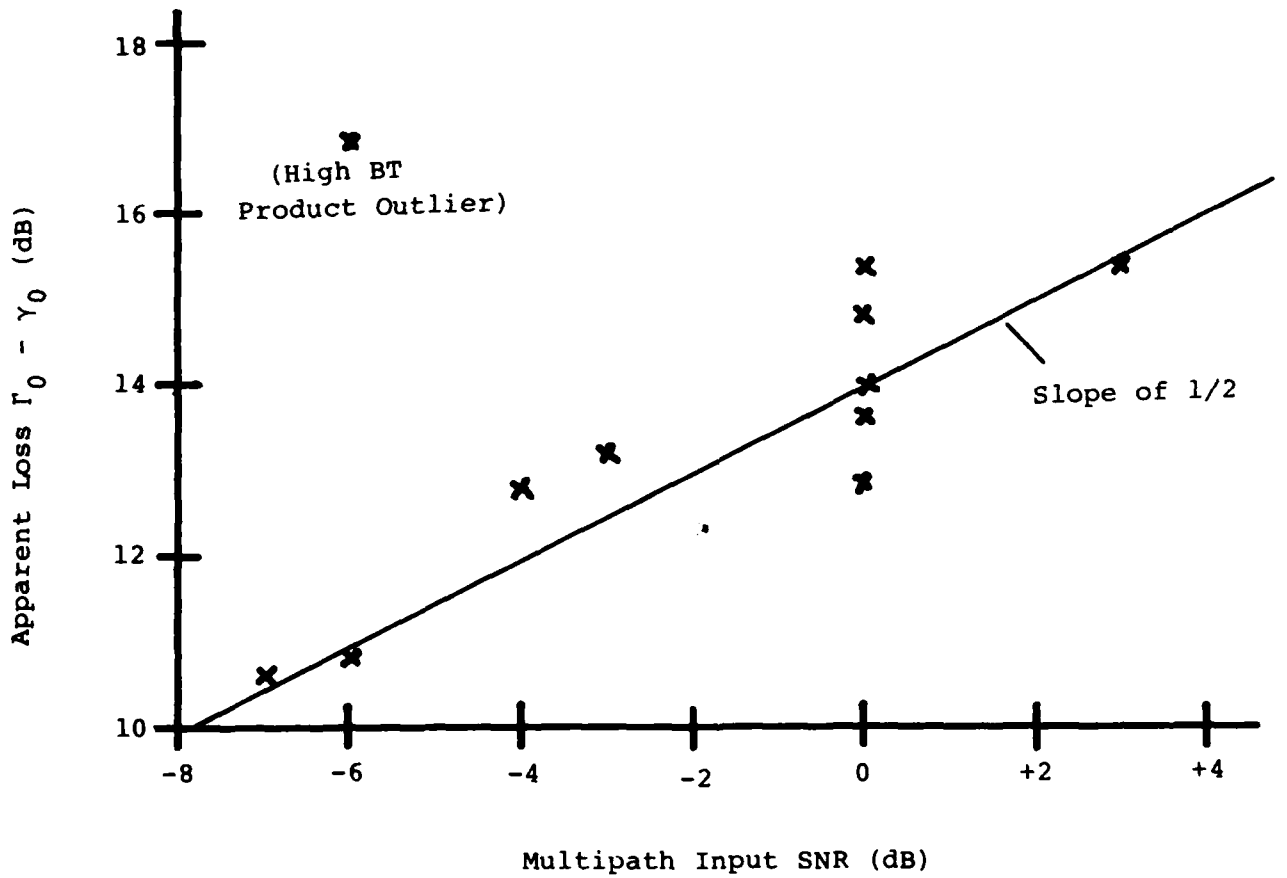

Figure 3-13. Apparent Loss as a Function of Multipath Input SNR (dB).

3.2.2.4 -- Continued

For a linear envelope detector with a sinewave plus zero mean Gaussian noise on the input, the first and second moments of the output, z, are given by Whalen (Anthony D. Whalen, Detection of Signals in Noise, Academic Press, New York, 1971, p 105) as

$$\mathcal{E}\{z\} = (2\sigma^2)^{\frac{1}{2}}\Gamma(\tfrac{3}{2})\,{}_1F_1(-\tfrac{1}{2};\ 1;\ -\tfrac{\alpha^2}{2})$$

$$\mathcal{E}\{z^2\} = (2\sigma^2)\Gamma(2)\,{}_1F_1(-1;\ 1;\ -\tfrac{\alpha^2}{2})$$

where σ^2 is the variance of the Gaussian noise, α is the ratio of the sinewave amplitude to the rms level of the noise, $\Gamma()$ is a gamma function and ${}_1F_1(a;\ b;\ x)$ is the confluent hypergeometric function.

If one computes the detector output SNR as

$$10\ \log_{10}\left(\frac{\mu_s^2}{2\sigma_s^2}\right)$$

where μ_s is the mean detector output and σ_s is the standard deviation of the detector output (both taken at the peak of the ambiguity function), then at high SNR values (say greater than 10 dB, the output SNR equals the input SNR. The complete relationship is shown in Figure 3-14. Superimposed on the theoretical curve are measured data developed from the output envelope statistics and γ_0 (developed from the P_d/P_{fa} measurements). These data provide additional support for the contention that to establish performance we can simply measure statistics at the peak of the ambiguity function and from these infer expected P_d/P_{fa} characteristics.

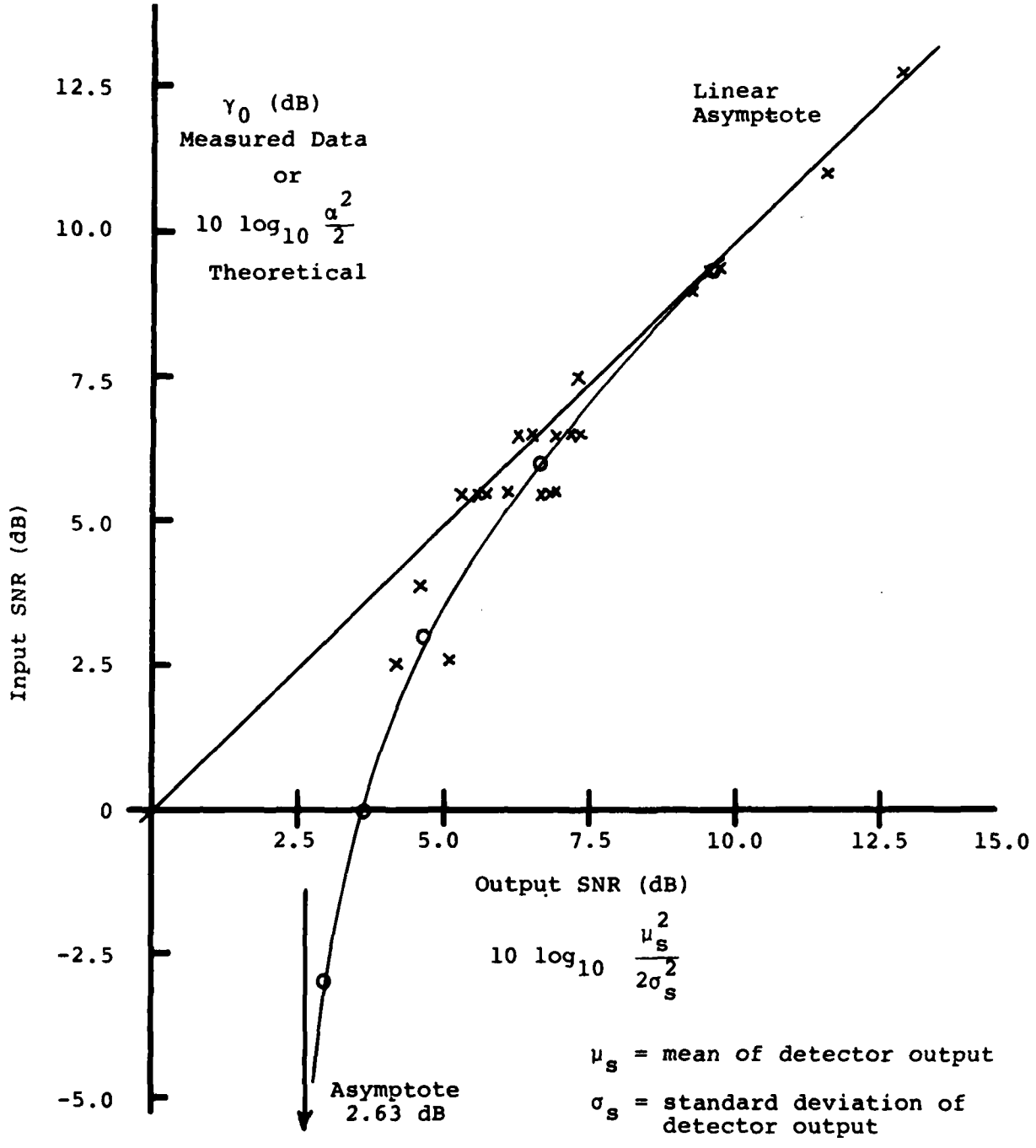

Figure 3-14. Input/Output SNR Relationships for the Linear Envelope Detection of a Sinewave in Gaussian Noise.

3.2.2.5 Processor Evaluation Based on Peak Envelope Statistics.

For each of the various measurement conditions, the measured mean and standard deviation values for the envelope of the peak of the ambiguity function can be used to compute an effective output SNR that in turn can be transformed through the theoretical curve of Figure 3-14 to an equivalent input SNR that will be called γ_1. These data will be compared with theoretical results based on an analysis of an ideal cross-correlation processor. The model in this case was reported in the Interim Technical Report, 1979. The ideal processor output SNR is defined as the ratio of the squared mean of the correlation estimate to its variance. The output SNR, Γ_1, is given by

$$\Gamma_1 = \frac{2B_nT\ SNR_1SNR_2}{1 + SNR_1 + SNR_2 + \lambda SNR_1SNR_2}$$

where $2B_nT$ is the time-bandwidth product and is in our case equal to n, the number of pulses; λ is a parameter, typically with a value near unity. The λ term takes into account the estimation error due to finite time integration.

The measured results have been compared with those of an ideal correlator for values of λ equal to one or zero and are presented in Figure 3-15. The data seem to be concentrated in a band with an apparent loss ranging from 10 to 13 dB and a second band with an apparent loss on the order of 16 dB. If the data are examined in terms of the apparent loss as a function of n, the results are summarized in Figure 3-16. Here it seems clear that the larger apparent losses are occurring when n is large. Large n corresponds to the higher duty cycle signals, in this case a PRI of about 19 μsec. Note that the number of pulses also corresponds to the processing time-bandwidth product or equivalently the processing gain. Performance analysis of the optical correlator, as reported in the 1979 Interim Report has suggested a processing gain of the form

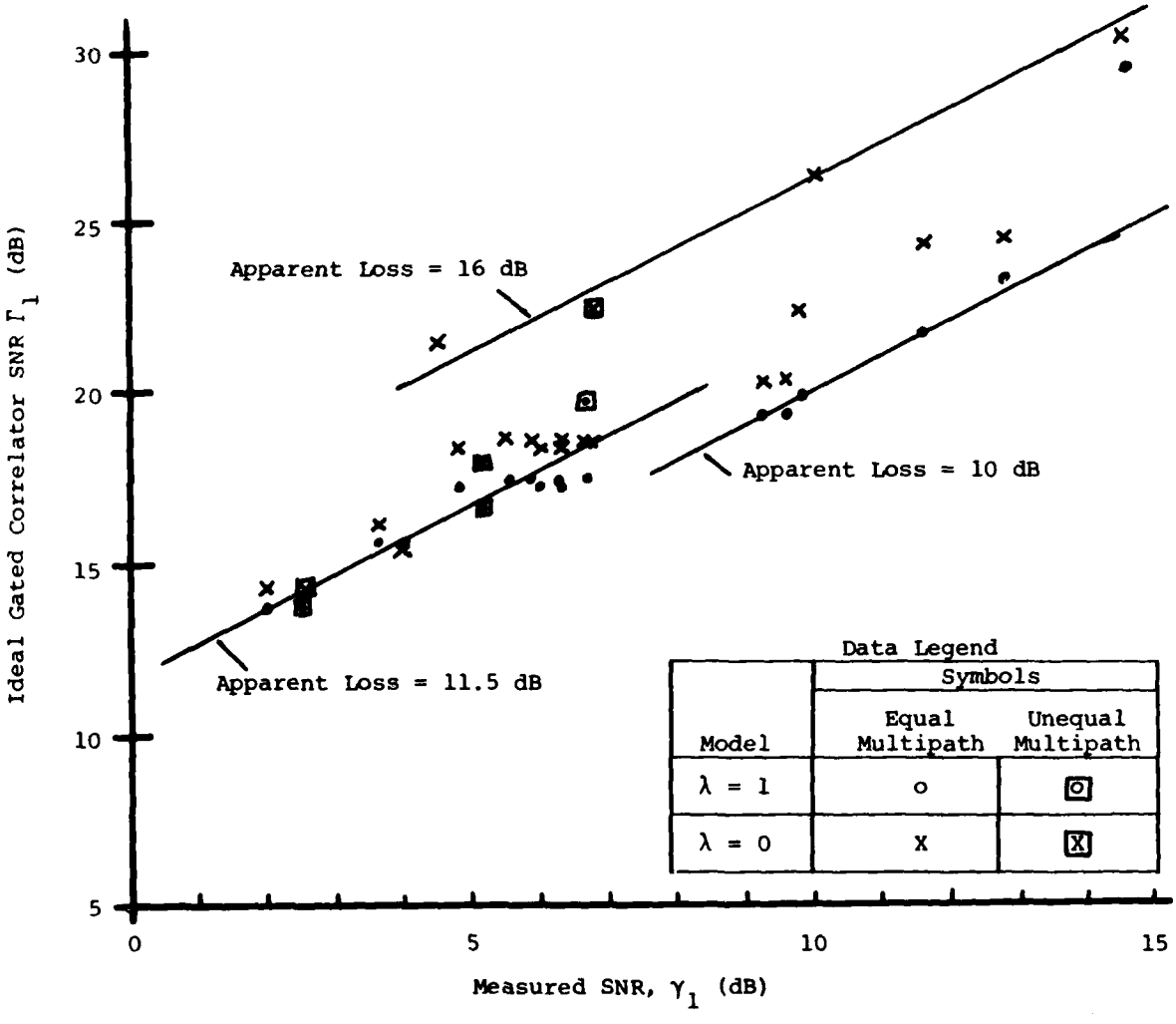

Figure 3-15. A Comparison of Processor Equivalent SNR for an Ideal Correlator and Corresponding Values Derived from Measured Peak Envelope Statistics.

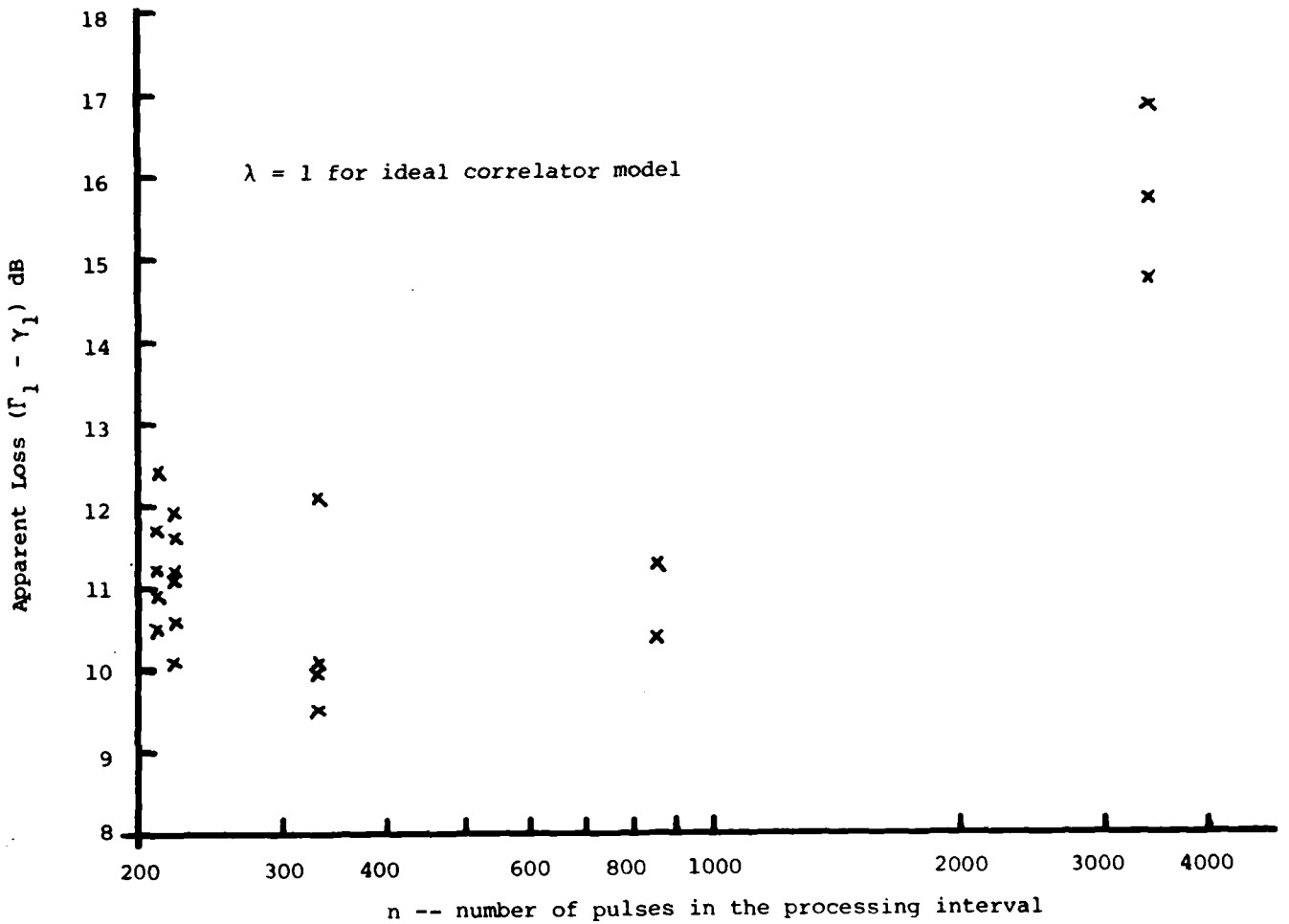

Figure 3-16. Apparent Processor Loss as a Function of the Number of Pulses.

3.2.2.5 -- Continued

$$\frac{n}{1 + k\frac{n}{(DR)^2}}$$

where k is a constant related to the signal modulation depths of the three optical processor inputs and DR is the dynamic range of the photodetector array. For very large n the processing gain approaches a constant given by $(DR)^2/k$. At this time, we have insufficient measurements to establish the presence of the effect, however, it is a candidate for controlled experiments in the future.

The apparent loss is plotted as a function of the multipath input SNR in Figure 3-17. These data may be further compared with the data presented in Figure 3-13. With the additional data available in Figure 3-17 the possible trend identified in Figure 3-13 is not apparent.

3.2.2.6 Summary of Quantitative Test Results.

The time integrating triple product processor has been configured as an ambiguity function processor and operated in a gated processing mode to evaluate its performance for the detection of multipath. The test signal is a repetitive pulse train with a 1 μsec pulse width and a PRI that was varied between 19 μsec and 312 μsec. The multipath delay was nominally 25 μsec and the pre-D bandwidth for the composite signal plus noise was varied from 300 kHz to 1 MHz.

Gated correlation processing allows one to increase the effective average SNR for pulse signals. The gate in this case was derived from the noisy pre-D signal and had a nominal width of 2 μsec.

A key attribute of the processor is its highly parallel processing capability. For the tests reported here the processor was configured to compute the real part of the complex cross ambiguity

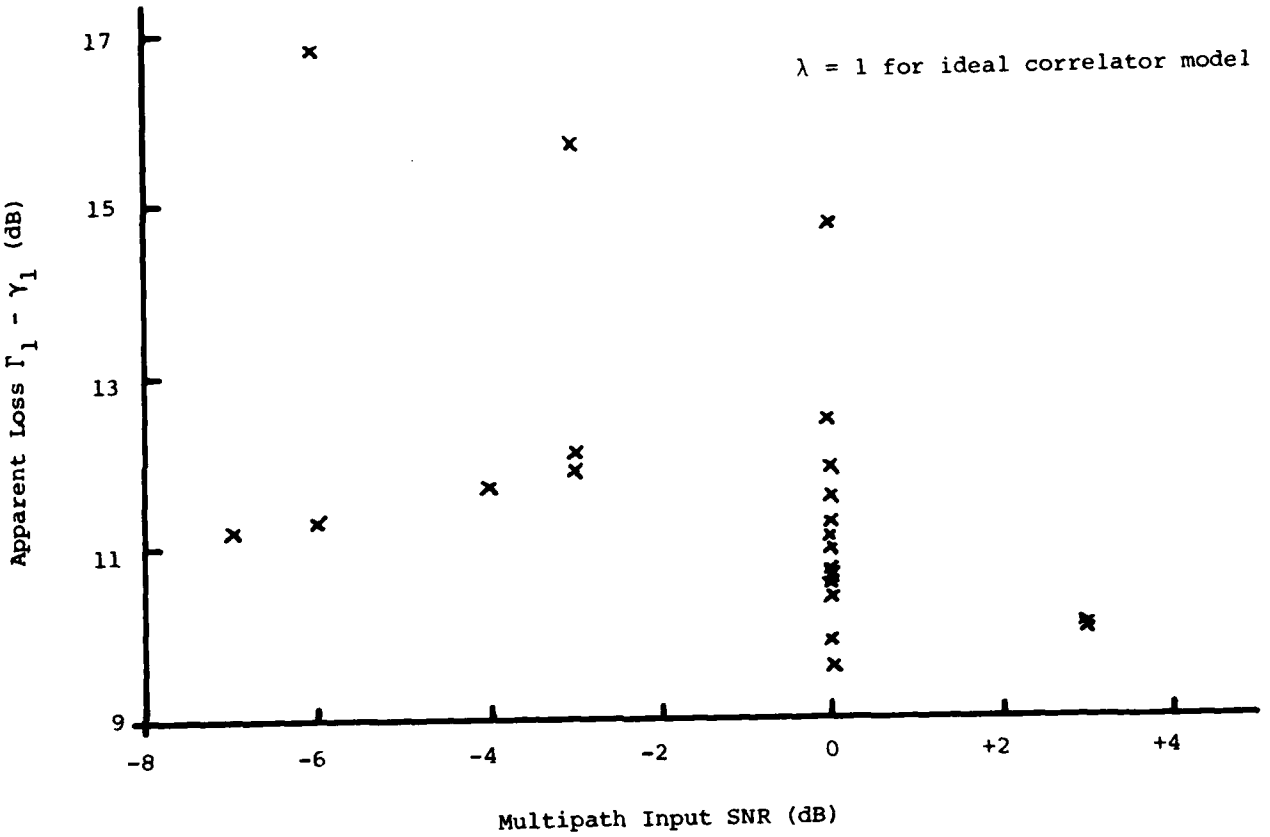

Figure 3-17. Apparent Loss as a Function of Multipath Input SNR (db), $\lambda = 1$ Model.

3.2.2.6 -- Continued

function in real time and for a region 20 μsec by 1.1 kHz. The measurement interval was (1/15) sec, however, the effective integration time depended upon the gate width and the signal PRI. The region of the ambiguity function that is processed may be centered wherever desired or sequentially stepped in a search scenario by the simple selection of a pre-computational delay parameter value and a synthesizer frequency parameter value.

The processor output values are in digital form and at a cursor selectable position a series of digital samples are used to compute the envelope of the complex ambiguity function via the Hilbert transform.

The performance evaluation was placed in the context of a detection problem, that is, is signal plus noise present or is noise only present. The signal here is the real part of the complex ambiguity function at a carrier and at the multipath delay and Doppler offset. The processor P_d/P_{fa} characteristics were estimated by performing a large series of tests at various input SNR's. Additional statistical characteristics such as the mean and variance of the envelope output were measured in both signal and noise only regions.

The measured data were processed to arrive at an effective SNR of a sinewave (phase unknown) in Gaussian noise that would be applied to a linear envelope detector for the detection process. This effective SNR is a consequence of the processor and can be compared with an equivalent SNR for an ideal correlator operating with the same input signals. The differences between the effective SNR's derived from measurements and comparable values for the ideal correlator represent an apparent loss in processing gain associated with this particular real processor implementation.

3.2.2.6 -- Continued

The apparent losses that were measured concentrated in a band ranging from 10 to 13 dB and in a second band with an apparent loss on the order of 16 dB. The higher apparent loss was observed at high processing time-bandwidth product and may be a manifestation of an effect anticipated by Kellman and associated with a signal modulation depths in the optical processor and dynamic range limtiations in the photo-detector array. It has been determined that a minimum of 3.25 dB of this apparent loss is due to the phase averaging technique used for bias elimination. Alternative bias elimination techniques are available that do not suffer this loss and that are relatively simple to implement. With the assumption that this is correct and if we consider the low-duty cycle signals (lower effective processing gain available in the measurement interval), then it is concluded that the apparent loss of the optical processor relative to ideal is on the order of 7 to 10 dB. The level of processing gain that is achievable is quite satisfactory for many applications. If the apparent loss could be reduced by another 3 to 6 dB many more applications would become viable. It is recommended that additional controlled tests be performed to establish the sources of the loss and evolve techniques to improve performance.

DETECTOR INTEGRATION ACOUSTO-OPTIC SIGNAL PROCESSING

P. KELLMAN
ESL Incorporated
Sunnyvale, California 94086

1. INTRODUCTION

Detector integration optical signal processing techniques presented in this paper are a generalization of the one dimensional time integrating correlator demonstrated by Sprague[1] and transversal filter architectures described by Whitehouse, et al[2]. The class of achievable signal processing functions is described, and examples of one and two dimensional realizations of spectral analysis and ambiguity function processing are given.

Detector integration optical processing methods implement time integrating, rather than spatial integrating, algorithms, which result in a processor with increased flexibility and multiple purpose. An important consequence of time integrating methods is the ability to operate on signals or imagery with very large time-bandwidth products ($\sim 10^6$) without having to store the entire time history as a spatial record. Therefore, an important class of two-dimensional and multi-channel processing algorithms may be performed without requiring two-dimensional spatial light modulator devices. Rather, the optical implementation presented utilizes acousto-optic devices and charge coupled image sensors, which are highly compatible input/output devices for signal processing applications. Further, these techniques may be realized with either coherent or non-coherent optical systems.

The one dimensional time integrating correlator is reviewed in Section 2 and a spectral analysis implementation is described in Section 3. Two dimensional detector integration processors are introduced in Section 4 and examples of ambiguity function processing and two dimensional spectral analysis are given in Sections 5 and 6.

2. TIME INTEGRATING CORRELATOR

The one dimensional time integrating correlator[1] is reviewed. Consider the optical realization shown conceptually in Figure 1. The light source is temporally modulated by a signal, $s_1(t)$, to produce an output intensity $I_1(t)$, which illuminates an acoustic delay line light modulator. A second signal, $s_2(t)$, is introduced into the acoustic cell, which spatially modulates the source intensity by an amount denoted by $I_2(t-x/v)$, where x is the spatial dimension and v is the acoustic velocity. The acoustic signal is Schlieren imaged onto a linear photodiode array; the intensity distribution in the image plane is given by the product $I_1(t)I_2(t-x/v)$.

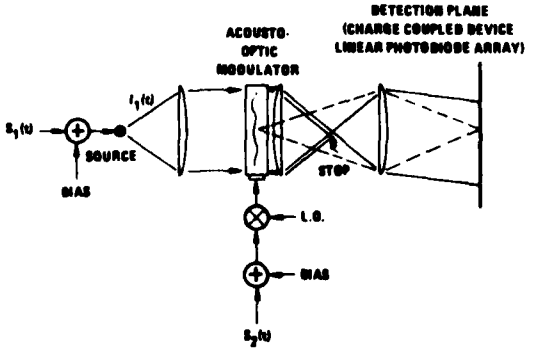

Figure 1. Time Integrating Correlator

The charge integration, directly proportional to exposure, is performed by detectors at discrete positions, x_i. The resultant output voltage at the i^{th} detector element is therefore:

$$R_{12}(\tau_i) = \int_T I_1(t) I_2(t-x_i/v)\,dt \qquad (1)$$

where $\tau_i = x_i/v$, and T, the integration time of the detector, is set by the timing of the charge transfer readout register. This is the desired correlation, where I_1 and I_2 are directly related to the input signals s_1 and s_2.

The range of relative delay between input signals is limited by the acoustic delay length, and the integration time is set by the detector readout period. In the spatial integration approach[3], the integration period is determined by the acoustic delay; in configurations employing fixed reference masks, the range of relative delay is unlimited, however, in correlators with active reference, the range is limited to the acoustic delay. Long integration and flexibility of variable integration are achieved with the time integrating approach.

In order to operate in a linear region of intensity modulation, it is necessary to bias the input signals. The resulting intensity modulation is:

$$I_1 = B_1 + s_1$$

$$I_2 \simeq \sin^2[B + s_2] \simeq B_2 + s_2 \qquad (2)$$

where the acousto-optic modulation is considered in the Bragg limit. In this case the spatial modulation is approximately linear for weak modulation biased at 50% diffraction efficiency. The output voltage may then be written as,

$$R_{12}(\tau_i) = \int I_1(t) I_2(t-x_i/v)dt$$

$$= \int s_1(t) s_2(t-x_i/v)dt + \int B_1 B_2 dt$$

$$+ B_1 \int s_2(t-x_i/v)dt + B_2 \int s_1(t)dt \quad . \quad (3)$$

The first term of Equation (3) is the desired correlation between s_1 and s_2. The second term is fixed bias, and the last terms are signal dependent, though effectively zero mean (signal components at frequencies higher than 1/T will integrate to zero).

Operation at low signal to bias ratio (modulation depth), in order to achieve linear intensity modulation, reduces the correlator dynamic range. Furthermore, wideband acousto-optic devices with high diffraction efficiency are difficult to realize. A technique, introduced in this paper, for overcoming this limitation, is described as follows. The acousto-optic deflector is modulated single sideband with the carrier offset by an amount greater than the signal bandwidth; in addition the illumination source must be modulated on a carrier with equal frequency offset. In this way, undesirable products resulting from nonlinear intensity modulation are offset in frequency, and integrated to zero. Consequently, low signal to bias ratio and high diffraction efficiency are not required. The spatial sampling in the detection plane must then be commensurate with the bandwidth of signal plus frequency offset. The spatial carrier can be eliminated by means of a grating in the image plane, thereby reducing the detector sampling requirement. Other, more general, functions can be realized with spatial masks, and by post detection electronic weighting.

Detector noise determines the achievable time-bandwidth product for a given sensitivity. Detector noise has a shot noise contribution due to the optical bias, as well as post integration readout noise due to reset charge uncertainty in charge transfer devices. The achievable time-bandwidth and dynamic range can be extended, however, by employing post detection digital integration. Baseline variation due to optical bias and detector array non-uniformities also reduces the dynamic range. However, this baseline may be effectively removed by electronic techniques.

3. TIME INTEGRATING SPECTRAL ANALYSIS

An approach to real time optical spectral analysis of electrical signals, that uses a time integrating, rather than spatial integrating, version of the chirp-z transform, is described. The large time-bandwidth correlation is accomplished by means of the correlator described in the previous section. A time integrating architecture, for correlation and spectral analysis, using oppositely traveling acoustic waves, has been described by Montgomery[4]. For time integrating realizations, frequency resolution is determined by the detector integration period, rather than the acoustic delay length, therefore, higher resolution can be achieved than by spatial integration. Variable resolution is attainable through variable detector integration. Use of non-coherent intensity modulation leads to detection of the magnitude spectrum rather than the power spectrum which yields a considerable increase in dynamic range. This approach to spectral analysis achieves a flexibility not readily achieved by coherent optical spatial methods. The chirp algorithm is reviewed, and the real implementation is discussed.

The Fourier transform integral of Equation (4) may be rewritten as Equation (5) by expressing $f \cdot t$ as $1/2[f^2 + t^2 - (t-f)^2]$.

$$S(f) = \int s(t) e^{-i2\pi ft} dt \quad (4)$$

$$S(f) = e^{-i\pi f^2} \int s(t) e^{-i\pi t^2} e^{i\pi(t-f)^2} dt \quad (5)$$

The complex realization is shown in Figure 2. The post phase weighting may be ignored if only the magnitude or power spectrum is required. This realization converts the integral transform to time invariant filtering of a preweighted signal, followed by post weighting.

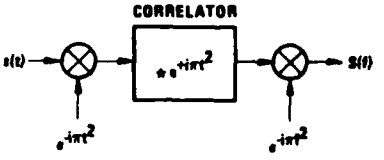

Figure 2. Complex Realization of Chirp Algorithm

In general, linear time-variant operations of the form:

$$y(\tau) = \int x(t) h(t,\tau) dt \quad (6)$$

may be implemented whenever the kernel can be decomposed as:

$$h(t,\tau) = a(t) b(t-\tau) c(\tau) \quad (7)$$

A necessary and sufficient condition for the above decomposition[5] is given as:

$$\frac{\partial^3 \log h}{\partial t^2 \partial \tau} + \frac{\partial^3 \log h}{\partial t \partial \tau^2} = 0 \quad (8)$$

The chirp algorithm may be realized with a single real correlation by translating the real chirp to a carrier frequency, f_o, greater than the signal analysis bandwidth, B. This implementation is shown in Figure 3. The desired difference frequency is translated to baseband, and the sum frequency is an out of band chirp that integrates to

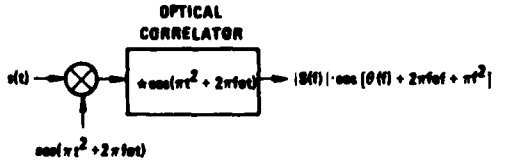

Figure 3. Single Channel Real Implementation of Chirp Algorithm

zero. The product of the difference frequency, which is a linear function of delay, and the input signal, is integrated, producing the spectrum.

Frequency resolution of this spectrum analyzer is inversely proportional to the detector integration time, T. The resolution is not set by the acoustic time delay which typically limits the use of acousto-optical processing to wideband analysis. A wide range of integration times are possible (0.1 - 10 msec) using self-scanned arrays of moderate size (e.g., 1024). Integration time periods can be extended easily by means of electronic accumulation.

The delay line length, τ, and the number of detectors, N, set the difference, $\Delta\tau$, between detector elements in the image plane. This determines the chirp bandwidth, B'. The required resolution or integration period fixes the chirp rate (see Figure 4). The above relations may be written as:

$$\begin{aligned} \tau &= N\cdot\Delta\tau \\ \Delta f &= 1/T \\ \frac{B'}{T} &= \frac{\Delta f}{\Delta\tau} \rightarrow B' = 1/\Delta\tau \\ B' &= N/\tau \end{aligned} \qquad (9)$$

The chirp bandwidth, B', will be greater than the analysis bandwidth, B, if the integration time, T, is greater than the delay line length, τ.

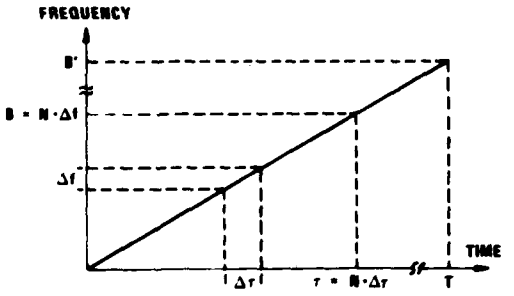

Figure 4. Instantaneous Frequency of Chirp

The samples must be spaced less than 1/T (modifying Equation 9) in order to satisfy Nyquist sampling of the signal plus the carrier offset. The spatial carrier may be eliminated by means of a grating in the image plane, or by electronic detection. The magnitude spectrum corresponds to the detected envelope; the phase modulates the carrier and may be detected as well, resulting in a complex spectrum output.

The dynamic range is primarily limited by the detectors, provided there is sufficient signal light power. If there are M distinguishable levels in the output voltage between the noise floor and the photoelement saturation value, the dynamic range in dB is given by 20 $\log_{10}$M, since incident exposure is directly proportional to spectral magnitude. This results in a considerable increase in dynamic range as compared to coherent optical spectral analysis in which incident exposure is related to spectral power density and the dynamic range is given by 10 $\log_{10}$M.

4. TWO-DIMENSIONAL PROCESSING

Two-dimensional integral transforms, for which the kernel is decomposable in the proper way may be implemented by detector integration optical processing. Two important examples are ambiguity plane processing and spectral analysis which are described in the next sections. The general class of achievable operations is described in this section.

Consider the optical realization shown conceptually in Figure 5. The optical train has a modulated illumination source, two acoustic delay line light modulators, and a matrix array of detectors. This configuration may be employed for several functions, determined by input signal and reference waveforms. It is assumed throughout this discussion, that two-dimensional processing is applied to either very long one-dimensional signals or to two-dimensional signals (e.g., imagery) that are in raster format. In this way, the input, x(t), will be a function of one variable, t; the output, $y(\tau_1,\tau_2)$, is a function of two variables.

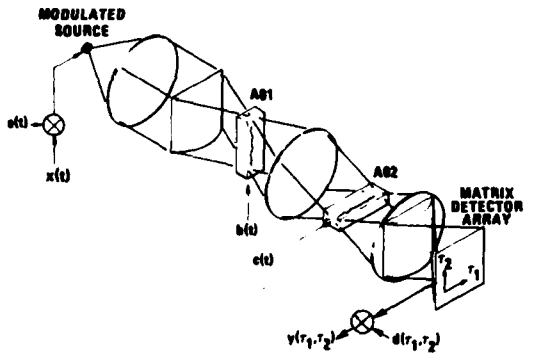

Figure 5. Generalized 2-D Detector Integration Processor

The light transmitted by the first acousto-optic modulator A01, is diffracted by the second, A02, in an orthogonal direction. Both acoustic signals are imaged on the detector plane. The desired image plane intensity distribution has a term proportional to the product of acoustic signals, $b(t-\tau_2)c(t-\tau_1)$, where $\tau_1 = x/v$ and $\tau_2 = y/v$ are time variables. The resultant detected output voltage is proportional to the integrated charge as in the previously described correlator. This structure implements integrals of the form:

$$y(\tau_1,\tau_2) = \int_T x(t)h(\tau_1,\tau_2,t)dt \qquad (10)$$

where

$$h(\tau_1,\tau_2) = a(t)b(t-\tau_2)c(t-\tau_1)d(\tau_1,\tau_2) \quad , \qquad (11)$$

{a, b, c, and d} are reference signals, and x(t) is the input signal. In this configuration, all signals are real. In order to perform complex computation, similar considerations apply that were given for one-dimensional processing. The output weighting, $d(\tau_1,\tau_2)$, may be applied electronically as indicated, or by means of a spatial mask in the image plane.

Alternate arrangements include applying inputs at A01 or A02. A dual input processor, that uses the same optical system, implements integrals of the form:

$$y(\tau_1,\tau_2) = \int x_1(t)x_2(t-\tau_1)h(\tau_1,\tau_2,t)dt \qquad (12)$$

where h is given by Equation (11), the source modulation is $x_1(t)$, and A02 is driven by $c(t)x_2(t)$. Additional input sources and multichannel acoustic devices may be employed as well. These possibilities are not detailed here.

The two-dimensional time integrating optical processor may be implemented with several modulation/detection schemes. A description of a coherent optical implementation using an interferometric reference beam has been given by Turpin[6]. Non-coherent implementation using an intensity modulated light emitting diode offers immunity to noise suffered in coherent imaging. The light budget is an important design consideration. Source collimation is required for efficient acousto-optic interaction. For acousto-optic modulation at low diffraction efficiencies, the doubly diffracted imaging scheme has substantial insertion loss. Alternatively, single diffraction imaging may be realized by utilizing the undiffracted light transmitted by A01 that is diffracted into the first order of A02. This signal is mixed, in the detection process, with the first order signal of A01 that passes undiffracted by A02. Both singly diffracted signals are in phase and may be Schlieren imaged. Input modulation must be designed such that the undesired terms are out of band.

The next examples demonstrate the strength of two-dimensional detector integration processing.

5. AMBIGUITY FUNCTION PROCESSING

Ambiguity function processing is important in resolution of delay and Doppler uncertainty. In application to radar signal processing or external signal parameter measurement, delay and Doppler are often time-varying. An ambiguity function snapshot is therefore desirable. A non-coherent optical parallel processing implementation for achieving such a snapshot is given in this section.

This example utilizes the 2-d optical system shown in Figure 5 which was generalized in the last section. Define the cross ambiguity function between two signals, s_1 and s_2, as:

$$\chi_{12}(t,\tau) = \int_T s_1(t)s_2(t-\tau)e^{-i2\pi ft}dt \qquad (13)$$

where τ and f are the delay and Doppler variables. The dual input optical processor output is described by Equation (12) which becomes:

$$y(\tau_1,\tau_2) = \int_T \left[s_1(t)e^{-i\pi t^2}\right]\cdot e^{i\pi(t-\tau_2)^2} s_2(t-\tau_1)dt$$

$$= e^{i\pi\tau_2^2}\cdot \int_T s_1(t)s_2(t-\tau_1)e^{-i2\pi t\tau_2}\,dt \qquad (14)$$

where {a,b} are complex chirp waveforms. This is the expression for the cross ambiguity function with a quadratic phase term that may be cancelled through post detection weighting. The real architecture may be realized by the method described for spectral analysis. In fact, the ambiguity function may be interpreted either as a multichannel spectrum analyzer given by:

$$\chi_{12}(f,\tau) = \mathcal{F}[s_1(t)s_2(t-\tau)] \qquad (15)$$

for multiple time delays, τ, or as a multichannel correlator given by:

$$\chi_{12}(f,\tau) = [s_1(t)\cdot e^{-i2\pi ft}]\star[s_2(t)] \qquad (16)$$

for multiple Dopplers, f. The one-dimensional processing considerations previously discussed are, therefore, applicable. The Doppler resolution is commensurate with the integration time, a coarse resolution may be maintained during acquisition period and a higher resolution zoom can be achieved by longer integration. Multiple correlation peaks or targets can be processed simultaneously since a linear system implementation is used.

6. TWO-DIMENSIONAL SPECTRAL ANALYSIS

A non-coherent optical time integrating approach to two-dimensional complex spectral analysis is described. This method is an extension of the technique described for one-dimensional analysis. Very large bandwidth (greater than 10^5) spectral analysis of electrical signals can be performed using this time domain approach, without requiring storage of the signal. Spectral analysis of raster scanned video imagery can be performed as well.

The optical system (Figure 5) described in the last sections is used in this example as well. The algorithm is implemented with three reference chirp waveforms. The source is modulated with the input signal, which is pre-multiplied by a chirp, and the other chirps modulate A01 and A02. The chirp rates are chosen such that the product of the three chirps result in a temporal sine wave, with frequency that is varying from pixel-to-pixel on the detector array. Each detector element integrates the product of this sine wave times the input signal, and, in this fashion, produces the spectrum. The frequency difference between output lines in one dimension is taken to be N times the frequency difference between lines in the other dimension, where N is the number of detectors per line. For a square array, the number of spectral samples is proportional to N^2. The technology is currently limited by detector array size, and detector readout rate.

The high rate chirps are folded over on the order of N times during the integration period, which creates a comb frequency sampling along the coarse frequency axis, with comb samples being a

function of the fine frequency axis. The real implementation is performed with frequency offset chirps, similar to the previous examples. Transforms of raster scan imagery are more complicated, requiring synchronization that is not described in this paper.

High resolution spectral analysis by detector integration processing has several advantages over coherent spatial techniques. These include, larger dynamic range, no signal storage, complex output, flexibility in processing, advanced device technology (acousto-optic), and non-coherent optical system implementation.

7. SUMMARY

Detector integration optical signal processing, as introduced in this discussion, has been generalized for one- and two-dimensional complex signal processing. These techniques are implemented by time integration and are well suited to time domain algorithms. The optical realization, utilizing acousto-optic input devices and charge coupled image sensor output, creates a processor that is compatible with signal processing systems. Such implementation affords very large time bandwidth signal processing without the storage problem associated with coherent spatial techniques. Flexibility of the transversal filter architecture is achieved by means of variable time integration and actively generated reference waveforms. The optical system described is multi-purpose as illustrated in the examples. Complex computation is performed without requiring a coherent optical system.

ACKNOWLEDGEMENT

The author acknowledges funding support by ESL Incorporated under the Internal Research and Development program. Special thanks to my colleagues at ESL, and to J.W. Goodman at Stanford University for their continued encouragement.

REFERENCES

1. R. Sprague and C. Koliopoulos, "Time Integrating Correlator," *Applied Optics* 15, 89 (January 1976).

2. H.J. Whitehouse, R.W. Means, and J.M. Speiser, "Signal Processing Architectures Using Transversal Filter Technology," Proceedings IEEE Symposium on Circuits and Systems, Boston, April 1975.

3. R. Sprague, "A Review of Acousto-Optic Signal Correlators," *Optical Engineering* 16, 467 (September/October 1977).

4. R. Montgomery, U.S. Patent 3,634,749 (1972).

5. H.J. Whitehouse, J.M. Speiser, and R.W. Means, "High Speed Serial Access Linear Transform Implementations," NUC Internal Report TN1026, (January 1973), reprinted in ARPA Quarterly Technical Report QR1, Image Transmission via Spread Spectrum Techniques.

6. T. Turpin, "Time Integrating Optical Processors," SPIE Symposium on Real-Time Signal Processing, San Diego, August 1978.

Coherent optical hybrid techniques for spectrum analysis

T. R. Bader
ESL Incorporated
Sunnyvale, California 94086

Abstract

A hybrid optical approach to coherent spectrum analysis realizes gains associated with time-integrating techniques while still retaining some of the advantages of space-integrating techniques. Measurement of large time-bandwidth spectra is performed with high sensitivity, efficiency, and range of detectable signal power levels, particularly in large bandwidth applications, where an optically transformed periodic chirp forms a distributed local oscillator as a reference for time integration.

Introduction

The continuing advancement of electro-optical component technologies is increasingly aiding realization of optical techniques for signal processing. These developments have been encouraged by the rapid advancement in electronic processing techniques and hardware. This latter, seemingly paradoxical, effect derives from the fact that the progress in electronic processing has made sophisticated but practical processors realizable provided the burden of very high throughput rates for certain operations can be borne, precisely in the area in which the parallel processing capabilities of optical techniques are most valuable.

Spectrum analysis is an operation that has become particularly well addressed by optical methods. In this paper we will focus our attention on two-dimensional coherent optical techniques for spectrum analysis, presenting a brief review of the space-integrating[1] and time-integrating[2,3,4] approaches and a discussion of hybrid implementations[5] that exhibit space-integrating and time-integrating characteristics. Our attention is directed toward the examination of those characteristics that make optical techniques most useful in processing systems, particularly bandwidth and time-bandwidth product, and a comparison of implementation variables such as optical efficiency and signal detectability. Since space-integrating, time-integrating, and hybrid techniques can be configured in two dimensions for compact, large time-bandwidth processing, the discussions below, organized to emphasize the close parallel among the techniques, will be given in terms of two-dimensional architectures.

Coherent Space-Integrating and Time-Integrating Spectrum Analysis

Space-integrating coherent processors rely on the physics of coherent light propagation, which permits a simple lens to transform a light amplitude into its amplitude spectrum. Since this can be performed in two dimensions, large blocks of information can be processed simultaneously. Figure 1 shows an example[1] of a two-dimensional spectrum analyzer using acousto-optic devices to deflect and modulate the laser light. Each acousto-optic beam deflector (AOBD) causes the light to be deflected in such a manner that the combined result is that the light focused at the recording medium is scanned in a multiline raster as it is modulated in intensity by the acousto-optic modulator (AOM).

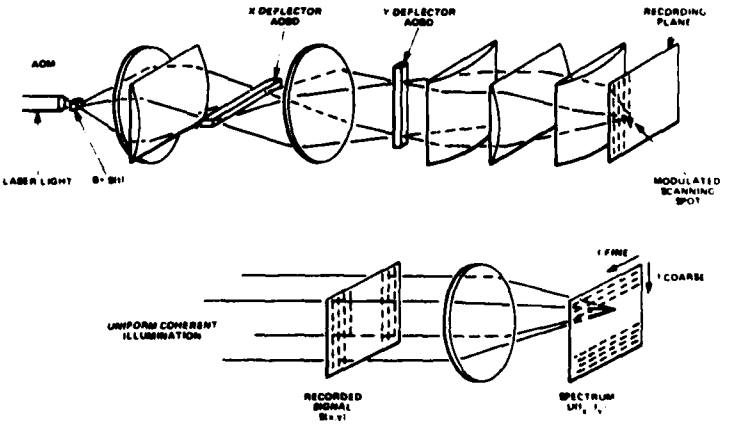

Figure 1. Two-dimensional space-integrating spectrum analyzer.

Since the recording medium responds to light intensity, the signal modulating the light power must be on a bias. The recording medium is used in a linear region of the amplitude transmittance versus exposure curve. After a full frame has been recorded the medium is illuminated with a uniform wave of coherent light. The transmitted amplitude is transformed by a lens to produce a two-dimensional intensity distribution that is proportional to the signal power spectrum arranged in a multiline format, one coordinate corresponding to coarse frequency increments and the other to fine tuning; in other words, the high resolution spectrum is folded into many horizontal lines (in Figure 1) in the same manner that the signal is folded into many vertical lines on the recording medium.

An analogous two-dimensional time-integrating analyzer[2] is shown in Figure 2, configured as the space-integrating system of Figure 1, except that the recording medium is removed and the scanning, modulated light is transformed by a lens to a modulated plane wave deflecting in two directions at a detector array plane. Here it interferes with a constant, uniform reference wave incident from an oblique angle. The signal, without a

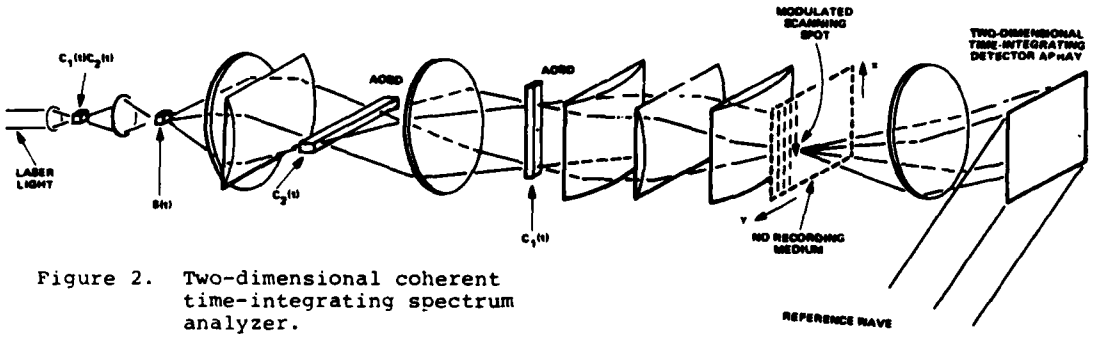

Figure 2. Two-dimensional coherent time-integrating spectrum analyzer.

bias, modulates the amplitude of the light at the AOM, rather than the intensity, with the result that the time-integrated energy distribution in the detection plane after a full frame is the amplitude spectrum. This technique of recording the spectrum is equivalent to recording an off-axis Fourier transform hologram of the transparency generated in the space-integrating technique of Figure 1 while scanning it with a focused spot rather than illuminating it all at once, as in Figure 1. The time-integrated spectrum is an amplitude spectrum on a spatial carrier, still maintaining all the phase information, that may be electronically demodulated. The exposure in the detection plane of the space-integrating analyzer is a power spectrum, requiring no demodulation; if an amplitude spectrum is desired, an off-axis reference wave, as in Figure 2, may be added, producing a Fourier transform hologram of the signal transparency, with precisely the amplitude spectrum distribution as that of Figure 2.

The time-integrating technique can be viewed as a heterodyne detection technique in

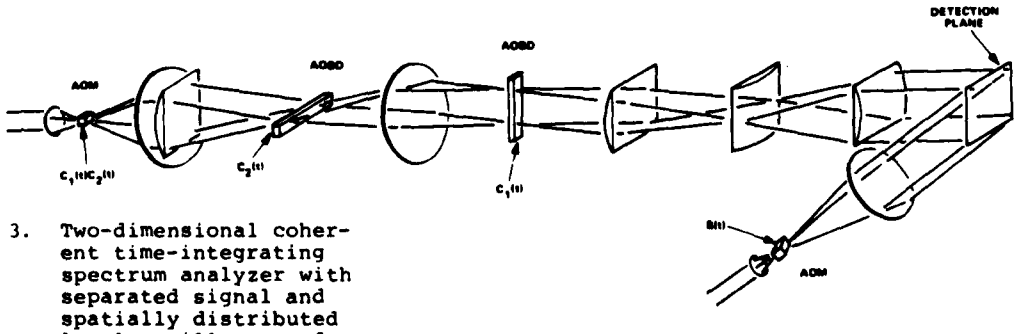

Figure 3. Two-dimensional coherent time-integrating spectrum analyzer with separated signal and spatially distributed local oscillator reference waves.

which the signal is detected by comparison with a local oscillator at every point in the detection plane, the frequency of the local oscillator being a function of the coordinate of the point.[2] Figure 3 is another optical scheme for a time-integrating analyzer; while Figure 2 was designed to illustrate the close relationship between time-integrating and space-integrating techniques (Figure 1), the rearrangement of Figure 3 is meant to help clarify the concept of the distributed local oscillator by creating a physical, corresponding to the mathematical, separation of the signal and the local oscillator reference. The relevant term in the power density integrated over time T_2 at the detector plane can be written

$$E(x,y) = \int_{-T_2/2}^{T_2/2} S(t)\ R(x,y,t)\ dt. \qquad (1)$$

The precise form of the local oscillator R(x,y,t) is discussed below.

Hybrid Spectrum Analysis

The above two approaches to high resolution spectral analysis exhibit different performance bounds and implementation requirements. The TI technique does not require a recording material for intermediate signal storage or the associated dual optical system (for recording and reading). Since the AOM is used in the intensity modulation mode in the space-integrating system, it has only half the bandwidth capability as the same device in the time-integrating system. In wide bandwidth applications a device with a low figure of merit (such as $LiNbO_3$) must be used because of acoustic attenuation. However, in a space-integrating system the requirement to drive the AOM with a bias at the linear region of the diffraction efficiency versus drive voltage curve may be impossible to meet. On the other hand, spatial integration is capable of providing much higher signal levels at the detector, and the power is localized to the signal area, whereas the presence of a signal in the time-integrating scheme contributes a bias to the entire detector. The significance of this is that the presence of a strong, but perhaps uninteresting, signal does not interfere with the detection of a much weaker signal that is not overlapping in frequency. The light power incident on the signal transparency can be increased to bring a weak signal into the dynamic range of the detector, allowing the strong signal to saturate. This cannot be done with a time-integrating system because a strong signal adds a saturating bias to the entire detector plane. (The important considerations of dynamic range improvement by heterodyne detection compared with direct detection do not qualify this observation if, for comparison purposes, a constant off-axis reference wave is added to the space-integrated spectrum at the detector.)

A hybrid spectrum analysis technique that succeeds in combining the above important features of space-integrating and time-integrating architectures is illustrated in Figure 4. Two important features distinguish this arrangment from that of Figure 3. First, the optical aperture of the AOM has been increased (to become an AOBD, by our definition), thus generating, by spatial integration, an amplitude spectrum at the detection plane. Second, the reference wave has been redefined to be the Fourier transform of the wave diffracted

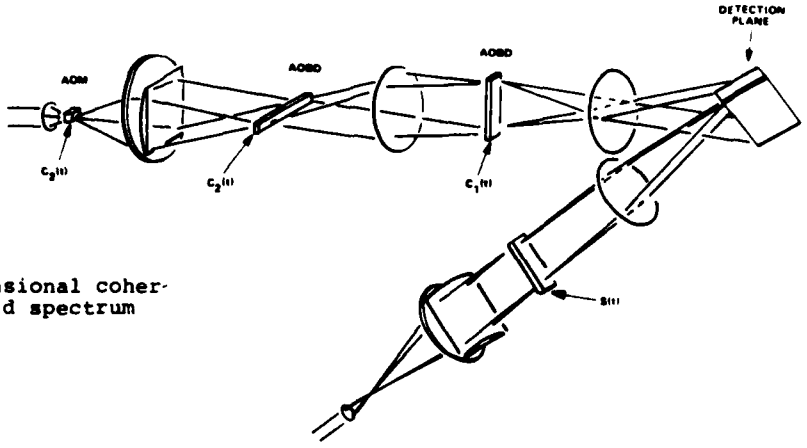

Figure 4. Two-dimensional coherent hybrid spectrum analyzer.

from the AOBD that is driven by the fast axis periodic chirp. The form of this is given below, but whatever form the reference wave takes, the relevant exposure term is

$$E(x,y) = \int_{-T_{2/2}}^{T_{2/2}} A(x,t)\ R(x,y,t)\ dt\ , \tag{2}$$

where

$$A(x,t) = \int_{-\infty}^{\infty} e^{-i2\pi f' t}\ U(f')\ \text{sinc}\ \pi T_1(\alpha v x - f')\ df' \tag{3}$$

is the signal, spatially distributed according to its amplitude spectrum, the estimate of which is limited by the delay time T_1 of the AOBD. v is the acoustic velocity, $\alpha = 2\pi/\lambda F$, λ is the optical wavelength and F is the focal length of the transform lens.

Spatially Distributed Local Oscillators

The reference wave of Figure 4 can be described[5] by

$$R(x,y,t) = e^{ikx} \sum_{p} e^{-i2\pi[p+(y/D)](t/T_1)}\ \text{sinc}\ \pi T_1[(\Delta f x/D) - (p/T_1)],\quad f_1 \le p/T_1 \le f_1+\Delta f \tag{4}$$

where k is the wave vector of the spatial carrier, f_1 is the minimum chirp frequency and Δf is the chirp bandwidth. (Unimportant quadratic phase factors have been omitted for simplicity.) The frequencies f_1 to $f_1+\Delta f$ are assumed to lie in the Bragg bandwidth of the AOBD, and the chirp period is equal to the delay time T_1. The distributed local oscillator described by Equation 4 and illustrated in Figure 5 is seen to consist of an array of grid lines, each grid line having width $1/T_1$ and frequency $[p+(y/D)]/T_1$.

Figure 5.

Representation of a two-dimensional distributed local oscillator reference amplitude. A periodic chirp is optically Fourier transformed in the x direction.

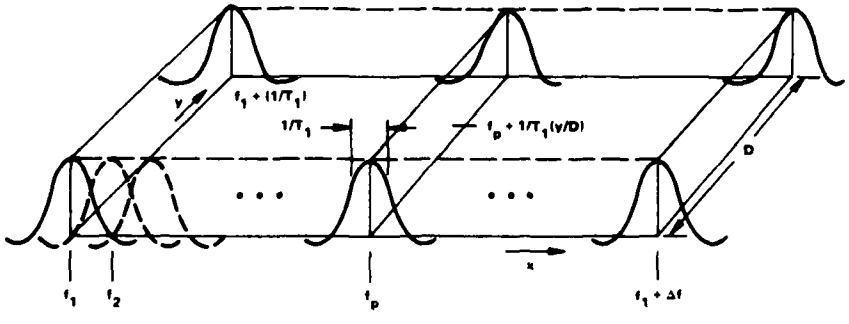

Let us now return to the reference wave of Figure 3 and consider the effect on the light amplitude of the chirp drive for the fast axis only. Considering the periodic chirp function

$$C_1(t) = \sum_{n} e^{i[a(t-nT_1)^2 + b(t-nT_1)]}\ \text{rect}\ \frac{t-nT_1}{T_1}, \qquad a = \frac{\pi\Delta f}{T_1}, \quad b = 2\pi f_1 \tag{5}$$

applied as a Doppler up-shift by the AOM and a down-shift by the AOBD, the net result is

$$R(x,t) = \sum_{n} e^{i[bx + 2axt - 2anT_1]}\ \text{rect}\ \frac{t-nT_1}{T_1}\ \text{rect}\ \frac{t-nT_1-x/v}{T_1}. \tag{6}$$

To render this in a more visible form, we define $G(t-nT_1)$ and use the identity

$$G(t-nT_1) = \text{rect}\ \frac{t-nT_1}{T_1}\ \text{rect}\ \frac{t-nT_1-x/v}{T_1} = \text{rect}\ \frac{x}{2vT_1}\ \text{rect}\ \frac{t-nT_1-x/2v}{T_1-\frac{x}{v}}. \tag{7}$$

With Equation 7 and the transform relationship

$$F(f) = \int_{-\infty}^{\infty} e^{i2\pi ft} G(t)dt = \text{rect}\ \frac{x}{2vT_1}\ e^{i2\pi fx/2v\left[T_1 - \left|\frac{x}{v}\right|\right]}\ \text{sinc}\ \pi f\left[T_1 - \left|\frac{x}{v}\right|\right], \tag{8}$$

Equation 6 can be written, after some manipulation, as

$$R(x,t) = \frac{e^{ibx + i2axt/v}}{T_1} \sum_p F\left[\frac{ax}{\pi v} - \frac{p}{T_1}\right] e^{-i2\pi\left[\frac{ax}{\pi v} - \frac{p}{T_1}\right]t} \tag{9}$$

If we now include the y deflection, neglecting any periodicity, substitute the explicit form for F (again omitting an unimportant quadratic phase factor), and include an angular offset, the two-dimensional spatially distributed local oscillator becomes

$$R(x,y,t) = e^{ikx} \sum_p e^{i2\pi[p+(y/D)]t/T_1} \left[1 - \left|\frac{x}{vT_1}\right|\right] \text{sinc}\left\{\pi T_1 \left[\frac{\Delta fx}{D} - p\right]\left[1 - \left|\frac{x}{vT_1}\right|\right]\right\},\ 0 \le x \le D. \tag{10}$$

Equation 10 represents a two-dimensional distributed local oscillator that is characterized by degradation in high frequency resolution when the fast axis AOBD is driven at high chirp repetition rates. As illustrated in Figure 6, the uniform modulus reference wave is composed of a set of grid lines (labeled by p), with spacing $1/T_1$ having frequencies $[p+(y/D)]T_1$, as does the distributed local oscillator of Equation 4, represented in Figure 5. However, the width of a grid line is larger by a factor $[1-(x/vT_1)]^{-1}$ and the peak is lower by $[1-(x/vT_1)]$. Noting that the optical aperture D is equal to $|v|\tau$, where τ is the acoustic transit time of the cell, the line width degradation factor is $[1-(x/D)(\tau/T_1)]^{-1}$. The ratio τ/T_1 is the fraction of the chirp that is within the AOBD aperture. As the chirp period T_1 approaches τ the grid lines get broader. This spreading results in an ambiguity at higher frequencies due to overlap or crosstalk onto neighboring frequency locations in the coarse frequency direction, observed as ghost signals in a measured signal that are separated by N_2 resolvable elements (where N_2 the time-bandwidth product in the y direction). A constraint is, therefore, placed on the chirp period, and in turn on the bandwidth and resolution of the system. A ratio $T_1/\tau = 4$ corresponds to a 33% spread at the maximum frequency, or about 10 dB crosstalk suppression at a nearest neighbor peak. If we choose this to be the maximum allowable error, then the bandwidth to which the AOBD must respond (N_1/τ) is four times larger than the system bandwith (N_1/T_1).

Figure 6.

Representation of a two-dimensional distributed local oscillator reference amplitude. A periodic chirp is imaged in the x direction.

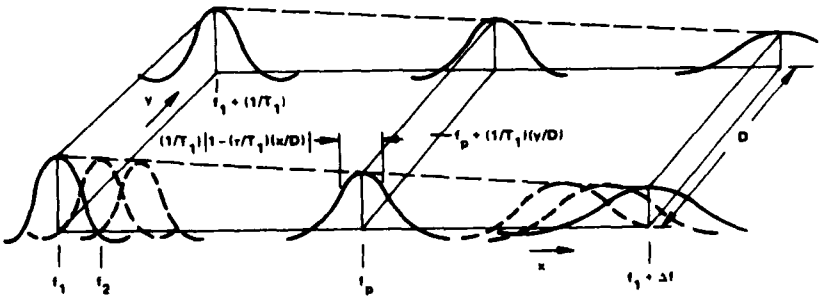

System Design and Performance Considerations

The preceding discussion of distributed local oscillators serves to illustrate one of the benefits of utilizing the Fourier transform properties of lenses with spatially modulated coherent light. Specifically, the full bandwidth capability of acousto-optic devices can be exploited. As an illustration of the operational limitations involved in using acousto-optic cells, Figure 7 contains some tradeoff curves relative to some representative materials. The solid lines represent rather soft upper bounds to the time-bandwidth product as a function of bandwidth, assuming a device bandwidth to center frequency ratio of 0.5, and limited by acoustic absorption. An acoustic attenuation of 3dB over the optical aperture

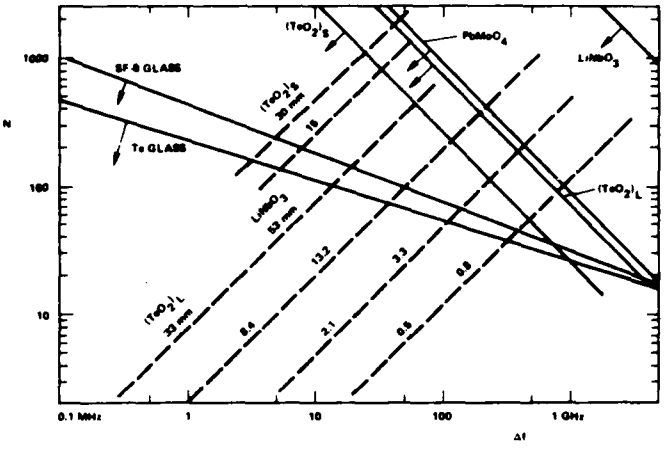

Figure 7. Acousto-optic device tradeoff curves for representative materials. Solid lines define acoustic attenuation bounds. $(TeO_2)_L$ and $(TeO_2)_S$ represent, respectively, the longitudinal and slow shear modes of TeO_2.

was assumed here. The dashed lines are lines of constant cell length; 30mm represents a practical upper limit in most cases. Figure 7 does not pretend to summarize all the constraints involved in fabricating acousto-optic devices, even for the materials represented, but to provide a reasonable basis of discussion of the operating regions of devices that might be realized for the systems we are presently considering.

As an example, a $LiNbO_3$ AOBD with 1 GHz bandwidth and time-bandwidth product of 10^3 is within the realm of existing technology, and may be used to implement a 1 GHz spectrum analyzer only if the distributed local oscillator is of the spatially transformed chirp variety in the fast axis direction (Equation 4). The number of resolvable frequencies of such a system would be 10^6 if the slow axis factor to the two-dimensional local oscillator was implemented as an imaged AOBD (rather than optically Fourier transformed), using a 25mm TeO_2 device in the slow shear mode with a chirp bandwidth of 25 MHz. The slow chirp period would be 1 ms, so that $T_2/\tau = 25$ for the slow axis device, large enough to avoid significant chirp fill time effects.

As a general rule the diffraction efficiency of an AO device, for the maximum rated drive power, decreases with the bandwidth of the device, at least in the high frequency region. Requiring a device several times wider in bandwidth than the signal to be analyzed could be a significant factor in optical power considerations. This is especially true where a change in acousto-optic material is involved. For example, a 120 MHz system with 700 resolvable frequencies in the coarse direction could be implemented with a 25mm TeO_2 device operated in the longitudinal mode in a hybrid system. A purely time-integrating system would require about 500 MHz of device bandwidth, implying a $LiNbO_3$ AOBD, a material with a much lower figure of merit,[6] and, as a result, lower optical efficiency.

Hybrid systems retain an important characteristic not shared with purely time-integration spectrum analysis; very weak signals can be detected in the presence of strong signals not overlapping in coarse frequency lines by raising the laser power incident on the signal AOBD, permitting the strong signal to saturate its line and raising the power of the weak signal into the dynamic range of the detector. In addition to the optical efficiency gains resulting from device bandwidth considerations, a large gain in efficiency in the signal path of the hybrid system of Figure 4 is achieved by concentrating the signal light into the spectrum, rather than distributing it uniformly over the detector.

The coherent hybrid approach, like the purely time-integrating technique, avoids the necessity of using an intermediate recording medium and associated optical readout complications. On the other hand, such recording media could be used in the detection plane to produce an intermediate recording of the amplitude spectrum, with real-time optical demodulation. This optical demodulation by coherent illumination and spatial filtering provides the two-dimensional detector array with the power spectrum, decreasing the number of required array elements because of the absence of the carrier, and permitting multi-frame time-integration detection.[2,3] (It should be emphasized that when recording media are used in the detection plane of hybrid systems the bandwidth advantages of such architectures are retained.) There is a degree of versatility of detection techniques therefore associated with time-integrating and hybrid schemes, a fact that may be of some significance in the wide bandwidth applications we are addressing, where the state of the art in detection hardware is presently the limiting implementation problem.

Summary

The hybrid approach to the two-dimensional coherent spectrum analysis combines some important features of space-integrating and time-integrating techniques. Spatially transformed periodic chirps provide a distributed local oscillator that permits time-integration detection at the full bandwidth of acousto-optic devices. The range of detectable signal levels can be extended well beyond the instantaneous dynamic range of the detector because of the spatial separation of the light energy in the spectrum. This spatial spectrum also results in higher optical efficiency; overall efficiency is improved further by permitting the use, for the same system bandwidth, of acousto-optic devices of lower bandwidth and therefore, higher achievable diffraction efficiency, a reflection of the tradeoffs involved in the performance of such devices. Some versatility exists in the methods available for optical detection, the aspect that presents the most difficult implementation problem for wide-bandwidth systems.

References

1. Thomas, C. E., "Optical Spectrum Analysis of Large Space Bandwidth Signals," Appl. Opt. 5, 1782 (1966).
2. Turpin, T. M., "Time Integrating Optical Processors," SPIE 154, 197 (1978).
3. Sprague, R. A. and Koliopoulos, C. L., "Time Integrating Acoustooptic Correlators," Appl. Opt. 15 (1976).
4. Kellman, P., "Time-Integrating Optical Processors," SPIE Symposium on Optical Processing Systems, Huntsville, 185 (1978).
5. Bader, T. R., "Acoustooptic Spectrum Analysis: A High Performance Hybrid Technique," to be published.
6. Uchida, N. and Niizeki, N., "Acoustooptic Deflection Materials and Techniques," Proc. IEEE 61, 1073 (1973).
7. Eschler, H. and Weidinger, F., "Acousto-Optic Properties of Dense Flint Glasses," J. Appl. Phys. 46 (1975).
8. Uchida, N., "Acoustic Attenuation in TeO_2," J. Appl. Phys. 43, 2915 (1972).
9. Yano, T., Fukumoto, A., and Watanabe , A., "Tellurite Glass: A New Acousto-Optic Material," J. Appl. Phys. 42, 3674 (1971).

Time integrating optical signal processing

P. Kellman

ESL, Incorporated
495 Java Drive
Sunnyvale, California 94086

Abstract. Time integrating acousto-optic processors realize flexible, multipurpose complex signal processing architectures based on correlation algorithms. One- and two-dimensional techniques are presented including examples of spectral analysis and ambiguity function processing. Noncoherent optical processor implementation using interferometric detection with electronic reference is described and experimental results are given.

Keywords. acousto-optics, signal processing, correlators, spectral analysis, ambiguity function, triple-product processor, chirp algorithm.

Optical Engineering 19(3), 370-375 (May/June 1980)

I. INTRODUCTION

Optical techniques for linear signal processing lend themselves naturally to large time-bandwidth product operations due to the high degree of parallelism found in optical systems. Parallel optical signal processing has traditionally exploited spatial integration[1,2] to realize functions such as filtering and spectral analysis. In this manner, the potential time-bandwidth product, or number of cycles integrated, is proportional to the large number of degrees of freedom of the optical system, though a practical limitation is imposed by input and output devices such as light modulators and detectors.

Integration in time rather than space may be used to realize extremely large time-bandwidth products. Time integrating techniques have recently been generalized for one- and two-dimensional complex signal processing.[3-5] Interest in time integrating techniques has resulted due to the attractive device technology as well as flexibility of time integrating algorithms. An important consequence of time integrating techniques is the ability to operate on signals with very large time-bandwidth product without having to store the entire time history as a spatial record. Therefore, an important class of two-dimensional and multichannel processing algorithms may be performed without requiring two-dimensional spatial light modulators. Acousto-optic devices and charge coupled image sensors are particularly well suited for time integrating processor implementation. Further, these signal processing techniques may be realized with either coherent or noncoherent optical systems.

The optical signal processing architectures discussed in this paper are based on acousto-optic or other traveling wave input modulation devices. Time integrating optical correlators were first demonstrated using translating optical masks,[6-9] and scanning detector systems.[7-10] In signal recording applications, time integrating techniques have been used to compensate Doppler shift.[11,12] Time integrating correlator implementation has been demonstrated using acousto-electric surface wave technology.[13] Acousto-optic implementations of one-dimensional time integrating correlation and spectral analysis have first been introduced by Montgomery,[14] Sprague, and Koliopoulos.[15] Two-dimensional time integrating techniques were introduced by Kellman[3,4] and Turpin.[5] In this paper, time integrating acousto-optic signal processing is reviewed, and the concept of interferometric detection with electronic reference is described. These techniques are generalized for complex computation, and examples of spectral analysis and ambiguity function processing are given.

This paper is organized as follows. Time integrating correlation is reviewed in Section 2 and interferometric implementation with electronic reference is described. Time integrating spectral analysis by means of the chirp algorithm is described in Section 3, and the experimental result of a noncoherent optical implementation is given. Two-dimensional processing is presented in Section 4 and examples of ambiguity function processing and spectral analysis are given in Sections 5 and 6.

Original manuscript OD-213 received November 12, 1979.
Accepted for publication December 3, 1979.
This paper was presented at the SPIE seminar on Acousto-Optic Bulk Wave Devices, November 27-29 1979, Monterey, California, and appears in SPIE Proceedings Volume 214

II. TIME INTEGRATING CORRELATION

The one-dimensional time integrating correlator is reviewed. Consider the optical realization shown conceptually in Figure 1. The

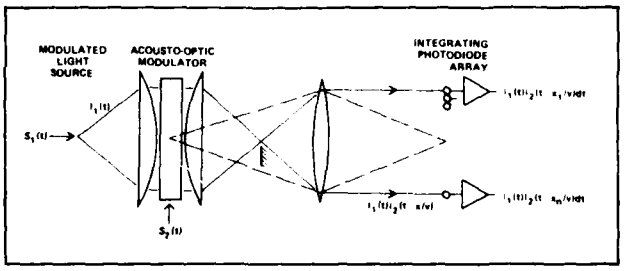

Figure 1. Time integrating correlator.

light source is temporally modulated by a signal, $s_1(t)$, to produce an output intensity $I_1(t)$, which illuminates an acoustic delay line light modulator. A second signal, $s_2(t)$, is introduced into the acoustic cell, which spatially modulates the source intensity by an amount denoted by $I_2(t-x/v)$, where x is the spatial dimension and v is the acoustic velocity. The acoustic signal is schlieren imaged onto a linear photodiode array; the intensity distribution in the image plane is given by the product $I_1(t)I_2(t-x/v)$. Distinction between coherent and noncoherent optical system implementation and interferometric versus noninterferometric detection will be described.

The charge integration, directly proportional to exposure, is performed by detectors at discrete positions, x_i. The resultant output voltage at the i^{th} detector element is therefore:

$$R_{12}(\tau_i) = \int_T I_1(t)I_2(t-x_i/v)dt \qquad (1)$$

where $\tau_i = x_i/v$, and T, the integration time of the detector, is set by the timing of the charge transfer readout register. This is the desired correlation, where I_1 and I_2 are directly related to the input signals s_1 and s_2. Several modulation/detection schemes may be employed in order to achieve a linear relationship.

The range of relative delay between input signals is limited by

the acoustic delay length, and the integration time is set by the detector readout period. The correlator time-bandwidth product, BT, may therefore be larger than the delay line time-bandwidth product, $B\tau$, since the integration time period may be longer than the acoustic delay. In spatial integrating correlators,[16] the integration period is determined by the acoustic delay; in configurations employing fixed reference masks, the range of relative delay is unlimited, however, in correlators with acoustic reference, the range is limited to the acoustic delay. Long integration and flexibility of variable integration are achieved with the time integrating approach.

The achievable processing gain is limited by the correlator dynamic range which is determined by the detector dynamic range and the signal-to-bias ratio. The signal-to-bias ratio depends on the light intensity modulation depth. Detector dynamic range is limited by saturation and is defined as the ratio of saturation level to rms noise. The processing gain and dynamic range can be extended, however, by post-detection digital integration.

In all approaches to time integrating optical correlation, the goal is to achieve a term in the detected light intensity that is proportional to the product of the input signals. Acousto-optic devices modulate optical phase, thus are basically nonlinear modulators of electric field amplitude or intensity. However, linear electric field modulation is approximated at low diffraction efficiency (depth of phase modulation). Linear intensity modulation is approximated by operation with an optical bias at high diffraction efficiency ($\pi/4$ phase shift) and a small signal modulation depth. This latter technique has been exploited by Sprague and Koliopoulous.[15] Interferometric detection may be used when acousto-optic modulation of electric field is linear. In one implementation, a coherent optical reference beam is used for interferometric detection. Another implementation is described that uses an electronic reference to realize interferometric detection with either coherent or noncoherent light. This approach is realized by adding a reference oscillator signal to the acoustic modulation, rather than using a reference beam with separate optical path. The basic difference between the coherent and noncoherent implementation is the spatial and temporal diversity of the illumination. Tolerance to angular and wavelength dispersion is determined by the acoustic diffraction and the Bragg condition. The magnitude transfer function, MTF, is related to the illumination and acoustic field by convolution of their angular spectrums.

In the interferometric schemes, it is assumed that acousto-optic modulation of the electric field is linearly proportional to the drive voltage, and that the imaging optics pass only the first diffraction order. This condition is approximated at low diffraction efficiency. Third order intermodulation may be in band and may contribute to the output. In special cases, these terms time-integrate to zero.

The implementation described uses an internally modulated diode source as shown in Figure 1. A reference oscillator signal is added to the acousto-optic deflector input with a frequency that is offset from the signal modulation; in addition the illumination source must be modulated on a carrier with equal frequency offset. Both single and double sideband modulation are analyzed.

The image intensity distribution, I, is given by the product of the source modulation, I_1, and acousto-optic modulation denoted by $I_2 = |E_2|^2$ where E_2 is the complex electric field modulation.

$$I(t,x) = I_1(t)I_2(t - x/v). \tag{2}$$

For double sideband modulation

$$\begin{aligned} I_1(t) &= A_1\left[1 + \sqrt{2}m_1 s_1(t)\cos(2\pi f_0 t)\right] \\ E_2(t) &= A_2^{1/2}\left[1 + \sqrt{2}m_2 s_2(t)e^{j2\pi f_0 t}\right]e^{j2\pi f_c t} \\ I_2(t) &= |E_2(t)|^2 \\ &= A_2\left[1 + 2m_2^2 s_2^2(t) + 2\sqrt{2}m_2 s_2(t)\cos(2\pi f_0 t)\right], \end{aligned} \tag{3}$$

where f_c is the frequency difference between the reference oscillator at f_c and the double sideband suppressed carrier modulation at $f_c + f_0$. The +1 diffraction order is passed by the imaging optics. A_1 and A_2 correspond to light intensity and diffraction efficiency respectively; m_1 and m_2 are constants that determine the modulation depth. It is assumed that signals s_1 and s_2 are bandlimited to a bandwidth B (i.e., $|S(f)| = 0, |f| > B$), and have unit average power. The spectrum of the input modulation is shown in Figure 2. The device bandwidth is $f_0 + B$.

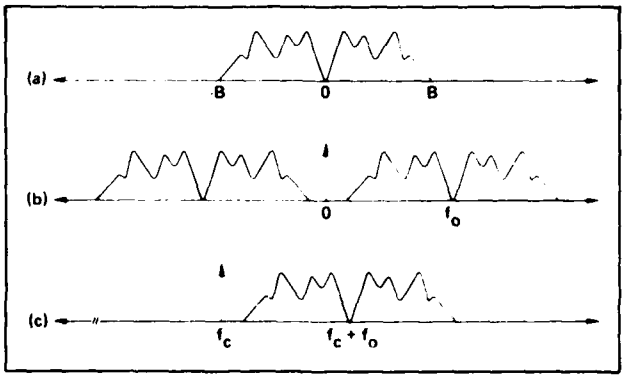

Figure 2. Spectrum of (a) input signal, (b) diode source modulation, and (c) acousto-optic deflector modulation for DSB example.

For $f_0 > 3B$ several cross terms effectively integrate to zero and the output becomes approximately

$$R(\tau) \simeq A_1A_2\left\{T + 2m_2^2 \cdot \int s_2^2(t-\tau)dt + 2m_1m_2\cos[2\pi f_0\tau] \cdot \int s_1(t)s_2(t-\tau)dt\right\} \tag{4}$$

where $\tau = x/v$. The first two terms are bias and the last term is the desired correlation on a spatial carrier, f_0. The bias terms may be eliminated through filtering. The ratio of signal-to-bias for maximum correlation is given by $\beta = 2m_1m_2/(1 + 2m_2^2)$.

For single sideband (SSB) modulation the bandwidth requirement is cut in half. The spectrum of the input modulation is shown in Figure 3. For $f_0 > 3/2$ B the output correlation is approximately:

$$R(\tau) = A_1A_2\left\{\int dt + m_2^2\int\left[s_2^2(t-\tau) + \tilde{s}_2^2(t-\tau)\right]dt + 2m_1m_2(R_{12}(\tau)\cos[2\pi f_0\tau] + \tilde{R}_{12}(\tau)\sin[2\pi f_0\tau])\right\} \tag{5}$$

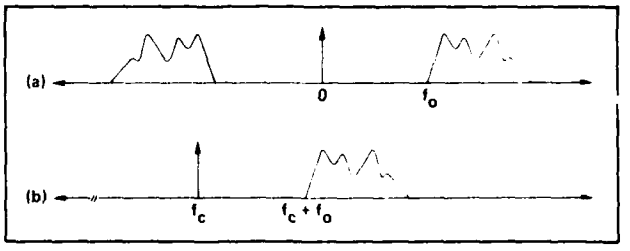

Figure 3. Spectrum of (a) diode source modulation, and (b) acousto-optic deflector modulation for SSB example.

where $R_{12}(\tau)$ is the desired correlation and $\tilde{R}_{12}$ is the Hilbert transform of $R_{12}(\tilde{R}_{12} = R_{12}\tilde{})$. The desired correlation R_{12} may be synchronously detected.

Complex correlation using real computation is described in the following. In general, calculation of complex multiplication or correlation requires four real operations. Alternatively, frequency translation may be utilized to realize complex correlation with a single real correlator at the expense of bandwidth. The time inte-

grating spectrum analyzer described in the next section is an example of complex correlation by this method. Further advantage of correlation at a carrier frequency is the ability to filter the desired correlation from additional bias terms. The expressions for complex correlation are derived in the following.

Define the correlation between complex signals x(t) and y(t) by:

$$R_{xy}(\tau) = \langle x(t)y^*(t-\tau)\rangle \tag{6}$$

where

$$x(t) = x_R(t) + ix_I(t)$$
$$y(t) = y_R(t) + iy_I(t)$$

and $\langle \cdot \rangle$ denotes ensemble average.

$$\mathrm{Re}|R_{xy}(\tau)| = \langle x_R(t)y_R(t-\tau)\rangle + \langle x_I(t)y_I(t-\tau)\rangle$$

$$\mathrm{Im}|R_{xy}(\tau)| = -\langle x_R(t)y_I(t-\tau)\rangle + \langle x_I(t)y_R(t-\tau)\rangle . \tag{7}$$

Consider the real correlation between $x_o(t)$ and $y_o(t)$,

$$R_{x_oy_o}(\tau) = \langle x_o(t)y_o(t-\tau)\rangle$$

$$x_o(t) = \mathrm{Re}\{x(t)e^{i2\pi f_o t}\} \tag{8}$$

$$y_o(t) = \mathrm{Re}\{y(t)e^{i2\pi f_o t}\}$$

where x(t) and y(t) are bandlimited with bandwidth B, and $f_o > B$.

$$R_{x_oy_o}(\tau) \approx \frac{1}{2}\mathrm{Re}\{R_{xy}(\tau)e^{i2\pi f_o\tau}\} . \tag{9}$$

Cross products at the sum frequency $2f_o$ average to zero for $f_o > B$. Thus, the correlation between x_o and y_o is at a carrier frequency f_o, with carrier phase modulated by the phase of R_{xy}, and envelope equal to the magnitude of R_{xy}. The real and imaginary parts of $R_{xy}(\tau)$ may be derived from $R_{x_oy_o}$ by synchronous detection (in quadrature).

III. TIME INTEGRATING SPECTRAL ANALYSIS

An approach to real time optical spectral analysis of electrical signals that uses a time integrating, rather than spatial integrating, version of the chirp z-transform, is described. The large time-bandwidth correlation is accomplished by means of the correlator described in the previous section. A time integrating architecture for correlation and spectral analysis, using oppositely traveling acoustic waves, has been described by Montgomery.[14] For time integrating realizations, frequency resolution is determined by the detector integration period, rather than the acoustic delay length, therefore, higher resolution can be achieved than by spatial integration. Variable resolution is attainable through variable time integration. Use of intensity modulation leads to detection of the magnitude spectrum rather than the power spectrum which yields a considerable increase in dynamic range. This approach to spectral analysis achieves a flexibility not readily achieved by coherent optical spatial methods. The chirp algorithm,[17,18] is reviewed, and the real implementation is discussed.

The Fourier transform integral

$$S(f) = \int s(t)e^{-i2\pi ft}\,dt \tag{10}$$

may be rewritten as

$$S(f) = e^{-i\pi f^2}\int s(t)e^{-i\pi t^2}e^{i\pi(t-f)^2}\,dt , \tag{11}$$

by expressing $f\cdot t$ as $\frac{1}{2}[f^2 + t^2 - (t-f)^2]$. The complex realization is shown in Figure 4. The post-phase weighting may be ignored if only the magnitude or power spectrum is required. This realization

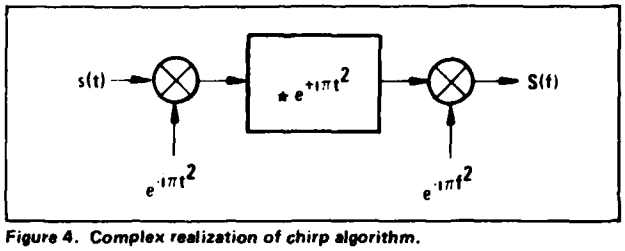

Figure 4. Complex realization of chirp algorithm.

converts the integral transform to time invariant filtering of a preweighted signal, followed by post-weighting.

The chirp algorithm may be realized with a single real correlation by translating the real chirp to a carrier frequency, f_o, greater than the signal analysis bandwidth, B. The desired difference frequency is translated to baseband, and the sum frequency is an out-of-band chirp that integrates to zero. The product of the difference frequency, which is a linear function of delay, and the input signal, is integrated, producing the Fourier transform. The magnitude spectrum corresponds to the detected envelope. The phase modulates the spatial carrier and may be detected as well, resulting in a complex output.

Frequency resolution of this spectrum analyzer is inversely proportional to the detector integration time, T. The resolution is *not* set by the acoustic time delay which typically limits the use of acousto-optical processing to wideband analysis. A wide range of integration times are easily realized (0.1–100 msec) using self-scanned arrays of moderate size (e.g., 1024). Integration time periods can be extended by means of electronic accumulation.

The delay line length, τ, and the number of detectors, N, set the delay, $\Delta\tau$, between detector elements in the image plane. This determines the chirp bandwidth B'. The required resolution or integration period fixes the chirp rate, α, (see Figure 5). The spatial

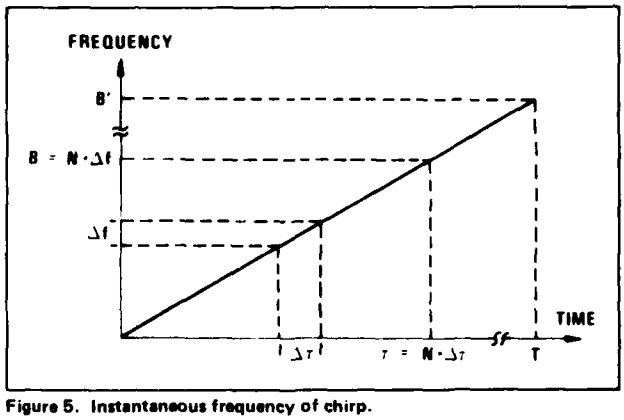

Figure 5. Instantaneous frequency of chirp.

bandwidth equals the chirp bandwidth, B', plus carrier frequency, f_o. Let k be the number of samples (detectors) per cycle of the highest frequency (k = 2 for Nyquist sampling), and define k' as the ratio of frequency offset to chirp bandwidth, f_o/B'. The above relationships may be written as:

$$N = k(f_o + B')\tau$$
$$\alpha = B'/T = B/\tau$$
$$k' = f_o/B' \geq 1 . \tag{12}$$

The time-bandwidth product is, therefore

$$BT = N/k(1+k') < N/4 . \tag{13}$$

The dynamic range is limited by detection noise. If there are M distinguishable levels in the output voltage between the noise floor and the photo element saturation value, and if β is the maximum ratio of signal-to-bias, then the dynamic range in dB is given by 20 $\log_{10} M\beta/(1+\beta)$, since incident exposure is directly proportional to spectral magnitude. This results in a considerable increase in dynamic range as compared to coherent optical power spectral analysis in which incident exposure is related to spectral power density and the dynamic range is given by 10 $\log_{10}$M.

An experimental breadboard was constructed using a noncoherent implementation with a light emitting diode source. The modulation was double sideband and the chirps had octave bandwidth (k′=1). The correlator output for a sine wave input is shown in Figure 6. In this photograph the envelope is observed since the

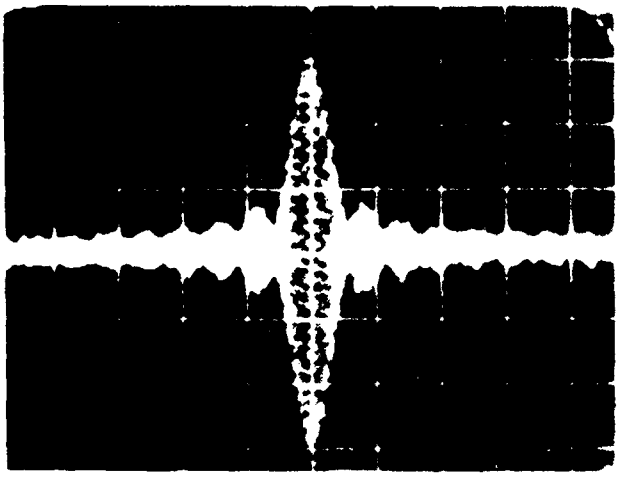

Figure 6. Time integrating spectrum analyzer output.

exposure covers multiple integration periods in which the signal phase is changing. Parameters of this example were: N = 1000, τ=40 μsec, B′=2.5 MHz, T=2 msec, BT=100, k=5, k′=1. The signal-to-bias ratio, β, was 20% and the detector dynamic range (peak to rms) was M=1000. The dynamic range observed was 40 dB (βM/2) since the bias was set at M/2 rather than optimized at M/(1+β). The dynamic range is 3 dB greater using SSB input modulation.

IV. TWO-DIMENSIONAL PROCESSING

Two-dimensional integral transforms, for which the kernel is decomposable in the proper way, may be implemented by time integrating optical processing. Two important examples are ambiguity plane processing and spectral analysis.

Consider the optical realization shown conceptually in Figure 7. The optical train has a modulated illumination source, two acoustic delay line light modulators, and a matrix array of detectors. This configuration may be employed for several functions, determined by input signal and reference waveforms. It is assumed throughout this discussion that two-dimensional processing is applied to either very long one-dimensional signals or to two-dimensional signals (e.g., imagery) that are in raster format. In this way, the input will be a function of one variable, t; the output $R(\tau_1,\tau_2)$ is a function of two variables.

The light diffracted by the first acousto-optic modulator A01, is diffracted by the second, A02, in an orthogonal direction. Both acoustic signals are imaged on the detector plane. The desired image plane intensity distribution has a term proportional to the product of acoustic signals, $s_1(t-\tau_1)s_2(t-\tau_2)$, where $\tau_1=y/v$ and $\tau_2=x/v$ are time variables. The resultant detected output voltage is proportional to the integrated charge as in the previously described

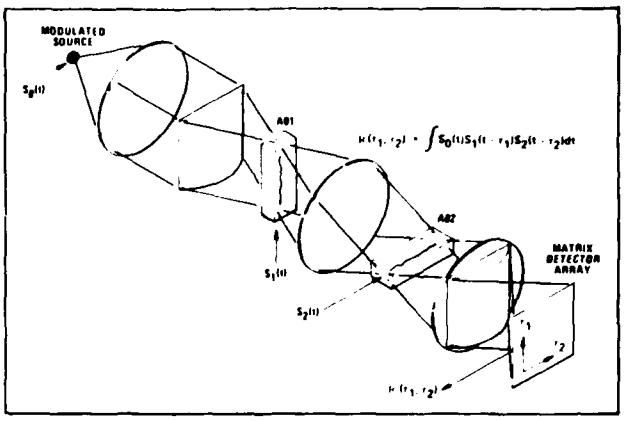

Figure 7. Two-dimensional time integrating optical processor.

correlator. This structure implements integrals of the form:

$$R(\tau_1,\tau_2) = \int_\Gamma s_0(t)s_1(t-\tau_1)s_2(t-\tau_2)dt \ . \tag{14}$$

In this configuration, all signals are real. In order to perform complex computation, similar considerations apply that were given for one-dimensional processing.

Hybrid realizations that use a combination of spatial and time integration can be used to implement a variety of other operations. An example of spectral analysis utilizing spatial integration for coarse resolution and time integration for fine resolution is described by Bader.[19]

The two-dimensional time integrating optical processor may be implemented with several modulation/detection schemes. A description of a coherent optical implementation using an interferometric optical reference has been given by Turpin.[5] Noncoherent implementation using an intensity modulated light emitting diode offers immunity to noise suffered in coherent imaging. Noncoherent optical implementation using a reference oscillator for interferometric detection may be used to realize complex operation. Input modulation must be designed such that undesired terms are out of band.

The next examples demonstrate the strength of two-dimensional time integrating processors.

V. AMBIGUITY FUNCTION PROCESSING

Ambiguity function processing is important in resolution of delay and Doppler uncertainty. In application to radar signal processing or external signal parameter measurement, delay and Doppler are often time-varying. An ambiguity function snapshot is therefore desirable. A noncoherent optical parallel processing implementation for achieving such a snapshot is given in this section.

This example utilizes the 2-D optical system shown in Figure 7 which was generalized in the last section. The cross ambiguity function between complex signals x(t) and y(t) may be defined as

$$A_{xy}(\tau,f) = \int_0^T x(t)y^*(t-\tau)e^{-j2\pi ft}\,dt \tag{15}$$

where the variables τ and f may be interpreted as delay and Doppler, respectively. A real implementation of the complex cross-ambiguity function is described that uses the architecture of Section 4. The spectral analysis operation is performed using the chirp algorithm. Complex correlation was derived in Section 2 and is easily extended to two-dimensional computation.

Define the complex input signals $s_0(t)$, $s_1(t)$, and $s_2(t)$ by

$$s_0(t) = x(t)e^{-i\alpha\pi t^2}$$

$$s_1(t) = y^*(t)$$
$$s_2(t) = e^{i\alpha\pi t^2} \quad , \qquad (16)$$

and consider the interferometric implementations of Section 2 with electronic reference. In the case of complex inputs, the intensity modulation is given by

$$I_0(t) = A_0\left[1 + \sqrt{2}m_0 \mathrm{Re}\left\{s_0(t)e^{i2\pi f_0 t}\right\}\right]$$
$$I_1(t) = A_1\left[1 + 2m_1^2|s_1(t)|^2 + 2\sqrt{2}m_1 \mathrm{Re}\left\{s_1(t)e^{i2\pi f_1 t}\right\}\right]$$
$$I_2(t) = A_2\left[1 + 2m_2^2|s_2(t)|^2 + 2\sqrt{2}m_2 \mathrm{Re}\left\{s_2(t)e^{-i2\pi f_2 t}\right\}\right] \qquad (17)$$

where double sideband modulation is assumed. The integrated intensity, $R(\tau_1,\tau_2)$,

$$R(\tau_1,\tau_2) = \int_0^T I_0(t)I_1(t-\tau_1)I_2(t-\tau_2)dt \qquad (18)$$

contains the desired ambiguity function term,

$$\mathrm{Re}\left\{A_{xy}(\tau_1,\alpha\tau_2)e^{-i[2\pi(f_1\tau_1 - f_2\tau_2) + \alpha\pi\tau_2^2]}\right\} , \qquad (19)$$

which is at a carrier frequency and may be filtered from other cross-product terms. The quadratic phase term may be cancelled through post-detection weighting. The variables τ_1 and τ_2 correspond to delay and Doppler respectively. The Doppler resolution is commensurate with the integration time; the analysis bandwidth is determined by Eq. (13). A coarse resolution may be maintained during a signal acquisition period, and a higher resolution zoom can be achieved by longer integration. Multiple correlation peaks or targets can be processed simultaneously since a linear system implementation is used.

Ambiguity function processing was demonstrated using the noncoherent optical implementation shown in Figure 7. Devices included a Hitachi HLP-20 light emitting diode, Fairchild SL62926 charge coupled device image sensor, and Isomet acousto-optic devices. The diode has a 30 MHz 3 dB bandwidth and was biased at an average optical power of approximately 10 mW. The image sensor has 380×488 elements and was operated with an integration period of 33.34 msec. The acousto-optic devices have a 30 MHz 1 dB bandwidth and 50 μsec delay. Chirp waveforms of very large time-bandwidth product ($BT \leq 2^{19} = 524{,}288$) were synthesized digitally. The delay range was limited to 36×27 μsec (4:3 aspect ratio) to increase the signal bandwidth. The image plane sampling was, therefore, 380÷36 μsec ≅ 10.6 MHz in one delay dimension and 488÷27 μsec ≅ 18.1 MHz in the other dimension. The overall system frequency response (MTF) was approximately 3 dB lower at the Nyquist limit (2 samples per cycle) 5 and 9 MHz, respectively. An example ambiguity function of a short psuedo-random code is shown in Figure 8. The Doppler range was 1-3.5 kHz determined by the chirp rate. The code repetition period was 6.2 μsec (31 length, 5 MHz rate), therefore, 4 correlation peaks are evident in the ambiguity function; the Doppler was 2 kHz. The time bandwidth product was 5 MHz × 33.34 msec = 166,700. No post-detection processing has been applied to the output video. A signal dependent bias variation, proportional to the pairwise cross-correlations between inputs, has not been filtered. The image has several blemishes due to the CCD camera. The sensor dynamic range is approximately 60 dB, and the maximum signal-to-bias ratio was 25%; the resultant input signal dynamic range was, therefore, 48 dB.

VI. SPECTRAL ANALYSIS

A noncoherent optical time integrating approach to two-dimensional complex spectral analysis is described. This method is an extension of the technique described for one-dimensional

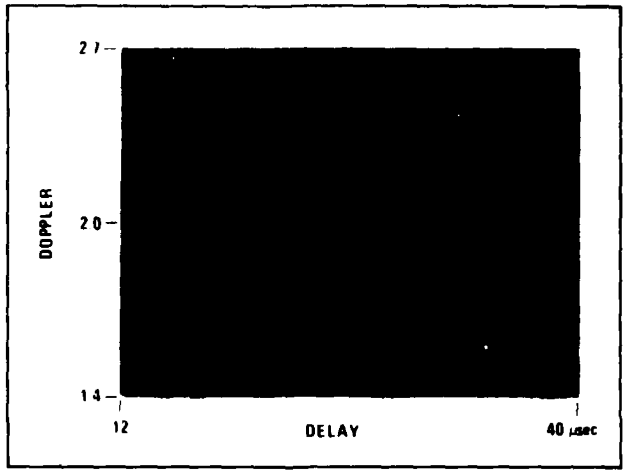

Figure 8. Ambiguity function for short code.

analysis. Very large time-bandwidth (greater than 10^5) spectral analysis of electrical signals can be performed using this time domain approach, without requiring storage of the signal. Spectral analysis of raster scanned video imagery can be performed as well.

The optical system (Figure 7) described in the last sections is used in this example as well. The algorithm is implemented with three reference chirp waveforms. The source is modulated with the input signal, which is premultiplied by a chirp, and the other chirps modulate A01 and A02. The chirp rates are chosen such that the product of the three chirps result in a temporal sine wave, with frequency that is varying from pixel to pixel on the detector array. Each detector element integrates the product of this sine wave times the input signal, and, in this fashion, produces the spectrum. The frequency difference between output lines in one dimension is taken to be N times the frequency difference between lines in the other dimension, where N is the number of detectors per line. For a square array, the number of spectral samples is proportional to N^2. The technology is currently limited by detector array size, and detector readout rate.

A two-dimensional chirp algorithm with three complex reference chirps is described next. The real implementation is performed with frequency offset chirps, similar to the previous examples. Define the transform (optical processor output) by

$$R(\tau_1,\tau_2) = \int_{-NT/2}^{NT/2} s(t)a(t)b(t-\tau_1)c(t-\tau_2)dt \qquad (20)$$

where

$$a(t) = \sum_n e^{-j\alpha\pi(t-nT)^2}\, \mathrm{rect}\left(\frac{t-nT}{T}\right)$$
$$b(t) = e^{j\alpha\pi t^2/N}\, \mathrm{rect}(t/NT)$$
$$c^*(t) = a(t)\, b(t) \ . \qquad (21)$$

Waveforms a(t) and c(t) are periodic chirps with period T and chirp rates α and $\alpha(N-1)/N$, respectively. Waveform b(t) is a low rate chirp with period NT and rate α/N. The chirp rates are chosen such that a constant difference frequency, $f = \alpha[\tau_1 + (N-1)\tau_2]/N$, is generated by the product $a(t)b(t-\tau_1)c(t-\tau_2)$. Frequency discontinuities occur during intervals $nT < t < nT + \tau_2$ due to the chirp transition traversing the acoustic delay aperture. This effectively reduces the integration time by the factor $(T-\tau_2)/T$. However, this may be completely compensated by increasing the chirp bandwidth. This effect is ignored in the following analysis, thus

$$a(t)b(t-\tau_1)c(t-\tau_2) = \sum_n e^{j[2\pi\alpha nT\tau_2 - 2\pi\alpha t[\tau_1 + (N-1)\tau_2]/N + \phi(\tau_1,\tau_2)]} \cdot \mathrm{rect}\left(\frac{t-nT}{T}\right)\mathrm{rect}\left(\frac{t}{NT}\right) \quad (22)$$

where

$$\phi(\tau_1,\tau_2) = \alpha\pi\left[\tau_1^2 + (N-1)\tau_2^2\right]/N \ .$$

The spectral phase weighting, $\phi(\tau_1,\tau_2)$ may be compensated post-detection. Equation (20) becomes

$$R(\tau_1,\tau_2) = e^{j\phi}\int NT\,\mathrm{sinc}(Tf)\,S\left[f-\alpha[\tau_1+(N-1)\tau_2]/N\right] \cdot \sum_n \mathrm{sinc}\left[NT(f+\alpha\tau_2-n/T\right]df \ . \quad (23)$$

As evidenced by the term $S[\alpha(\tau_1 + (N-1)\tau_2)/N]$, the variables τ_1 and τ_2 may be interpreted as fine and coarse frequency, respectively. Integration over N chirp repetitions has created a comb sampling along the coarse frequency axis, with comb samples a function of the fine frequency axis. The spectral resolution is proportional to 1/NT where NT is the total integration period.

VII. SUMMARY

Time integrating optical techniques for one- and two-dimensional complex signal processing have been described. Signal processing architectures utilizing actively generated reference waveforms such as chirps realize a wide range of algorithms and variable time integration allows further flexibility. Particularly attractive is the multipurpose capability of the time integrating optical processor, e.g., the same optical system is used for both spectral analysis and ambiguity function processing.

The technique of interferometric detection with electronic reference was described. In this implementation, a local oscillator is added to the acoustic modulation rather than a coherent optical reference added to the image. This method, therefore, permits noncoherent optical implementation, with the advantages of directly modulated diode light sources and increased immunity to artifacts of coherent optical imaging systems. The correlation is performed at a carrier, thereby enabling complex operation. Furthermore, the interferometric method circumvents the difficult requirement for acoustic modulation at a high diffraction efficiency bias point, that is necessary for linear operation in the noninterferometric technique.

The optical implementation, utilizing acousto-optic input and integrating image sensor output devices, creates a processor that is highly compatible with signal processing systems. Such implementation affords very large time-bandwidth product signal processing without the input signal storage requirement associated with spatial integrating methods. The requirement for high resolution, large dynamic range output image sensors becomes the key device limitation. Acousto-optic devices are available with time-bandwidth product much greater than the number of resolvable image samples.

The key attributes of time integrating techniques are summarized in the following: extremely large time-bandwidth correlations may be performed, independent of the device time-bandwidth product; a flexible, multipurpose processor is realized by use of actively generated reference waveforms and variable time integration; an important class of two-dimensional algorithms, including complex spectral analysis and ambiguity function processing, may be performed without having to store the entire time history as a spatial record; the system may be implemented with noncoherent diode sources, acousto-optic devices, and integrating image sensors.

ACKNOWLEDGMENT

The author acknowledges funding support by ESL, Incorporated under the Internal Research and Development program and by the Air Force Office of Scientific Research under contract F49620-78-C-0102.

REFERENCES

1. L. J. Cutrona, E. N. Leith, C. J. Palermo, and L. J. Porcello, "Optical Data Processing and Filtering Systems," IRE Trans. Info. Theory, Vol. IT-6, pp. 386-400, June 1960.
2. J. W. Goodman, "Operations Achievable with Coherent Optical Information Processing Systems," Proc. IEEE, Vol. 65, pp. 29-38, January 1977.
3. P. Kellman, "Detector Integration Acousto-Optic Signal Processing," Proc. Int. Optical Computing Conf., London, England, pp. 91-95, September 1978.
4. P. Kellman, "Time Integrating Optical Processors," *Optical Processing Systems*, Proc. Soc. Photo-Opt. Instr. Eng. 185, 130-139 (1979).
5. T. Turpin, "Time Integrating Optical Processors," *Real-Time Signal Processing*, Proc. Soc. Photo-Opt. Instr. Eng. 154, 196-203 (1978).
6. C. Skenderoff, et al., "Radar Receiver Having Improved Optical Correlator Means," U.S. Patent 3 483 557, December 1969.
7. A. J. Talamini, Jr. and E. C. Farnett, "New Target for Radar: Sharper Vision with Optics," Electronics, Vol. 38, pp. 58-66, December 1965.
8. J. K. Parks, "Optical Correlation Detector for the Audio Frequency Range," J. Acoust. Soc. Amer. 37, 268-277 (1965).
9. K. Bromley, "An Optical Incoherent Correlator," Opt. Acta 21, 35-41 (1974).
10. M. A. Monahan, R. P. Bocker, K. Bromley, and A. Louie, "Incoherent Electro-Optical Processing with CCD's," in Dig. Int. Optical Computing Conf. (Washington, DC) (IEEE Catalog 75 C40941-5C), April 1975.
11. M. Arm, M. King, A. Aimette, and L. B. Lambert, in *Proceedings of the Symposium on Modern Optics*, F. Fox, Ed. (Polytechnic Press, Brooklyn, NY, 1967), pp. 691-702.
12. J. W. Goodman, "Temporal Filtering Properties of Holograms," Appl. Optics 6, 857-859 (1967).
13. R. W. Ralston, D. H. Hurlburt, F. J. Leonberger, J. H. Cafarella, and E. Stern, "A New Signal-Processing Device, The Integrating Correlator," 1977 Ultrasonics Symposium Proceedings, New York, pp. 623-628.
14. R. M. Montgomery, "Acousto-Optical Signal Processing System," U.S. Patent 3 634 749, January 1972.
15. R. A. Sprague and C. L. Koliopoulos, "Time Integrating Acousto-Optic Correlator," Appl. Optics 15, 89-92 (1976).
16. R. Sprague, "A Review of Acousto-Optic Signal Correlators," Optical Engineering 16, 467-474 (1977).
17. L. R. Rabiner, R. W. Schafer, and C. M. Rader, "The Chirp Z-Transform Algorithm and Its Application," Bell System Technical Journal, pp. 1249-1292, May-June 1969.
18. H. J. Whitehouse, R. W. Means, and J. M. Speiser, "Signal Processing Architectures Using Transversal Filter Technology," Proceedings of the IEEE Symposium on Circuits and Systems, Boston, April 1975.
19. T. R. Bader, "Coherent Optical Hybrid Techniques for Spectrum Analysis," *Optical Processing Systems*, Proc. Soc. Photo-Opt. Instr. Eng. 185, 140-146 (1979).

Coherent hybrid optical processors

T. R. Bader
ESL Incorporated, Sunnyvale, California 94086

Abstract

Utilization of both space and time integration in acousto optic signal processing overcomes some of the limitations of purely space integrating and purely time integrating techniques. A one-dimensional configuration for coherent hybrid spectrum analysis is used to show that this approach exhibits superior dynamic range characteristics, including a unique sidelobe suppression property. A coherent hybrid ambiguity function processor is discussed to illustrate the important advantages that may be exploited by using both space and time integration in delay-Doppler plane processing.

Introduction

Acousto-optic techniques are becoming increasingly attractive for wide band parallel processing because of the real-time capability, the maturing system architectures and components, and the potential for small size and low power requirements. Time integration techniques [1-4] in one and two dimensional systems have overcome some of the device-related limitations by permitting long time processing for spectrum analysis, correlation, ambiguity function processing and other two-parameter processes. Hybrid space/time integration approaches [5-6] have been shown to retain some important characteristics of space integration and permit extended time processing by time integration. This paper presents a summary of some recent results on hybrid space/time integration approaches to signal processing. Two topics are addressed. First, some further considerations of coherent hybrid spectrum analysis are presented, emphasizing aspects of system dynamic range. It is shown that the combination of space and time integration leads to a superior performance that makes this approach attractive even for one-dimensional systems. Most noteworthy is the unique behavior of hybrid systems of suppressing sidelobes.

The second part of this paper extends the coherent hybrid approach to the generation of cross ambiguity functions. It is shown that the combination of space and time integration here also leads to superior performance in dynamic range and signal handling ability.

Spectrum Analysis

A relatively simple but highly successful application of acousto optics in signal processing is the familiar acousto optic power spectrum analyzer. This is referred to as a space integrating technique because the Fourier transform integral is over a spatial coordinate. The usefulness of such a technique derives from the fact that processing of many channels is performed in parallel over a wide bandwidth. Important limitations encountered with this approach are that the frequency resolution is limited to the inverse of the acoustic transit time, the number of channels is limited to the time-bandwidth product of the device, and the dynamic range is frequently severely limited by the detector noise, since the detector senses the signal power.

Time-integrating AO techniques overcome these limitations by coherent detection of the signal by many local oscillators distributed over the signal band. Here the complex spectral amplitude is detected so that the detector noise is significantly less important. The frequency resolution is the inverse of the integration time and is (along with the analysis bandwidth) electronically scaleable. The number of parallel channels can be extended in two dimensions to the product of the time-bandwidth products of two Bragg cells. Time-integrating techniques, however, have their own limitations, including the constraint to lower bandwidths and a dynamic range that degrades as the number of occupied channels increases.

Previous studies [5,6] have shown that hybrid configurations utilizing both space and time integration can retain important performance characteristics of both space and time integrating approaches. Here we continue the discussion of hybrid spectrum analysis by describing a one dimensional configuration, focusing on the characteristics that principally affect the system's dynamic range. Such a system is shown schematically in Figure 1.

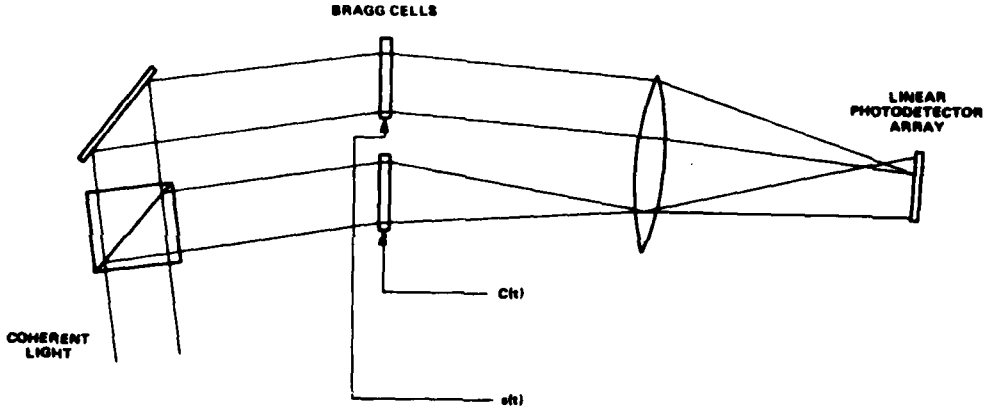

Figure 1. One dimensional coherent hybrid spectrum analyzer

Coherent light is diffracted from two Bragg cells, one driven by the signal and the other by a periodic chirp, such that they are both Doppler-shifted in the same direction. Both optical waves are Fourier transformed by a lens onto a detector array, where they interfere to form a fringe complex. This fringe pattern is integrated over time T_1 equal to the Bragg cell delay time. The resulting exposure is a sampling of the signal's amplitude spectrum on a spatial carrier determined by the mean relative angle between the incident waves.

The signal in Figure 1 is assumed to lie in the band of the Bragg cell. If v is the acoustic velocity, x is the coordinate in the detector plane and z is the coordinate in the Bragg cell driven by signal s t), the amplitude at the detector is

$$S(x,t) = \int_{vT_1} s(t + z/v)\, e^{-i2\pi\alpha xz}\, dz = c\int e^{i2\pi f' t} u(f')\, \text{sinc}\, \pi T_1(\alpha vx - f')\, df' \qquad (1)$$

where u(f) is the signal amplitude spectrum, $\alpha = 1/\lambda F$, λ is the optical wavelength and F is the focal length of the lens. Consider a CW signal of frequency f. Then

$$S(x,t) = S_o e^{i2\pi ft}\, \text{sinc}\, \pi T_1(\alpha vx - f). \qquad (2)$$

The periodic chirp, unlike the time-integrating techniques, has a chirp length and period equal to the Bragg cell delay T_1. Its bandwidth represents the system's analysis bandwidth and can be as large as that of the Bragg cell. The Fourier transform of the light diffracted from this periodic chirp can be considered a local oscillator in the detector plane that has a frequency that is a linear function of position on the array. It can be approximately described, as shown in the Appendix by

$$R(x,t) = R_o \sum_p e^{i2\pi pt/T_1 + i\Omega(p)}\, \text{sinc}\, \pi T_1[\alpha vx - p/T_1] \qquad (3)$$

The normalized exposure after some time $T_2 \geq T_1$ is

$$E(x) = \frac{1}{T_2}\int_{-T_2/2}^{T_2/2} |R(x,t)e^{ikx} + S(x,t)|^2\, dt$$

$$= |R_o|^2 + |S_o|^2\, \text{sinc}^2 \pi T_1(\alpha vx - f)$$

$$+ 2|R_o S_o| \sum_p \text{sinc}\pi T_2(f - p/T_1)\ \ \text{sinc}\pi T_1(\alpha vx - p/T_1)$$

$$\times\, \text{sinc}\pi T_1(\alpha vx - f)\ \ \cos[kx + \psi + \Omega(p)]. \qquad (4)$$

When $T_2 = T_1$ it can be shown that the Whittaker-Shannon sampling theorem leads to the identity

$$\sum_p e^{i\Omega(p)}\ \mathrm{sinc}\pi T_1[f-p/T_1]\ \mathrm{sinc}\pi T_1[\alpha vx-p/T_1] = e^{i\Omega(\alpha vxT_1)+i2\pi\nu_o\alpha vx}\ \mathrm{sinc}\pi T_1[f-\alpha vx] \quad (5)$$

where $\nu_o = (f-f_m)T_1/\Delta f$; f_m and Δf are the minimum frequency and width of the band. Substitution of Equation 5 into Equation 4 yields the signal term

$$E_s(x) = 2|R_oS_o|\ \ \mathrm{sinc}^2\pi T_1[\alpha vx - f]\ \ \cos[kx + \psi + \Omega'(\alpha vxT_1)]. \quad (6)$$

Thus the signal envelope, the peak of which is proportional to $|S_o|$, has a sinc^2 form, rather than sinc as in the time-integrating and space integrating techniques. An important consequence of this is that the sidelobes are down by a factor of two in dB compared with those techniques. Sidelobes of the very bright zero order (undiffracted by the acoustic wave) that extend into the signal band are similarly suppressed. This inherent sidelobe suppression is the result of the combined effect of the localization of the signal illumination at the detector by spatial integration (i.e., the optical Fourier transform) and localization of the interference fringe pattern by time integration. In real space integrating and time integrating systems the profile of a spectral line is not actually a sinc function but is modified by the apodization of the optical wave illuminating the Bragg cell, among other things. Similar apodizing behavior applies to hybrid systems; moreover, if $P(\alpha vx-f)$ is the profile of the spectral amplitude for a space or time integrating spectrum analyzer, that for a hybrid system can be shown to be $P^2(\alpha vx-f)$.

A source of noise in optical processors that can limit the dynamic range is light scattered from optical elements, particularly the Bragg cells. Such scattered light is not Doppler shifted, and therefore in time integrating and hybrid systems, the only terms in the exposure that do not integrate to zero are products containing only scatter elements. If $s_n(x)$ and $r_n(x)\exp(ikx)$ are the scatter amplitude components at the detector, the exposure term $2|s_n\ r_n|\cos(kx+\phi)$ has a smaller variance than the signal power by a factor $\overline{|s_n\ r_n|^2}\ /\ |R\ S|^2$. Therefore the dynamic range referred to scatter noise is twice as large (in dB) for systems using time integration than for purely space integrating systems. The $|s_n|^2$ and $|r_n|^2$ terms are also small, but are furthermore at low spatial frequencies, out of the signal band).

It will be noted that in Eq. 4 the bias term contributed by the signal is localized and does not contribute a bias to other signals in the band. Unlike time integrating techniques that exhibit reduced dynamic range for multiple signals because of a uniform bias contributed by each signal, hybrid techniques retain a high multiple signal or broad band capability.

Let us now consider the dynamic range as limited by detector noise. The output voltage of a linear detector array is proportional to the exposure, where we can write

$$V(x) = \alpha|R|^2 + \alpha|S|^2 + 2\alpha|RS|\cos\phi(x)\ .$$

The signal term remaining after bandpass filtering is

$$V_s(x) = 2\alpha|RS|\cos\phi(x)\ .$$

This is a maximum when $\alpha|R|^2 = \alpha|S_M|^2 = V_{sat}/4$, where V_{sat} is the saturation voltage. Thus the maximum detected signal power is

$$\overline{|2\alpha RS_M\cos\phi(x)|^2} = V^2_{sat}/8\ .$$

We define the minimum detected signal power to be

$$\overline{|2\alpha RS_m\cos\phi(x)|^2} = \sigma^2\ ,$$

where σ is the rms detector noise over one frequency resolution element. The dynamic range related to detector noise is therefore

$$DR \equiv |S_M/S_m|^2 = (V_{sat}/\sigma)^2/8\ .$$

A space integrating power spectrum analyzer has a dynamic range $DR_o \equiv V_{sat}/\sigma$ so that the advantage in dynamic range of interferometric techniques is described by the relationship

$$DR = (DR_o)^2/8 \quad .$$

This advantage is directly analogous to the well-known improvement in dynamic range of optical heterodyne detection compared with direct detection.[7]

Ambiguity Function Processing

Two dimensional AO techniques have been found useful for simultaneous display of time delay and Doppler shift of two signals in the form of their cross-ambiguity function

$$\chi[\tau,f] = \int_{-\infty}^{\infty} S_1(t) S_2^*(t-\tau) e^{-i2\pi ft}\, dt \quad . \tag{7}$$

There are numerous implementations [2-4] of time integrating techniques, both coherent and incoherent, all of which are characterized by the property that the detector is in an image plane of one or both of the Bragg cells driven by the signals. Let T_1 be the Bragg cell delay. The exposure of the two dimensional detector with coordinates τ and f after time T_2 is generally of the form

$$E(\tau,f) = B + C + \operatorname{rect}_{\varepsilon T_1}\tau \; \chi[\tau,f] * \operatorname{sinc}\pi T_2 f \cos(k\tau + \phi), \tag{8}$$

where "*" signifies convolution, B is a bias term that is more or less uniform over the detector, C is a zero mean correlation noise, the rect function reflects the delay range limitation to the Bragg cell delay (ε = 1 or 2, depending on the particular implementation) and the sinc function indicates that the Doppler Rayleigh resolution is the inverse of the integration time. The cos term represents a spatial carrier that has been arbitrarily chosen to be in the τ direction.

Let us consider as an example a long pseudorandom signal of bandwidth Δf_s. The cross ambiguity function between the signal and a shifted and delayed version over a time window T_2 is shown schematically in Figure 2, exhibiting[6] the familiar "thumbtack" shape with a sharp peak of width $1/\Delta f_s$ and $1/T_2$ in the delay and Doppler direction respectively, (when the peak is not too far from the center). The correlation noise or self-clutter is spread over a delay and Doppler area $\Delta f_s T_2$. Figure 3 shows the cross-ambiguity function measured by a time integrating processor integrating for time T_2. It is a small area cut out of the function of Fig. 2, where the delay range is limited by the Bragg cell delay, according to Eq. 7, and the Doppler range is chosen for convenience. The bias term is also included. A point to be noted is that if one of the two signals to be processed contains more than one delayed or shifted component, each component adds a bias contribution, thus reducing the dynamic range per component in a manner analogous to the multiple signal dynamic range reduction in time integrating spectrum analyzers.

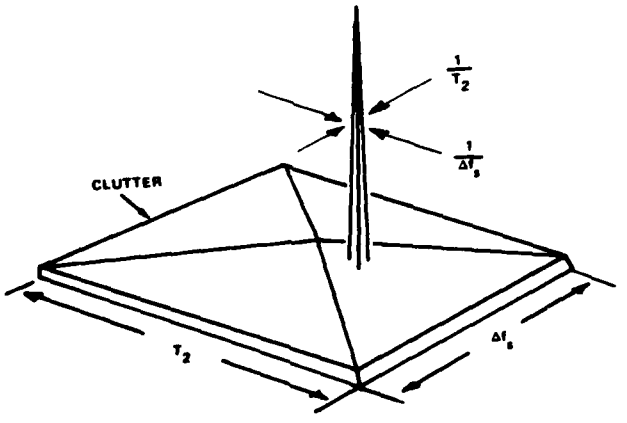

Figure 2. Cross Ambiguity Function of a Pseudorandom Signal

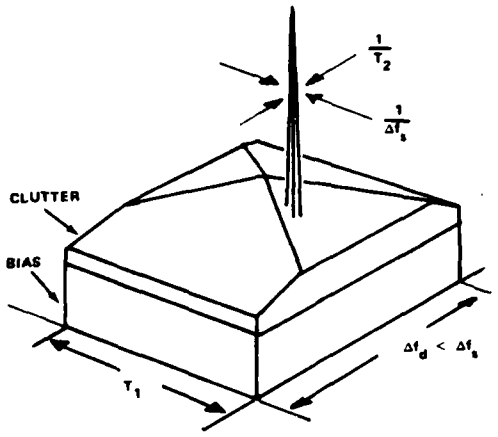

Figure 3. Cross Ambiguity Function for Time Integrating Processor

Space integrating techniques [4,9] have been used to generate the cross ambiguity function; the constraint encountered when acousto-optic devices are used in real time is that the Doppler resolution is limited to the inverse of the Bragg cell delay time. Furthermore, unless the optical wave is coherently detected the technique suffers from the same dynamic range limit as a power spectrum analyzer; that is, the absolute square of the ambiguity function is detected, permitting the detector noise to be a more serious problem.

The combination of space and time integration can be applied to ambiguity function processing to provide improved performance. Consider the optical schematic of Figure 4. It consists basically of a space integrating ambiguity function generator designed to facilitate expansion of the Doppler coordinate so that a small portion of the Doppler range fills the detector array and a spatially distributed local oscillator that provides a coherent reference for time integration. The first Bragg cell driven by $S_1(t)$ is imaged with magnification m_1 onto the second cell orthogonal to it, driven by $S_2(t)$. Diffraction orders of the two cells of opposite sign are selected. This image plane is rotated by angle θ with respect to coordinates x and y with respect to which Fourier transformation and imaging with magnification m_2, respectively, are performed. The resulting optical amplitude at the detector is

$$A(\tau,f;t) = ce^{-i\psi(\tau,f)} \operatorname{rect}\frac{\tau}{2T_1} \left\{ \chi(\tau,f)\, e^{i2\pi f(t-\tau/2)} \right\} * P(\tau,f) , \tag{8}$$

where

$$\tau = y\cos\theta / vm_1m_2 \quad , \quad f = xv/(\lambda F\cos\theta)$$

are the delay and Doppler coordinates, respectively, F is the focal length of the transform lens, and where

$$P(\tau,f) = (T_1 - |\tau|)\ \operatorname{sinc}\pi(T_1 - |\tau|)f$$

represents the Doppler resolution function. The best resolution is seen to be $1/T_1$ corresponding to small delays.

The objective of the hybrid scheme is to cut out a small band of the ambiguity function, reducing the Doppler range, and improve the Doppler resolution by time integration. Adding the reference wave R exp $i[2\pi(v/\lambda F)xt - kx]$ and integrating the absolute square of the result over time $T_2 \gg T_1$ leads to an exposure

$$E(\tau,f) = R^2 + \left|c[T_1-|\tau|]\ \chi(\tau,f)\right|^2 * \operatorname{sinc}^2\pi T_1 f$$

$$+ 2R[T_1-|\tau|]\left|c\chi(\tau,f) * \operatorname{sinc}\pi T_2 f\right| \cos(k'x+\psi')$$

$$\text{for} \quad |\tau| \leq T_1 \quad . \tag{9}$$

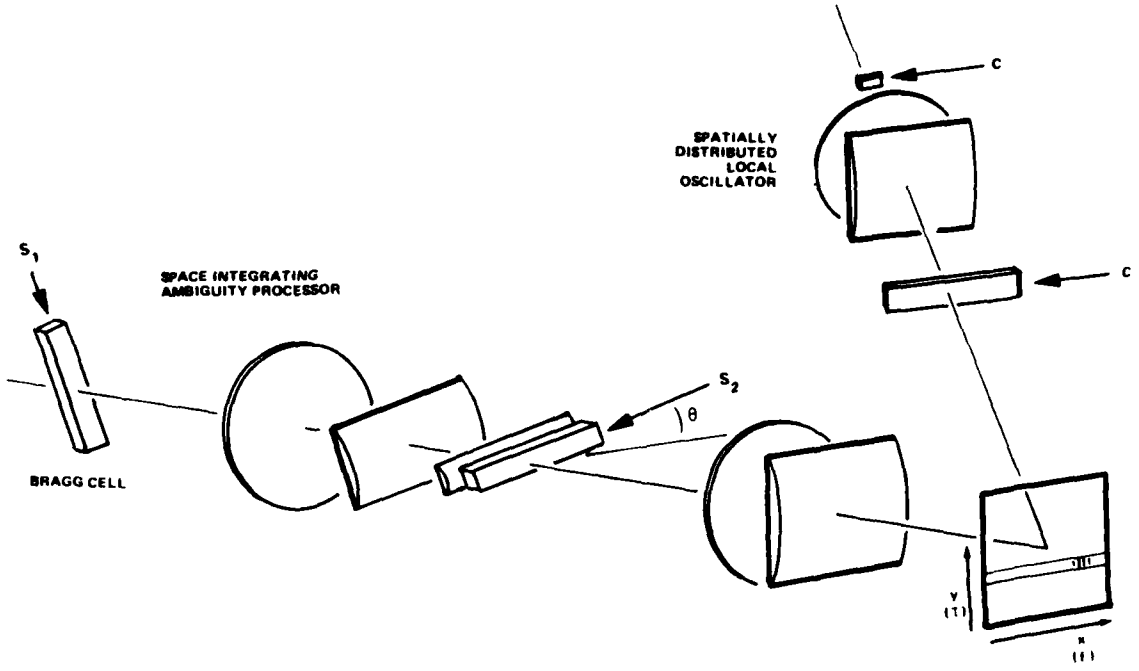

Figure 4. Schematic of Coherent Hybrid Ambiguity Function Processor

For our psendorandom signal this is represented in Figure 5. The broad Doppler peak has been reduced by time integration to a peak with a spatial carrier that is $1/T_2$ wide. An important characteristic of this measured cross ambiguity function is that the bias contribution from the signal arm of the interferometer is confined to the delay bias. Multiple signal components generating peaks separated by at least the delay resolution $1/\Delta f_s$ do not degrade the dynamic range as a result of bias accumulation, as is the case for purely time integrating processors. If the chosen Doppler range is larger than the Doppler resolution of the space-integrating processor above, then some localization of bias in the Doppler direction is also maintained.

Because of the time integration aspect, optical scatter noise, as in the spectrum analyzer, integrates out except for small second order terms.

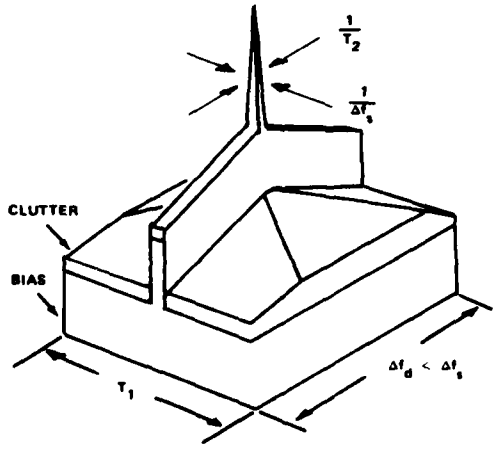

Figure 5. Ambiguity Function For Coherent Hybrid Processor.

Summary

Using the examples of one dimensional spectrum analysis and two dimensional ambiguity function processing, some of the limitations of purely space integrating and purely time integrating techniques for acoustooptic signal processing can be overcome by utilizing both space and time integration. Dynamic range advantages resulting from the coherent detection aspect of interferometric techniques are enhanced by optical scatter noise reduction, localized bias for superior multiple signal handling ability, and, in the case of spectrum analysis, a reduction in spectral sidelobes. The inherent sidelobe suppression property of coherent hybrid spectrum analysis is an important factor in many applications, particularly those involving threshold detection, and is characteristic of no other known optical technique.

The author acknowledges support for this work by the Air Force Office of Scientific Research under contract F49620-78-C-0102.

Appendix

An acoustooptic device having sound velocity v is driven by a periodic chirp of length T_1, period T_1, bandwidth Δf and minimum frequency f_m such that the amplitude of the up-shifted diffracted light is

$$r(t,\xi) = \sum_n e^{i[a(t-nT_1+\xi/v)^2 + b(t-nT_1+\xi/v)]} \operatorname{rect}(t-nT_1+\xi/v)/T_1 \quad \operatorname{rect}\xi/D \qquad \text{(A-1)}$$

where

$$a = \frac{\pi\Delta f}{T_1} , \qquad b = 2\pi f_m$$

At the detector plane, an optical Fourier transform plane of the Bragg cell, the convolution theorem yields

$$R(x,t) = \int_{-\infty}^{\infty} r(t,\xi)\, \exp(-i2\pi\alpha\xi x)\, d\xi = D\int_{-\infty}^{\infty} V(x-x',t)\, \operatorname{sinc}\pi\alpha Dx'\, dx' \qquad \text{(A-2)}$$

where

$$V(x,t) = \sum_n \int_{-\infty}^{\infty} e^{i[a(t-nT_1+\xi/v)^2 + b(t-nT_1+\xi/v)] - i2\pi\alpha x\xi} \operatorname{rect}(t-nT_1+\xi/v)/T_1\, d\xi \qquad \text{(A-3)}$$

The change of variables $z = t-nT_1+\xi/v$ leads to

$$V(x,t) = v\sum_{n=-\infty}^{\infty} e^{-i2\pi\alpha vx(t-nT_1)} \int_{-\infty}^{\infty} e^{iaz^2 - i(2\pi\alpha vx-b)z} \operatorname{rect}(z/T_1)\, dz . \qquad \text{(A-4)}$$

Using the identity

$$\sum_{n=-\infty}^{\infty} e^{ian} = 2\pi\sum_{p=-\infty}^{\infty} \delta(a + 2\pi p) , \qquad \text{(A-5)}$$

where $\delta(x)$ is the Dirac delta function, we have

$$V(x,t) = c\, e^{i2\pi\alpha vxt} \sum_p \delta[x-(p/\alpha vT_1)] \int_{-\infty}^{\infty} e^{i[az^2 - (2\pi\alpha vx-b)z]} \operatorname{rect}(z/T_1)\, dz \qquad \text{(A-6)}$$

Substitution of Equation A-6 into Equation A-2 yields

$$R(x,t) = c_1 \sum_p \Phi(p/T_1)\, e^{i2\pi pt/T_1} \operatorname{sinc}\pi T_1[\alpha vx-p/T_1] , \qquad \text{(A-7)}$$

where c_1 is a constant and

$$\Phi(p/T_1) = \int_{-\infty}^{\infty} e^{i[az^2 + (b-2\pi p/T_1)z]} \, rect(z/T_1) \, dz \quad . \tag{A-8}$$

The function $|\Phi(p/T_1)|$ describes the uniformity of the modulus in the transform plane of the Bragg cell in our model. For convenience of discussion of spatially distributed local oscillators we can derive an approximation to Equation A-8 in the limit of large N. Using the convolution theorem,

$$\Phi(p/T_1) = T_1 \int_{-\infty}^{\infty} G[(p/T_1)-\xi'] \, sinc \, \pi T_1 \xi' \, d\xi' \quad , \tag{A-9}$$

where

$$G[(p/T_1)-\xi'] = c_2 \, e^{-i\pi^2[(p/T_1)-(b/2\pi)-\xi']^2/a} \quad . \tag{A-10}$$

In the expansion of the exponent in Equation A-10 the $(\xi')^2$ term can be considered negligible, because at the first null of the sinc function in Equation A-9, $\xi'=1/T_1$ and

$$\pi^2(\xi')^2/a = \pi/\Delta f T_1 = \pi/N \ll 1 \quad .$$

Therefore we can write approximately

$$R(x,t) = c_2 \sum_p e^{i2\pi pt/T_1 - i[(2\pi p/T_1)-b]^2/4a} \, sinc \, \pi T_1 [avx - (p/T_1)], \tag{A-11}$$

where p runs over intergers from $f_m T_1$ to $(f_m+\Delta f)T_1$, and where we have observed that $D = vT_1$. c_2 is a complex constant.

References

1. Sprague, R. A. and C. L. Koliopoulos, "Time Integrating Acoustooptic Correlators," Appl. Opt. 15, 89 (1976).

2. Kellman, P., "Detector Integration Acousto-Optic Signal Processing," Proc. Int. Opt. Computing Conference, London, p. 91 (1978).

3. Turpin, T.., "Time Integrating Optical Processors," SPIE Symposium on Real Time Processing, San Diego, 154, 196 (1978).

4. Cohen, J., "Ambiguity Processing Architectures Using One- Dimensional Acoust-Optic Transducers," SPIE Symposium on Real Time Signal Processing II, 180, 134, (1979).

5. Bader, T. R., "Acoustooptic Spectrum Analysis: A High Performance Hybrid Technique," Appl. Opt. 18, 1668 (1979).

6. Bader T. R., "Coherent Optical Hybrid Techniques for Spectrum Analysis," SPIE Symposium on Optical Processing Systems, Huntsville, 185, 140 (1979).

7. Pratt, W. K. Laser Communication Systems, J. Wiley and Sons,N.Y., 1969, Chapter 10

8. Said, R. A. K.,et al., "Crosspath Real Time Optical Correlator and Ambiguity Function Processor," Proc. IEE 120, 423 (1971).

9. Rihaczeh, A. W., Principles of High Resolution Radar, McGraw-Hill Book Company, N.Y., 1969, Chapter 5.

TIME-INTEGRATING PROCESSORS USING BRAGG CELLS

Todd R. Bader
ESL Incorporated
Sunnyvale, CA

Acousto-optic methods are currently gaining wide use in electronic signal processing systems in a variety of applications, particularly communications and radar signal processing. The motivation for acousto-optic techniques is the associated wide bandwidth and parallel processing capability. The blossoming realization of high performance hardware is a result of the currently maturing technologies of key devices, including the acousto-optic devices themselves and, equally important, coherent and noncoherent light sources and high quality optical detectors.

The acousto-optic devices (Bragg cells) used in signal processing systems are real-time spatial light modulators; that is, a signal impressed on the piezoelectric transducer is represented (due to an acousto-optic interaction in the medium) as a traveling spatial variation of the light amplitude emerging from the device. The light diffracted by a component of this traveling sound wave is also Doppler shifted in optical frequency by the frequency of that component, a significant property relative to the use of A-O devices for time-integrating coherent processing.

Bragg cells are currently available in high quality devices operating in bandwidths that range from several MHz to perhaps 2 GHz, and with transit time x bandwidth products up to about 2000. The required bandwidth determines the acousto-optic material used. Generally the materials with the best acousto-optic coupling have the lowest bandwidth capability.

The most straightforward application of acousto-optic devices for signal processing is a power spectrum analyzer (or Bragg receiver) in which an array of photodetectors samples the optical intensity pattern in the back focal plane of a lens that Fourier Transforms the coherent light amplitude diffracted from a Bragg cell. Also, a variety of simple optical systems, both coherent and noncoherent, can be implemented to measure cross-correlation functions between two signals. Bragg receivers and time-integrating optical correlators are particularly useful for sensitive detection of narrowband and spread spectrum signals, respectively. Both algorithms use a time-integrated detected signal to improve sensitivity. This post-detection integration has the additional benefit of reducing the processor output data rate, easing the requirements placed on the detector array. Interferometric techniques for coherent detection may be used for complex amplitude spectrum analysis at the cost of more sophisticated detector array and post-detection processing technology.

SPSE Symposium on Optical Data Display, Processing and Storage.
Las Vegas, March 198

AD-A106 778 ESL INC SUNNYVALE CA F/G 9/3
TIME INTEGRATING OPTICAL SIGNAL PROCESSING.(U)
JUL 81 T R BADER, P KELLMAN, H N SHAVER F49620-78-C-0102
UNCLASSIFIED AFOSR-TR-81-0700 NL

Two-dimensional systems composed of a light source, Bragg cells, two-dimensional detector arrays and simple passive components can be configured to perform a variety of processing algorithms. High resolution spectrum analysis is performed by extending frequency resolution in the transverse direction of a coherent spectrum analyzer by time-integration. Complex spectra of imagery, for example, can be generated in this way by providing an input electronic signal in the form of a raster scanned image. Real-time cross correlation of two images is performed by generating an inverse 2-D transform of the product of their spectra. Another 2-D process well-matched to A-O techniques is the generation of ambiguity functions. This is a valuable method of measuring the cross correlation of a signal with a version of it having an unknown Doppler-shift.

Acousto-optic processing performance is presently limited by detector array technology. Although systems are currently being fielded with high performance A-O processors, these are mostly one-dimensional. Detector technology is rapidly advancing, however, and the near future should see a growing volume and variety of one- and two-dimensional acousto-optic signal processors for numerous applications.